

UNIVERSITY OF BELGRADE
FACULTY OF PHYSICS

MASTER THESIS

**Polaron Mobility Obtained by a
Variational Approach for a Class of
Lattice Models**

STUDENT: MILAN KORNJAČA

ADVISOR: DR NENAD VUKMIROVIĆ

MAY 2017

The work presented in this thesis was performed in Scientific Computing Laboratory of the Institute of Physics, Belgrade, under the supervision of Dr Nenad Vukmirović. I would like to thank Nenad for all the patience and time invested in this thesis and above all for the fresh ideas in the moments when they were most needed. I would like to thank Veljko Janković, for the practical help in numerous occasions, as well as for a great working atmosphere.

Contents

1	Introduction	1
1.1	Fröhlich and Holstein Polarons	2
1.2	Lattice Fröhlich Polaron	6
1.3	Finite Temperature Green's Functions	9
1.4	Kubo Formula for Mobility	11
1.5	Overview of the Thesis	16
2	Variational Lang-Firsov Unitary Transformation	17
2.1	Lang-Firsov Unitary Transformation	17
2.2	Gibbs-Bogolyubov Bound and Equations for Variational Parameters	20
2.3	Numerical Solution for the Variational Parameters in 1D Model	22
3	Approximate Solutions for Kubo Formula and Spectral Properties of Lattice Fröhlich Polaron	27
3.1	Approximate Solution to Kubo Formula	27
3.2	Matsubara Functions via Dyson Expansion	30
3.3	Analytic Continuation and Retarded Green's Functions	33
4	Polaron Mobility Estimates in Extreme Parameter Regions	39
4.1	Low Temperature and Weak Coupling Limit for Polaron Mobility	39
4.1.1	Non-Adiabatic Regime ($J_{\mathbf{C}} > \hbar\omega_0$)	41
4.1.2	Adiabatic Regime ($J_{\mathbf{C}} < \frac{\hbar\omega_0}{2}$)	42
4.1.3	Mixed Regime ($\frac{\hbar\omega_0}{2} < J_{\mathbf{C}} < \hbar\omega_0$)	44
4.2	High Temperature and Strong Coupling Limit for Polaron Mobility	44
5	Numerical Results	48
5.1	Parameters of Numerical Calculation	48
5.2	Polaronic Spectra	49
5.3	Current-Current Correlations	55
5.4	Mobility	57
6	Conclusion	65
A	The Proof of Expressions Used for the Calculations of Phonon Thermal Averages	66

Chapter 1

Introduction

Electron-phonon interaction is a very important topic for understanding the properties of solids, in particular their transport properties. Transport properties of metals, semiconductors and ionic crystals are all decisively influenced by electron phonon-interaction. In semiconductors and ionic crystals, the concept of polaron, a composite particle that consists of an electron and the cloud of phonons bound to it, is useful for understanding the effects of electron-phonon interaction.

The beginnings of the polaron concept can be traced back to the works of Landau and Pekar in the early thirties [1], but it was Fröhlich who first systematically described and studied the polaron [2]. In years that followed, the basic properties of Fröhlich polaron were established, but also the number of "species" of polarons was significantly enlarged beyond the initial Fröhlich type. Although the basic physics is the same, different polaron types are needed to describe the effects of electron-phonon interaction in real materials in which band structure, as well as the strength and range of the interaction, can vary to a great degree. In recent decades, interest in polaron physics is reinvigorated. The polaronic or polaron-like effects are expected to be important for transport in organic semiconductors as well as quantum dot solids [3] on the one hand and systems such as an impurity in a Bose-Einstein condensate on the other hand [4]. There is even an alternative theory of high-temperature superconductivity in cuprates based on the polaronic effects [5].

The main subject of this thesis is the mobility of a specific family of polarons in a wide range of coupling strengths and temperatures. The description of the model studied and its relation to other polaron models can be found in sections 1.1 and 1.2. Standard Matsubara Green's function techniques that were used for the calculation of polaronic spectral properties are briefly described in section 1.3. Linear response theory essential for the calculation of mobility is covered in section 1.4. In the final section of the chapter, an overview of the thesis is given.

1.1 Fröhlich and Holstein Polarons

Electron-phonon interaction is present in any solid, but its strength may vary greatly depending on the electronic properties of the solid as well as the type of phonons that electrons couple to. The thesis will concentrate on polar materials, such as ionic solids and compound semiconductors. Optical phonons, as vibrations of ions or different atoms, produce polarization field in the solid, which electrons couple to. Transverse optical phonons in which the displacement is normal to the wave vector do not produce strong electric fields. Acoustic phonons do not produce polarization of the medium unless the crystal is piezoelectric, so the coupling to them is usually small. Thus, the interaction with longitudinal optical (LO) phonons is usually the dominant form of electron-phonon interaction in polar materials [6].

An electron moving in the polar medium induces polarization around itself and in turn it may become self-trapped by the field of induced polarization. This basic picture is the root of the polaron idea. Polaron is an entity consisting of an electron and the polarization it carries around, or equivalently of an electron and the phononic cloud it is bound to. Properties of a polaron such as its effective mass or the response to the external fields are different than that of a band electron. Since there is an interest in transport properties of materials in which electron-phonon interaction is sufficiently strong so that the polaron picture may be valid, it is important to understand properties of polarons [7]. More specifically, in the materials with the strongest type of electron-phonon interactions, that of the polar LO coupling, polarons are shown to govern the transport properties [6].

The most common model that describes polarons is the Fröhlich model. It is derived in the free electron approximation (continuum approximation) taking into account the interaction of the electron with one LO mode. The dispersion of the LO mode is taken to be flat as in Einstein approximation. Hamiltonian of this model is:

$$H_{Fröhlich} = \frac{\mathbf{p}^2}{2m_b} + \sum_{\mathbf{q}} \hbar\omega_0 b_{\mathbf{q}}^{\dagger} b_{\mathbf{q}} + \sum_{\mathbf{q}} (V_{\mathbf{q}} b_{\mathbf{q}} e^{i\mathbf{q}\mathbf{r}} + V_{\mathbf{q}}^* b_{\mathbf{q}}^{\dagger} e^{-i\mathbf{q}\mathbf{r}}) \quad (1.1)$$

$$V_{\mathbf{q}} = -i \frac{\hbar\omega_0}{q} \left(\frac{4\pi\alpha}{V} \right)^{\frac{1}{2}} \left(\frac{\hbar}{2m_b\omega_0} \right)^{\frac{1}{4}} \quad \alpha = \frac{e^2}{\hbar} \sqrt{\frac{m_b}{2\hbar\omega_0}} \left(\frac{1}{\epsilon_{\infty}} - \frac{1}{\epsilon_0} \right)$$

where ω_0 is the frequency of the LO mode, V is the system volume, m_b is the electron band mass, α is the dimensionless electron-phonon coupling constant, while ϵ_{∞} and ϵ_0 are the high-frequency and static dielectric constants of material, respectively.

One of the features of the Fröhlich model is that it connects interaction strength parameter with the measurable properties of material such as the dielectric constants, effective mass and phonon frequencies. The approximate derivation of this relation will be presented for the strong coupling ($\alpha \gg 1$). It will be assumed that an electron in the material is localized on the length scale of l_1 . Electron's charge distribution

will be approximated by a uniformly charged sphere of radius l_1 . Additional energy that comes from electron-phonon interaction will be found as a difference between the self-energies of electrons in cases where the lattice polarization has an effect and doesn't, respectively.

The electrostatic energy of the sphere without the presence of ions is $\frac{3}{5} \frac{1}{4\pi} \frac{e^2}{l_1}$. Self-energy of the electron with polarization fields that can adiabatically follow him, as is the case for strong coupling, is $\frac{3}{5} \frac{1}{4\pi} \frac{e^2}{\epsilon_0 l_1}$. On the other hand, the self-energy of an electron in the high-frequency case for which ionic polarization cannot follow the electron is $\frac{3}{5} \frac{1}{4\pi} \frac{e^2}{\epsilon_\infty l_1}$, because the electron charge is screened by the amount given by the static dielectric constant. Total interaction energy of the electron and its polarization is equal to the difference of these two self-energies and is proportional to:

$$U_{int} = -\frac{e^2}{l_1} \left(\frac{1}{\epsilon_\infty} - \frac{1}{\epsilon_0} \right). \quad (1.2)$$

A rough estimate of the range of the electronic localization can be made by taking into account the kinetic energy of the localized electron:

$$E_{kin} = \frac{\hbar^2}{2m_b l_1^2}. \quad (1.3)$$

After minimizing the total energy with respect to the l_1 , the result is:

$$l_1 = \frac{e^2 m_b}{\hbar^2 \left(\frac{1}{\epsilon_\infty} - \frac{1}{\epsilon_0} \right)}, \quad E_{tot} = -\frac{e^4 m_b}{2\hbar^2 \left(\frac{1}{\epsilon_\infty} - \frac{1}{\epsilon_0} \right)^2}. \quad (1.4)$$

Comparing the result above with the exact result for the Fröhlich model binding energy in the strong coupling limit ($-\alpha^2$), the connection between coupling constant and measurable quantities is obtained. In table 1.1 the measured Fröhlich coupling constants for several polar materials are given. It can be seen that they lay in quite a wide range that includes both weak and strong couplings [7].

A large amount of work has been done within the Fröhlich model and much is known - polaron binding energies, spectral properties, mobility in limiting cases, etc. However, the model is inadequate in dealing with strong (or not even strong) electron-phonon interaction in at least one way. In assuming the validity of the continuum approximation, Fröhlich model assumes that the spatial extent of the electronic wave function is at least several lattice constants, ideally greater. However, electron-phonon interaction can cause length to be even shorter. The result in the strong limit gives for the spatial extent of the electronic wave function is approximately [7]:

$$l_1 = \sqrt{\frac{\hbar}{m_b \alpha^2 \omega_0}}. \quad (1.5)$$

Table 1.1: Fröhlich coupling constants for several polar materials. The table is taken from [7].

Material	α	Material	α
InSb	0.023	AgCl	1.84
InAs	0.052	KI	2.5
GaAs	0.068	TlBr	2.55
GaP	0.2	KBr	3.05
CdTe	0.29	Bi ₁₂ SiO ₂₀	3.18
ZnSe	0.43	CdF ₂	3.2
CdS	0.53	KCl	3.44
α -Al ₂ O ₃	1.25	CsI	3.67
AgBr	1.53	SrTiO ₃	3.77
α -SiO ₂	1.59	RbCl	3.81

In the weak limit ($\alpha \ll 1$), the following expression is valid for the characteristic length [7]

$$l_2 = \sqrt{\frac{\hbar}{m_b \omega_0}}. \quad (1.6)$$

There is a number of materials where the length (either l_1 or l_2) is not sufficiently higher than lattice constant because of the strong electron-phonon interaction, the best example being transition metal oxides and, depending on what is considered large enough, it may include even alkali-halides. Furthermore, there are materials in which electron band mass is sufficiently large to make l_1 or l_2 length small. These include organic semiconductors and quantum dot solids [5].

Because of the need to go further beyond continuum approximation of Fröhlich, various lattice polaron models were proposed [8]. Polarons are labeled by either large or small depending on the characteristic length of polaronic wave function [6]. In that sense Fröhlich model can be seen as an extreme case of a large continuum polaron mainly valid when bandwidths are large and electron-phonon interaction not too strong. Furthermore, standard Fröhlich Hamiltonian is derived for the long range (unscreened) electron-phonon interaction. On the other end of a polaronic family there is another well known model, the Holstein polaron.

Holstein model is a small lattice polaron model in which the range of the electron-phonon interaction is assumed to be minimal, so that electron interacts only with phonons on a site it is currently found. The short-range electron-phonon interaction is thought to be good approximation for non-polar materials in which long-range electrostatic forces are absent. But in general, Holstein model is an approximation for small bandwidths and interaction ranges, quite the opposite of the Fröhlich case. Standard Holstein Hamiltonian is written with the tight-binding approximation for

electrons. For a single LO mode with flat dispersion it assumes the form:

$$H_{Holstein} = - \sum_{\mathbf{m}, \mathbf{n}} t_{\mathbf{n}} c_{\mathbf{m}+\mathbf{n}}^\dagger c_{\mathbf{m}} + \sum_{\mathbf{m}} \hbar\omega_0 b_{\mathbf{m}}^\dagger b_{\mathbf{m}} - \sum_{\mathbf{m}} \sum_{\mathbf{q}} \hbar\omega_0 g^2 c_{\mathbf{m}}^\dagger c_{\mathbf{m}} (b_{\mathbf{m}}^\dagger + b_{\mathbf{m}}), \quad (1.7)$$

where g^2 is the dimensionless electron-phonon coupling constant, \mathbf{m} and \mathbf{n} are site position vectors and $t_{\mathbf{n}}$ is the transfer integral from central site to site \mathbf{n} . Its connection with measurable properties of a material is not as clear as in the Fröhlich case because it is related exclusively to the microscopic details of a material. Yet it may be inferred from the measurement of the properties strongly affected by polaronic nature of charge carriers, with the assumption that the model itself is valid for a material in question. Also, first principle calculations may provide estimates, as has been done for quantum dot systems [9].

Important point to consider when describing Holstein and other lattice polaron Hamiltonians is that a simple strong/weak interaction classification is not entirely adequate. While in the Fröhlich case the only relevant parameter is the coupling constant α , it is the ratio of coupling and transfer integral that determines strong and weak interaction ranges for the lattice case. However, this ratio, $\frac{g^2 \hbar\omega_0}{t}$ for Holstein model, can be small or large independent of the g^2 or t , so there are regions of parameters in which a character of interaction is not entirely clear. For this reason, besides weak ($\frac{g^2 \hbar\omega_0}{t} \ll 1$) and strong ($\frac{g^2 \hbar\omega_0}{t} \gg 1$) Holstein limit, there exist adiabatic $t \ll \hbar\omega_0$ and nonadiabatic $t \gg \hbar\omega_0$ limits. In the adiabatic limit phonons can follow the electronic motion. Most materials would correspond to nonadiabatic region, however there are examples in which this is not so clear and even ones in which adiabatic condition can be full-filled (quantum dot solids) [9].

From all the properties of Fröhlich and Holstein models, mobility estimates are the most important for further comparison. Two limiting cases are especially illuminating.

In the limit of weak interactions, low temperatures and large electronic bandwidths, carriers exhibit band-like behaviour. In this case electron-phonon interaction is one possible source of scattering that limits otherwise infinite mobility to finite values. If we are interested in a material in which electron-phonon interaction is dominant scattering mechanism, we can expect that the scattering rate is proportional to the number of phonons, determined by the temperature, and to the strength of interaction. This is confirmed by the exact result in the weak interaction low temperature limit of the Fröhlich model which correspond well to the range of the parameters described¹ [7]:

$$\mu = \frac{e}{2\alpha} (e^{\beta\hbar\omega_0} - 1) \propto \frac{1}{\alpha n_{ph}} \quad (1.8)$$

¹It should be noted that this result, although 50 years old, remains controversial. In some calculations an additional factor of 3 arises [7]. However, this doesn't influence our discussion.

In the opposite limit of high temperatures, strong interaction and small bandwidths, often used approximation is that of a diffusive motion of electrons. It is assumed that if polaron band is narrow enough the band-like mobility is suppressed. Since one of the consequences of strong electron-phonon interaction is band narrowing, a well known result for the Holstein Hamiltonian, very narrow polaron bands form in this region of parameters. Holstein proposition is that if this is true, main contribution to the mobility comes from electron hopping from one site to the other site. This random walk of electron is then modeled by Markovian process with a certain probability of a nearest neighbour hop. In turn, the mobility is proportional to the hopping probability. To make a hop, electron must overcome bonding with the phonon cloud on the site it is currently on. In other words, there is a barrier that electron must overcome in a hop. Result for a hopping mobility with these assumptions is of the form [6]:

$$\mu_h \propto t^2 \beta^{\frac{3}{2}} e^{-\beta E_a}, \quad (1.9)$$

where E_a is the activation energy that corresponds to the height of the hopping barrier which is of the order of the polaron binding energy. For the Holstein polaron in the strong coupling limit this binding energy is $g^2 \hbar \omega_0$.

The temperature dependence of the hopping mobility shows an activation behaviour in a certain temperature range, followed by power law decrease for very high temperature as opposed to exponential decrease of a band-like mobility seen in (1.8). However, since the result is derived in the limit of high temperatures, it is unclear to what temperature range it can be applied and whether activation behaviour is to be expected. Also, it is an open question to what extent can the band-like mobility be disregarded and in what range we can use one or the other theory of polaron mobility [10], [11]. It is clear that in order to resolve these questions, a unified theory of polaron mobility is needed. One of the steps in that direction may be achieved by using model Hamiltonians somewhere in between the extremes that Fröhlich and Holstein represent.

1.2 Lattice Fröhlich Polaron

A class of polaronic models that may be suitable for the ranges of conditions not covered by models presented in 1.1 are lattice Fröhlich polarons. The Hamiltonian of the lattice Fröhlich polaron, written for an arbitrary phonon dispersion ($\omega_{\mathbf{q}}$), is:

$$H = H_e + H_{ph} + H_{e-ph} = - \sum_{\mathbf{m}, \mathbf{n}} t_{\mathbf{mn}} c_{\mathbf{m}}^{\dagger} c_{\mathbf{n}} + \sum_{\mathbf{q}} \hbar \omega_{\mathbf{q}} b_{\mathbf{q}}^{\dagger} b_{\mathbf{q}} - \sum_{\mathbf{m}, \mathbf{n}} \hbar \omega_{\mathbf{q}} f_{\mathbf{m}-\mathbf{n}} c_{\mathbf{n}}^{\dagger} c_{\mathbf{m}} (b_{\mathbf{m}}^{\dagger} + b_{\mathbf{m}}), \quad (1.10)$$

where

$$b_{\mathbf{m}} = \frac{1}{\sqrt{N}} \sum_{\mathbf{q}} b_{\mathbf{q}} e^{-i\mathbf{q}\mathbf{m}}, \quad (1.11)$$

and where $f_{\mathbf{m}-\mathbf{n}}$ are the coefficients of electron-phonon interaction. The case in which they are zero except for $\mathbf{m} = \mathbf{n}$ corresponds to the Holstein Hamiltonian, while the case in which their Fourier transform is equal to the coefficients $V_{\mathbf{q}}$ in the Fröhlich Hamiltonian can be viewed as a Fröhlich polaron on a lattice. The model can be derived by considering classical interaction of the electron and the LO phonon polarization cloud, as will be shown on an 1D example [12]. It is this Hamiltonian that the thesis will be concerned with. While some of the results will be provided for the general Hamiltonian, it is a specific 1D variant of the model that will be investigated numerically, namely because of the computational convenience.

The basis for derivation of the lattice Fröhlich Hamiltonian is the interaction between the electron and the polarization that comes from LO phonons. Classically, this interaction has the form:

$$V_{int}(\mathbf{r}_{el}) = - \sum_{\mathbf{m}} e \frac{\mathbf{p}_{\mathbf{m}} \cdot (\mathbf{r}_{el} - \mathbf{m})}{|\mathbf{r}_{el} - \mathbf{m}|^3}, \quad (1.12)$$

where $\mathbf{p}_{\mathbf{m}}$ is the dipole moment of a molecule at site \mathbf{m} and \mathbf{r}_{el} is the electron position vector. The following steps in the derivation of lattice Fröhlich Hamiltonian will depend on the details of the crystal lattice and phonon polarization directions, but they are, in principle, similar. The 1D model used for numerical investigations consists of a linear chain with a polar molecule at each site. Atoms that molecule is built of can oscillate in a line of a chain which corresponds to one LO phonon mode. Dipole moment of a molecule can be assumed to be proportional to the displacement of atoms, $\xi_{\mathbf{m}}$. Thus, interaction energy is proportional to:

$$V_{int}(\mathbf{r}_{el}) \propto \sum_{\mathbf{m}} \frac{\xi_{\mathbf{m}}}{|\mathbf{r}_{el} - \mathbf{m}|^2}. \quad (1.13)$$

The matrix elements of the electron-phonon interaction are given by $\int d^3\mathbf{r}_{el} \psi_{\mathbf{n}'}^*(\mathbf{r}_{el}) V_{int}(\mathbf{r}_{el}) \psi_{\mathbf{n}}(\mathbf{r}_{el})$, where $\psi_{\mathbf{n}}(\mathbf{r}_{el})$ is the orbital function of the electron at site \mathbf{n} . The matrix elements are the largest for $\mathbf{n}' = \mathbf{n}$, since the orbital overlap between different molecules is usually exponentially smaller. The full treatment should include the "off-diagonal" matrix elements, or at least nearest neighbor ones. Yet, situation for the electron-phonon interaction is substantially different than that for the tight-binding approximation for electronic band structure. While in the tight-binding approximation including nearest neighbors' transfer is obligatory, as it gives the first nontrivial term, the first and the largest contribution for the electron-phonon interaction already comes from "diagonal" matrix elements. Including nearest neighbor overlap is more analogous to taking the next-nearest neighbour transfer in the TBA. With this

in mind, and using standard bosonic quantization:

$$\xi_{\mathbf{m}} \propto \frac{1}{\sqrt{N}} \sum_{\mathbf{q}} (b_{\mathbf{q}}^{\dagger} e^{i\mathbf{q}\mathbf{m}} + b_{\mathbf{q}} e^{-i\mathbf{q}\mathbf{m}}) \propto b_{\mathbf{m}}^{\dagger} + b_{\mathbf{m}}, \quad (1.14)$$

the electron-phonon part of the Hamiltonian can be written as:

$$H_{e-ph} = - \sum_{\mathbf{m}, \mathbf{n}} \hbar\omega_{\mathbf{q}} f_{\mathbf{m}-\mathbf{n}} c_{\mathbf{n}}^{\dagger} c_{\mathbf{n}} (b_{\mathbf{m}}^{\dagger} + b_{\mathbf{m}}), \quad (1.15)$$

with:

$$f_{\mathbf{m}-\mathbf{n}} \propto \frac{1}{|\mathbf{n} - \mathbf{m}|^2}. \quad (1.16)$$

The derived form of electron-phonon interaction is clearly that of a lattice Fröhlich type. The interaction has an infinite range, and its spatial dependence corresponds to the 1D Fröhlich lattice model². However, the interaction with the central site is not well defined. This is to be expected, since electron certainly does not see a dipole field from the molecule it is "currently" on. Finding the ratio of the interaction of electron with the central atom and the neighboring ones would require a first principle calculation, but without it, one must resort to inclusion of two different coupling constants. Thus, the final form of the interaction coefficients is:

$$f_{\mathbf{m}-\mathbf{n}} = \alpha_1 \delta_{\mathbf{m}, \mathbf{n}} + \frac{\alpha_2 C^2}{|\mathbf{m} - \mathbf{n}|^2} (1 - \delta_{\mathbf{m}, \mathbf{n}}), \quad (1.17)$$

where C is the lattice constant.

It is useful to redefine the couplings to have one coupling constant that determines overall interaction strength and the other that describes the relative strength of interaction with the central atom and all the other atoms (in a sense, the electron-phonon interaction range). It can be done in multiple ways, but here the procedure of Alexandrov [12] used for a different 1D lattice Fröhlich Hamiltonian will be loosely followed. As a measure of the interaction strength, the binding energy of the polaron in the strong-coupling limit is used. This binding energy, as will be shown, is given by:

$$\begin{aligned} \frac{\Delta E_{e-ph}}{\hbar\omega_0} &= - \sum_{\mathbf{q}} f_{\mathbf{q}}^2 = - \sum_{\mathbf{m}} f_{\mathbf{m}}^2 = -\alpha_1^2 - 2\alpha_2^2 \sum_{j=1}^N \frac{1}{j^4} = -\alpha_1^2 - \kappa\alpha_2^2, \\ f_{\mathbf{q}} &= \frac{1}{\sqrt{N}} \sum_{\mathbf{m}} f_{\mathbf{m}} e^{i\mathbf{q}\mathbf{m}}. \end{aligned} \quad (1.18)$$

²It should be noted that continuum Fröhlich polaron does not have a nice extension to the 2D or 1D case. While all the quantities calculated in the 3D Fröhlich model are regular, analogous 2D and 1D models suffer from ultraviolet divergences. Divergences are the consequences of the continuum approximation and as such they vanish on a lattice. Furthermore, some 3D Fröhlich models that use different phonon dispersion from the flat one also suffer from UV divergences [4]. While the continuum Fröhlich model is simple, it is not very robust.

For a sufficiently large number of atoms, $\kappa \approx \frac{\pi^4}{45} \approx 2.16$. The coupling constants are redefined as:

$$\begin{aligned}\alpha_1 &= \alpha \cos \psi \\ \alpha_2 &= \frac{1}{\sqrt{\kappa}} \alpha \sin \psi.\end{aligned}\tag{1.19}$$

The binding energy in the strong-coupling limit becomes $-\alpha^2$, thus the coupling constant α determines the overall interaction strength. The parameter ψ tells how much the Hamiltonian is Holstein-like or Fröhlich-like. The case of $\psi = 0$ corresponds to the Holstein Hamiltonian, while in the opposite extreme, $\psi = \frac{\pi}{2}$, the interaction with the central molecule is nonexistent. The ratio of the interaction coefficients for the central molecule and the nearest neighbor is:

$$\frac{f_0}{f_1} = \sqrt{\kappa} \cot \psi \approx 1.47 \cot \psi\tag{1.20}$$

The coefficients are equal for $\psi \approx \frac{\pi}{3}$, which can be taken as the upper limit of the sensible values for ψ . It is not expected that the interaction with the neighboring molecule is stronger than that with the central one.

It is this 1D lattice Fröhlich Hamiltonian class that will be investigated in detail in the following chapters³. However, the analytic results that will be derived are valid for the general lattice Fröhlich case. Before the results, a brief description of the methods used is presented.

1.3 Finite Temperature Green's Functions

Retarded and advanced Green's functions provide a systematic way of obtaining electronic correlations needed for the calculation of transport properties.

$$\begin{aligned}G_{\mathbf{k}}^{ret}(t) &= -ih(t)\langle c_{\mathbf{k}}(t)c_{\mathbf{k}}^\dagger + c_{\mathbf{k}}^\dagger c_{\mathbf{k}}(t) \rangle \\ G_{\mathbf{k}}^{adv}(t) &= ih(-t)\langle c_{\mathbf{k}}(t)c_{\mathbf{k}}^\dagger + c_{\mathbf{k}}^\dagger c_{\mathbf{k}}(t) \rangle\end{aligned}\tag{1.21}$$

In the expression above, $h(t)$ denotes the Heaviside step function, c -operators are electronic creation and annihilation operators and averaging is to be done over the grand canonical ensemble.

Since the thesis is concerned with the transport properties at finite temperatures, Matsubara formalism is used. The starting point of the formalism are the imaginary

³For numerical calculations flat phonon dispersion, $\omega_{\mathbf{q}} = \omega_0$, is used.

time Matsubara Green's functions, defined as [6]:

$$\begin{aligned} G_{\mathbf{k}}(\tau) &= -\langle T_{\tau} c_{\mathbf{k}}(\tau) c_{\mathbf{k}}^{\dagger} \rangle = -\langle T_{\tau} e^{\tau(H-\mu N)} c_{\mathbf{k}} e^{-\tau(H-\mu N)} c_{\mathbf{k}}^{\dagger} \rangle, \\ D_{\mathbf{k}}(\tau) &= -\langle T_{\tau} b_{\mathbf{k}}(\tau) b_{\mathbf{k}}^{\dagger} \rangle, \end{aligned} \quad (1.22)$$

for the fermions and bosons, respectively, with T_{τ} denoting the standard fermionic and bosonic time-ordering and b -operators being phononic creation and annihilation operators. In the expression above, N is the total number of particles and μ is the chemical potential.

Definitions above allow in the interaction picture for the transformation of the thermodynamic averages with respect to the full Hamiltonian into averages with respect to the non-interacting part. Corresponding S-matrix can then be calculated via standard Dyson series. Additional benefit is that only connected diagrams need to be summed.

$$\begin{aligned} G_{\mathbf{k}}(\tau) &= -\frac{\langle T_{\tau} S(\hbar\beta) c_{\mathbf{k}}^I(\tau) (c_{\mathbf{k}}^I)^{\dagger} \rangle_0}{\langle S(\hbar\beta) \rangle_0} = -\langle T_{\tau} S(\hbar\beta) c_{\mathbf{k}}^I(\tau) (c_{\mathbf{k}}^I)^{\dagger} \rangle_{0,connected} \\ S(\hbar\beta) &= \sum_{n=0}^{\infty} \frac{(-1)^n}{n! \hbar^n} \int_0^{\hbar\beta} d\tau_1 \dots \int_0^{\hbar\beta} d\tau_n \left[T_{\tau} V_{int}^I(\tau_1) \dots V_{int}^I(\tau_n) \right] \end{aligned} \quad (1.23)$$

In the expressions above, $\langle \dots \rangle_0$ denotes thermodynamic averaging with respect to the non-interaction part, while V_{int}^I is the interaction part of the Hamiltonian in the interaction picture.

Perturbative calculations of the Dyson series in the thesis are made feasible for arbitrarily strong electron-phonon interaction by previously applying a suitable canonical transformation that makes the interaction part of the Hamiltonian small.

Imaginary frequency Matsubara Green's functions are defined as Fourier transforms of the imaginary time functions:

$$\begin{aligned} G_{\mathbf{k}}(ip_n) &= \int_0^{\hbar\beta} d\tau e^{ip_n\tau} G_{\mathbf{k}}(\tau), \quad G_{\mathbf{k}}(\tau) = \frac{1}{\hbar\beta} \sum_n e^{-ip_n\tau} G_{\mathbf{k}}(ip_n), \quad p_n = \frac{(2n+1)\pi}{\hbar\beta} \\ D_{\mathbf{k}}(i\omega_n) &= \int_0^{\hbar\beta} d\tau e^{i\omega_n\tau} D_{\mathbf{k}}(\tau), \quad D_{\mathbf{k}}(\tau) = \frac{1}{\hbar\beta} \sum_n e^{-i\omega_n\tau} D_{\mathbf{k}}(i\omega_n), \quad \omega_n = \frac{2n\pi}{\hbar\beta}. \end{aligned} \quad (1.24)$$

The importance of the imaginary frequency Matsubara functions lies in the fact that they can give retarded and advanced Green's functions in frequency domain via analytic continuation:

$$\begin{aligned} \lim_{\delta \rightarrow 0} G(\omega + i\delta) &= G^{ret}(\omega) \\ \lim_{\delta \rightarrow 0} G(\omega - i\delta) &= G^{adv}(\omega). \end{aligned} \quad (1.25)$$

The benefit of Matsubara formalism is that it allows for the standard diagrammatic expansions to be used, which is not possible to do with the regular Green's functions without introducing additional diagrams. The price to be paid for this is the additional step of analytic continuation.

It is convenient to separate Green's functions into the non-interacting part and the self-energy part that comes from the interaction, as given by Dyson equation:

$$G_{\mathbf{k}}^{ret}(\omega) = \frac{G_{\mathbf{k}}^{0ret}(\omega)}{1 - \Sigma_{\mathbf{k}}^{ret}(\omega)G_{\mathbf{k}}^{0ret}(\omega)}, \quad G_{\mathbf{k}}^{0ret}(\omega) = \frac{1}{\omega - \frac{E_{\mathbf{k}} - E_f}{\hbar} + i\delta}, \quad (1.26)$$

where $E_{\mathbf{k}}$ is the electron band dispersion and E_f is the Fermi energy.

From the retarded Green's functions, another useful quantity can be derived - the spectral function.

$$\Lambda_{\mathbf{k}}(\omega) = -2\text{Im}[G_{\mathbf{k}}^{ret}(\omega)] = \frac{-2\text{Im}[\Sigma_{\mathbf{k}}^{ret}(\omega)]}{\left(\omega - \frac{E_{\mathbf{k}} - E_f}{\hbar} + \text{Re}[\Sigma_{\mathbf{k}}^{ret}(\omega)]\right)^2 + \left(\text{Im}[\Sigma_{\mathbf{k}}^{ret}(\omega)]\right)^2} \quad (1.27)$$

The spectral function is directly related to the density of states, and it can be used for the calculation of thermodynamic averages of any single-electron observable. Knowing the spectral properties of the Hamiltonian will allow for the calculation of the transport properties as given by the linear response theory. In particular, the following averages will be used:

$$\begin{aligned} \langle c_{\mathbf{k}}^\dagger(t)c_{\mathbf{k}} \rangle &= \int_{-\infty}^{\infty} \frac{d\omega}{2\pi} e^{i\omega t} n_F(\omega) \Lambda_{\mathbf{k}}(\omega), \\ \langle c_{\mathbf{q}}(t)c_{\mathbf{q}}^\dagger \rangle &= \int_{-\infty}^{\infty} \frac{d\omega}{2\pi} e^{-i\omega t} (1 - n_F(\omega)) \Lambda_{\mathbf{q}}(\omega), \end{aligned} \quad (1.28)$$

where n_F denotes Fermi distribution. The expressions can be proven by expanding averages and spectral functions in the eigenbasis of total Hamiltonian [6], a procedure that will be shown several times in the latter text, but will be omitted here for the sake of conciseness.

1.4 Kubo Formula for Mobility

Linear response theory provides a systematic way to describe the transport properties of systems in conditions close to equilibrium. The great advantage of the theory is the fact that the transport properties are connected to much more easily obtainable equilibrium properties of the system. As such, it will be used for the calculation of polaron mobility in conjunction with described Green's functions approach, which will provide the necessary equilibrium quantities.

There are two basic assumptions of the theory [13]. The first one is that the external field is sufficiently small so that it couples linearly to the system in question. In the case of interest, external field is the electric field that couples linearly to the dipole moment of the system:

$$H' = -\mathbf{d} \cdot \mathbf{E}. \quad (1.29)$$

Operator of the dipole moment of the system is:

$$\mathbf{d} = \sum_n q \mathbf{r}_n, \quad (1.30)$$

where \mathbf{r}_n is the position operator of carrier n of charge q .

The second assumption is that system is in the equilibrium before the field was applied. More precisely, without external field (Hamiltonian H_0 ⁴), system is in equilibrium, so that its density matrix satisfies:

$$\rho_{E=0} = \frac{e^{-\beta(H_0 - \mu N)}}{\text{Tr} e^{-\beta(H_0 - \mu N)}} \quad (1.31)$$

After the field is turned on, the system evolves under Hamiltonian $H = H_0 + H'$:

$$i\hbar \frac{d\rho(t)}{dt} = [H_0 + H', \rho(t)]. \quad (1.32)$$

The condition required for the validity of the approach can then be written as the equality of the corresponding density matrices in the moment when the field is turned on (for simplicity, this moment is labeled as $t = 0$):

$$\rho(0) = \rho_{E=0} \quad (1.33)$$

Since the interaction with the applied field is weak, the new density operator will not differ much from the initial one. Thus if it is written:

$$\rho(t) = \rho(0) + f(t), \quad (1.34)$$

operator $f(t)$ will be a perturbation. Rewriting the differential equation for density operator as an equation for f and taking only terms that are at most the first order in f and H' , gives:

$$i\hbar \frac{df(t)}{dt} = [H_0, f(t)] + [H'(t), \rho(0)], \quad (1.35)$$

which is equivalent to⁵:

$$i\hbar \frac{d}{dt} \left(e^{i\frac{H_0}{\hbar}t} f(t) e^{-i\frac{H_0}{\hbar}t} \right) = [H'_I(t), \rho(0)], \quad (1.36)$$

⁴In the case considered, this would be the full lattice Fröhlich Hamiltonian.

⁵The equilibrium statistical operator commutes with H_0 .

where H'_I is the H' in the interaction picture with regards to the H_0 as the free Hamiltonian. Integrating with initial condition $f(0) = 0$ and keeping only terms linear in H'_I gives:

$$f(t) = \frac{1}{i\hbar} e^{-i\frac{H_0}{\hbar}t} \int_0^t dt' [H'_I(t'), \rho(0)] e^{i\frac{H_0}{\hbar}t'} \quad (1.37)$$

The response of interest is the electric current. The current operator is given by[13]:

$$\mathbf{j}(\mathbf{r}) = \frac{q}{2m} \sum_n \left(\mathbf{p}_n \delta(\mathbf{r} - \mathbf{r}_n) + \delta(\mathbf{r} - \mathbf{r}_n) \mathbf{p}_n \right), \quad (1.38)$$

where \mathbf{p}_n is the momentum operator of carrier n with mass m .

Let it be supposed, for the sake of simplicity, that the applied electric field is in fixed direction labeled by b . The component of current density measured in direction a can be found by averaging the current operator with respect to the density matrix:

$$J^a(\mathbf{r}, t) = \text{Tr} \left(\rho(t) j^a(\mathbf{r}) \right). \quad (1.39)$$

Using the integral equation derived for $f(t)$, the cyclic property of trace, and defining $\mathbf{j}(\mathbf{r}, t) = e^{i\frac{H_0}{\hbar}t} \mathbf{j}(\mathbf{r}) e^{-i\frac{H_0}{\hbar}t}$, gives:

$$J^a(\mathbf{r}, t) = \text{Tr} \left(\rho(0) j^a(\mathbf{r}) \right) + \frac{1}{i\hbar} \int_0^t dt' \text{Tr} \left(\rho(0) [j^a(\mathbf{r}, t), H'_I(t')] \right) \quad (1.40)$$

The first part is zero because no net current can be present in an equilibrium state.

In order to get the current measured macroscopically, average over the volume of the system should be taken. In writing the H' , it was already assumed that the electric field is homogeneous throughout this volume.

$$J^a(t) = \frac{1}{V} \int d^3\mathbf{r} J^a(\mathbf{r}, t) = -\frac{1}{i\hbar V} \int_0^t dt' \text{Tr} \left(\rho(0) [j^a(t), d^b(t')] \right) E^b(t'), \quad (1.41)$$

where the operator $j^a(t)$ is given by:

$$j^a(t) = \frac{q}{m} \sum_n p_n^a. \quad (1.42)$$

Comparing with the definition of the conductivity tensor:

$$J^a(t) = \sum_b \int_0^t dt \sigma^{ab}(t, t') E^b(t'), \quad (1.43)$$

the following is obtained:

$$\sigma^{ab}(t, t') = -\frac{1}{i\hbar V} \text{Tr} \left(\rho(0) [j^a(t), d^b(t')] \right). \quad (1.44)$$

Using the cyclic property of trace and the form of $\rho(0)$, it can be shown that:

$$\sigma^{ab}(t, t') = \sigma^{ab}(t - t') = -\frac{1}{i\hbar V} \text{Tr} \left(\rho(0) [j^a(t - t'), d^b(0)] \right). \quad (1.45)$$

Thus, the regime in question does not have time dispersion and the optical conductivity tensor is well defined.

$$\sigma^{ab}(\omega) = \int_0^\infty dt e^{i\omega t} \sigma^{ab}(t) = -\frac{1}{i\hbar V} \int_0^\infty dt e^{i\omega t} \text{Tr} \left(\rho(0) [j^a(t), d^b(0)] \right) \quad (1.46)$$

The integrals above are to be calculated with $\omega = \omega + i\eta$, $\eta \rightarrow 0$, which corresponds to turning the electric field at $t = 0$.

To proceed further, the dipole moment operator can be related to the current operator by the equation:

$$\frac{d[d^b(t)]}{dt} = j^b(t), \quad (1.47)$$

which is a direct consequence of the continuity equation for the electric charge [6]. Integration gives:

$$d^b(0) = d^b(t) - \int_0^t dt' j^b(t'). \quad (1.48)$$

The equal-time commutation relation is also valid:

$$[j^a(t), d^b(t)] = -i\hbar \frac{N_c q^2}{m} \delta_{ab}, \quad (1.49)$$

where N_c is the total number of carriers. Using the last two expressions combined with (1.46) gives:

$$\begin{aligned} \sigma^{ab}(\omega) &= i \frac{n_c q^2}{m\omega} \delta_{ab} + \frac{1}{i\hbar V} \int_0^\infty dt e^{i\omega t} \int_0^t dt' \text{Tr} \left(\rho(0) [j^a(t - t'), j^b(0)] \right) \\ &= i \frac{n_c q^2}{m\omega} \delta_{ab} + \lim_{\eta \rightarrow 0} \frac{1}{i\hbar V} \int_0^\infty dt' \text{Tr} \left(\rho(0) [j^a(t'), j^b(0)] \right) \int_{t'}^\infty dt e^{i(\omega + i\eta)t} \\ &= i \frac{n_c q^2}{m\omega} \delta_{ab} + \frac{1}{\hbar\omega V} \int_0^\infty dt e^{i\omega t} \text{Tr} \left(\rho(0) [j^a(t), j^b(0)] \right) \end{aligned} \quad (1.50)$$

The last expression is known as one of the forms of Kubo formula for optical conductivity. Electrical conductivity can be obtained from it by taking the real part and then letting $\omega \rightarrow 0$. However, a more suitable form of the Kubo formula in which current-current commutators are replaced by correlators, will be used for calculations.

In order to derive the alternative form of Kubo formula, the real part of expression (1.50) is taken and then expanded in the eigenstate basis of H_0 :

$$\begin{aligned} \text{Re } \sigma^{ab}(\omega) = \text{Re} \lim_{\eta \rightarrow 0} \frac{1}{\hbar\omega V} \int_0^\infty dt e^{i(\omega+i\eta)t} \sum_{m,n} \left(\frac{e^{-\beta(E_n - \mu N_n)}}{\text{Tr } e^{-\beta(H_0 - \mu N)}} - \frac{e^{-\beta(E_m - \mu N_n)}}{\text{Tr } e^{-\beta(H_0 - \mu N)}} \right) \\ \cdot e^{-i\frac{E_m - E_n}{\hbar}t} \langle n | j^a(0) | m \rangle \langle m | j^b(0) | n \rangle, \end{aligned} \quad (1.51)$$

where E_m and E_n are energies of corresponding eigenstates. It is taken into account in the expression above that the current operators conserve carrier number. After doing the time integration, the expression becomes:

$$\begin{aligned} \text{Re } \sigma^{ab}(\omega) = \frac{\pi}{\hbar\omega V} \sum_{m,n} \left(\frac{e^{-\beta(E_n - \mu N_n)}}{\text{Tr } e^{-\beta(H_0 - \mu N)}} - \frac{e^{-\beta(E_m - \mu N_n)}}{\text{Tr } e^{-\beta(H_0 - \mu N)}} \right) \langle n | j^a(0) | m \rangle \\ \cdot \langle m | j^b(0) | n \rangle \delta\left(\omega - \frac{E_m - E_n}{\hbar}\right) = \frac{1}{2\hbar\omega V} \sum_{m,n} \left(\frac{e^{-\beta(E_n - \mu N_n)}}{\text{Tr } e^{-\beta(H_0 - \mu N)}} - \frac{e^{-\beta(E_n + \hbar\omega - \mu N_n)}}{\text{Tr } e^{-\beta(H_0 - \mu N)}} \right) \\ \cdot \int_{-\infty}^\infty dt \langle n | j^a(0) | m \rangle \langle m | j^b(0) | n \rangle e^{i\left(\omega - \frac{E_m - E_n}{\hbar}\right)t} \\ = \frac{1 - e^{-\beta\hbar\omega}}{2\hbar\omega V} \sum_n \int_{-\infty}^\infty dt e^{i\omega t} \frac{e^{-\beta(E_n - \mu N_n)}}{\text{Tr } e^{-\beta(H_0 - \mu N)}} \langle n | j^a(t) j^b(0) | n \rangle. \end{aligned} \quad (1.52)$$

Finally, the Kubo formula is rewritten in terms of current correlations:

$$\text{Re } \sigma^{ab}(\omega) = \frac{1 - e^{-\beta\hbar\omega}}{2\hbar\omega V} \int_{-\infty}^\infty dt e^{i\omega t} \langle j^a(t) j^b(0) \rangle, \quad (1.53)$$

where the average on the right denotes thermodynamic average with respect to H_0 . From (1.53) it is not clear whether the expression on the right is indeed real. However, this can easily be shown by expanding the operator average into the averages of the hermitian and the antihermitian part, which are themselves odd and even functions of time.

If the mobility is being calculated, DC limit ($\omega \rightarrow 0$) must be taken and the expression divided by the carrier concentration and charge:

$$\mu^{ab} = \frac{\beta}{2N_c q} \int_{-\infty}^\infty dt e^{i\omega t} \langle j^a(t) j^b(0) \rangle. \quad (1.54)$$

This formula will be the starting point for polaron mobility calculations.

1.5 Overview of the Thesis

The properties of the lattice Fröhlich models will be investigated in the thesis, with the ultimate goal of calculating its mobilities in a wide temperature and coupling strength range. In order for the calculation based on perturbative techniques to be made possible, a suitable canonical transformation will be applied as described in chapter 2. The transformation is tailored in such a way that after its application, interacting part of the Hamiltonian is small. This is possible in a wide temperature and coupling strength range because of the variational character of the transformation. In chapter 2, equations for the variational parameters will be derived and numerical results for free particle properties will be presented.

After the canonical transformation is applied, calculation of the polaronic spectral properties can be done by standard techniques described in section 1.3. The calculations will be presented in chapter 3. They will ultimately lead to a self-consistent equation for the polaronic self-energy which must be solved numerically.

However, the starting point of chapter 3 will be the Kubo formula derived in section 1.3. It will be shown that, under certain assumptions, the formula can be transformed to an expression that is determined by the knowledge of polaronic spectral functions. This expression will be used for numerical calculation of polaron mobility. In order to check the validity of these calculations as well as to provide the mobility estimates in the parameter ranges in which numerics is too costly, the limiting cases will be investigated in chapter 4. The limits in which relatively simple expressions for the mobility can be derived are weak coupling/low temperature and strong coupling/high temperature limits.

Finally, numerical results for the polaron mobility and spectral properties in the 1D model will be presented in chapter 5. The comparisons will be made with the appropriate limiting cases. The analyses will show the differences and similarities between different Hamiltonians in the class investigated. Chapter 6 will include a brief conclusion of the thesis.

Chapter 2

Variational Lang-Firsov Unitary Transformation

The subject of this chapter is the unitary transformation that will enable mobility calculations with standard perturbation techniques. The transformation applied is a variant of the Lang-Firsov transformation that is usually used for the Holstein polaron in the strong coupling limit, the difference being that the applied transformation is variational. The variational nature of the transformation makes it suitable for describing various coupling regimes. The equations for the corresponding variational parameters will be derived using Gibbs-Bogolyubov bound. At the end of the chapter, numerical solutions for the 1D model of interest will be presented.

2.1 Lang-Firsov Unitary Transformation

The transformation that will be applied on the lattice Fröhlich Hamiltonian (1.10) is an extension of the Lang-Firsov unitary transformation¹, which has the form:

$$H' = e^{-S} H e^S, \quad S = \frac{1}{\sqrt{N}} \sum_{\mathbf{m}, \mathbf{n}} \sum_{\mathbf{q}} f_{\mathbf{m}-\mathbf{n}} c_{\mathbf{n}}^\dagger c_{\mathbf{n}} (b_{\mathbf{q}}^\dagger - b_{-\mathbf{q}}) e^{i\mathbf{q}\mathbf{m}} \quad (2.1)$$

Lang-Firsov transformation is traditionally used for the description of the strong-coupling regime of the Holstein polaron. When the kinetic part of the Hamiltonian is negligible in comparison with electron-phonon interaction ($t_{\mathbf{n}} \rightarrow 0$), Lang-Firsov transformation exactly diagonalizes Holstein Hamiltonian [7]. The transformation is successful because it couples electron to phononic cloud, thus taking the electronic states to the polaronic ones [14]. However, the same picture is valid not only for Hol-

¹Also known as Merrifield's transformation [14].

stein Hamiltonian. Lang-Firsov transformation diagonalizes the whole lattice Fröhlich class of Hamiltonians in the strong coupling limit.

On the other hand, if the weak coupling limit is to be described, no unitary transformation is needed since the perturbation techniques are directly applicable. One way to include this fact in the transformation that aims to describe polarons in various coupling regimes is to make a Lang-Firsov transformation dependent on a set of variational parameters ($D_{\mathbf{m}-\mathbf{n}}$), so that it takes the form:

$$S = \frac{1}{\sqrt{N}} \sum_{\mathbf{m}, \mathbf{n}} \sum_{\mathbf{q}} D_{\mathbf{m}-\mathbf{n}} c_{\mathbf{n}}^{\dagger} c_{\mathbf{n}} (b_{\mathbf{q}}^{\dagger} - b_{-\mathbf{q}}) e^{i\mathbf{q}\mathbf{m}}. \quad (2.2)$$

It would be expected that after the optimization of the free energy², parameters $D_{\mathbf{m}-\mathbf{n}}$ will take the values $f_{\mathbf{m}-\mathbf{n}}$ in the strong-coupling limit, thus exactly diagonalizing the Hamiltonian. In the opposite limit, they would go to zero, so the unitary transformation will be close to unity. The variational parameters describe the degree to which the electron is dressed by its polaronic cloud. With both the weak and the strong limits being covered by the same transformation, it can be expected that the transformation will transfer a major part of the electron-phonon interaction to the diagonal part of the transformed Hamiltonian for intermediate coupling as well [14].

The following notation will be introduced:

$$\begin{aligned} f_{\mathbf{q}} &= \frac{1}{\sqrt{N}} \sum_{\mathbf{m}} f_{\mathbf{m}} e^{i\mathbf{q}\mathbf{m}}, & D_{\mathbf{q}} &= \frac{1}{\sqrt{N}} \sum_{\mathbf{m}} D_{\mathbf{m}} e^{i\mathbf{q}\mathbf{m}} \\ c_{\mathbf{m}} &= \frac{1}{\sqrt{N}} \sum_{\mathbf{k}} c_{\mathbf{k}} e^{-i\mathbf{k}\mathbf{m}}, & \theta_{\mathbf{m}} &= e^{\sum_{\mathbf{q}} D_{\mathbf{q}} (b_{\mathbf{q}}^{\dagger} - b_{-\mathbf{q}}) e^{i\mathbf{q}\mathbf{m}}}. \end{aligned} \quad (2.3)$$

Fourier coefficients of the electron-phonon interaction must satisfy the hermiticity condition, $f_{\mathbf{q}} = f_{-\mathbf{q}}^*$. Similarly, $D_{\mathbf{q}} = D_{-\mathbf{q}}^*$ holds for the variational parameters as the unitarity condition. For convenience, it will be taken that the Bravais lattice corresponding to the crystal lattice in question has inversion symmetry, and thus $f_{\mathbf{q}} = f_{-\mathbf{q}}$. Then, optimal variational parameters will also incorporate this symmetry, $D_{\mathbf{q}} = D_{-\mathbf{q}}$. Direct consequence is that both $f_{\mathbf{q}}$ and $D_{\mathbf{q}}$ are real. Also, by definition, $\theta_{\mathbf{m}}^{\dagger} \theta_{\mathbf{m}} = I$.

Electronic and phononic operators are transformed with the help of the Baker-Campbell-Hausdorff formula:

$$e^A B e^{-A} = B + [A, B] + \frac{1}{2!} [A, [A, B]] + \frac{1}{3!} [A, [A, [A, B]]] + \dots \quad (2.4)$$

²Extension from the ground state energy that is optimized in the zero temperature case.

and standard commutation relations. The result is:

$$\begin{aligned} c_{\mathbf{m}} &\rightarrow e^{-S} c_{\mathbf{m}} e^S = \theta_{\mathbf{m}} c_{\mathbf{m}} \\ b_{\mathbf{q}} &\rightarrow e^{-S} b_{\mathbf{q}} e^S = b_{\mathbf{q}} + \sum_{\mathbf{k}} D_{\mathbf{q}} c_{\mathbf{k}-\mathbf{q}}^{\dagger} c_{\mathbf{k}} \end{aligned} \quad (2.5)$$

The transformed Hamiltonian is then:

$$\begin{aligned} H' &= H'_e + H'_{ph} + H'_{e-ph} \\ H'_e &= - \sum_{\mathbf{k}_1, \mathbf{k}_2} \sum_{\mathbf{m}, \mathbf{n}} \left(\frac{1}{N} t_{\mathbf{m}\mathbf{n}} \theta_{\mathbf{m}}^{\dagger} \theta_{\mathbf{n}} e^{i(\mathbf{k}_1 \mathbf{m} - \mathbf{k}_2 \mathbf{n})} \right) c_{\mathbf{k}_1}^{\dagger} c_{\mathbf{k}_2} \\ H'_{ph} &= \sum_{\mathbf{q}} \hbar \omega_{\mathbf{q}} b_{\mathbf{q}}^{\dagger} b_{\mathbf{q}} + \sum_{\mathbf{k}, \mathbf{q}} \hbar \omega_{\mathbf{q}} D_{\mathbf{q}} c_{\mathbf{k}-\mathbf{q}}^{\dagger} c_{\mathbf{k}} (b_{\mathbf{q}}^{\dagger} + b_{-\mathbf{q}}) + \sum_{\mathbf{k}, \mathbf{q}} \hbar \omega_{\mathbf{q}} D_{\mathbf{q}}^2 c_{\mathbf{k}}^{\dagger} c_{\mathbf{k}} \\ &\quad - \sum_{\mathbf{q}, \mathbf{k}, \mathbf{k}'} \hbar \omega_{\mathbf{q}} D_{\mathbf{q}}^2 c_{\mathbf{k}+\mathbf{q}}^{\dagger} c_{\mathbf{k}'-\mathbf{q}}^{\dagger} c_{\mathbf{k}} c_{\mathbf{k}'} \\ H'_{e-ph} &= - \sum_{\mathbf{k}, \mathbf{q}} \hbar \omega_{\mathbf{q}} f_{\mathbf{q}} c_{\mathbf{k}-\mathbf{q}}^{\dagger} c_{\mathbf{k}} (b_{\mathbf{q}}^{\dagger} + b_{-\mathbf{q}}) - 2 \sum_{\mathbf{k}, \mathbf{q}} f_{\mathbf{q}} D_{\mathbf{q}} c_{\mathbf{k}}^{\dagger} c_{\mathbf{k}} \\ &\quad + 2 \sum_{\mathbf{q}, \mathbf{k}, \mathbf{k}'} \hbar \omega_{\mathbf{q}} f_{\mathbf{q}} D_{\mathbf{q}} c_{\mathbf{k}-\mathbf{q}}^{\dagger} c_{\mathbf{k}'+\mathbf{q}}^{\dagger} c_{\mathbf{k}} c_{\mathbf{k}'} \end{aligned} \quad (2.6)$$

The last terms in expressions for H'_{ph} and H'_{e-ph} are two-particle interactions. Polaronic properties are important for materials where electronic concentration in the conduction band is small (semiconductors, ionic solids), so they are usually described in a single-electron model [15]. The same will be done in this thesis. As a consequence, the aforementioned terms are exactly zero in the Hilbert space spanned by the single-electron (or single-polaron) states. Alternatively, it could have been explicitly stated when Hamiltonian was initially written that it corresponds to a single electron system³. In that case, the transformed Hamiltonian would have to be projected to the single-electron subspace. The final result would be the same, two-particle terms would vanish.

In order to separate the diagonal part of the H'_e , the following identity will be used:

$$\theta_{\mathbf{m}}^{\dagger} \theta_{\mathbf{n}} = (\theta_{\mathbf{m}}^{\dagger} \theta_{\mathbf{n}} - \langle \theta_{\mathbf{m}}^{\dagger} \theta_{\mathbf{n}} \rangle_0) + \langle \theta_{\mathbf{m}}^{\dagger} \theta_{\mathbf{n}} \rangle_0, \quad (2.7)$$

where $\langle \dots \rangle_0$ denotes phononic thermodynamic average over the free phononic part of the Hamiltonian. The average can be calculated using the commutator $[b_{\mathbf{q}} - b_{-\mathbf{q}}^{\dagger}, b_{\mathbf{q}'}^{\dagger} - b_{-\mathbf{q}'}] = 0$:

$$\begin{aligned} \langle \theta_{\mathbf{m}}^{\dagger} \theta_{\mathbf{n}} \rangle_0 &= \left\langle e^{\sum_{\mathbf{q}} D_{\mathbf{q}} (b_{\mathbf{q}} - b_{-\mathbf{q}}^{\dagger}) e^{-i\mathbf{q}\mathbf{m}}} e^{\sum_{\mathbf{q}'} D_{\mathbf{q}'} (b_{\mathbf{q}'}^{\dagger} - b_{-\mathbf{q}'}') e^{i\mathbf{q}'\mathbf{n}}} \right\rangle_0 \\ &= \prod_{\mathbf{q}} \left\langle e^{D_{\mathbf{q}} [b_{\mathbf{q}}^{\dagger} (e^{i\mathbf{q}\mathbf{n}} - e^{i\mathbf{q}\mathbf{m}}) - b_{\mathbf{q}} (e^{-i\mathbf{q}\mathbf{n}} - e^{-i\mathbf{q}\mathbf{m}})]} \right\rangle_0 \\ &= e^{-\frac{1}{2} \sum_{\mathbf{q}} D_{\mathbf{q}}^2 |e^{i\mathbf{q}\mathbf{n}} - e^{i\mathbf{q}\mathbf{m}}|^2 (2n_{\mathbf{q}} + 1)}. \end{aligned} \quad (2.8)$$

³Fröhlich Hamiltonian, as written in 1.1, clearly describes single-electron system.

Additionally, for the last step, average $\langle e^{\mu b^\dagger + \nu b} \rangle_0 = e^{\frac{1}{2}(2n+1)\mu\nu}$ is used. It can be proven by carefully expanding the exponential and averaging term by term, as shown in appendix A.

Using the consequence of translation symmetry, $t_{\mathbf{m}\mathbf{n}} = t_{\mathbf{m}-\mathbf{n}}$, inversion symmetry, and redefining the energy reference point so that $t_0 = 0$, the diagonal part of H'_e becomes:

$$\frac{1}{N} \sum_{\mathbf{m}, \mathbf{n}} t_{\mathbf{m}\mathbf{n}} e^{i(\mathbf{k}_1 \mathbf{m} - \mathbf{k}_2 \mathbf{n})} \langle \theta_{\mathbf{m}}^\dagger \theta_{\mathbf{n}} \rangle_0 = \delta_{\mathbf{k}_1, \mathbf{k}_2} \sum_{\mathbf{R}^+} 2t_{\mathbf{R}} \cos(\mathbf{k}_1 \mathbf{R}) e^{-\sum_{\mathbf{q}} D_{\mathbf{q}}^2 (1 - \cos \mathbf{q} \mathbf{R}) (2n_{\mathbf{q}} + 1)}. \quad (2.9)$$

R^+ denotes one half of the crystal sites (the other half are inversion images of the selected ones).

Transformed Hamiltonian becomes:

$$\begin{aligned} H' &= H_0 + V_1 + V_2 \\ H_0 &= \sum_{\mathbf{k}} c_{\mathbf{k}}^\dagger c_{\mathbf{k}} \left[\sum_{\mathbf{R}^+} -2t_{\mathbf{R}} \cos(\mathbf{k} \mathbf{R}) e^{-\sum_{\mathbf{q}} D_{\mathbf{q}}^2 (1 - \cos \mathbf{q} \mathbf{R}) (2n_{\mathbf{q}} + 1)} \right. \\ &\quad \left. + \sum_{\mathbf{q}} \hbar \omega_{\mathbf{q}} (D_{\mathbf{q}}^2 - 2f_{\mathbf{q}} D_{\mathbf{q}}) \right] + \sum_{\mathbf{q}} \hbar \omega_{\mathbf{q}} b_{\mathbf{q}}^\dagger b_{\mathbf{q}} \\ V_1 &= - \sum_{\mathbf{k}, \mathbf{q}} \hbar \omega_{\mathbf{q}} (f_{\mathbf{q}} - D_{\mathbf{q}}) c_{\mathbf{k}-\mathbf{q}}^\dagger c_{\mathbf{k}} (b_{\mathbf{q}}^\dagger + b_{-\mathbf{q}}) \\ V_2 &= - \sum_{\mathbf{k}_1, \mathbf{k}_2} \left[\frac{1}{N} \sum_{\mathbf{m}, \mathbf{n}} t_{\mathbf{m}-\mathbf{n}} (\theta_{\mathbf{m}}^\dagger \theta_{\mathbf{n}} - \langle \theta_{\mathbf{m}}^\dagger \theta_{\mathbf{n}} \rangle_0) e^{i(\mathbf{k}_1 \mathbf{m} - \mathbf{k}_2 \mathbf{n})} \right] c_{\mathbf{k}_1}^\dagger c_{\mathbf{k}_2} \end{aligned} \quad (2.10)$$

2.2 Gibbs-Bogolyubov Bound and Equations for Variational Parameters

In order to find the equations for variational parameters, Gibbs-Bogolyubov theorem will be used. The theorem provides an upper bound for the free energy of the system. Free energy is the relevant quantity to optimize, since the mean number of phonons, and thus the effect of electron-phonon interaction, depend strongly on temperature. The theorem itself states that the following inequality is valid for two bound, hermitian operators (Hamiltonians), H and H_0 :

$$F(H) = -\frac{1}{\beta} \ln \text{Tr}(e^{-\beta H}) \leq -\frac{1}{\beta} \ln \text{Tr}(e^{-\beta H_0}) + \langle H - H_0 \rangle_{H_0}. \quad (2.11)$$

The importance of the inequality is that it can be employed to give an upper bound on the system's free energy only by calculating the averages over the non-interacting part of the Hamiltonian. This bound can then be used as a functional which can be optimized to provide variational parameters. In the case considered, the Hamiltonian

is already conveniently separated for the use of Gibbs-Bogolyubov inequality:

$$F(\mathbf{D}) = -\frac{1}{\beta} \ln \text{Tr}(e^{-\beta H(\mathbf{D})}) \leq -\frac{1}{\beta} \ln \text{Tr}(e^{-\beta H_0(\mathbf{D})}) + \langle V_1 + V_2 \rangle_{H_0(\mathbf{D})} \quad (2.12)$$

Thermodynamic averages over phononic degrees of freedom give $\langle V_1 + V_2 \rangle_{H_0(\mathbf{D})} = 0$, so that the free-energy functional that will be used for optimization is:

$$\mathcal{F}(\mathbf{D}) = -\frac{1}{\beta} \ln \text{Tr}(e^{-\beta H_0(\mathbf{D})}). \quad (2.13)$$

Calculating the trace of the diagonal Hamiltonian is straightforward. In the following expressions for $\mathcal{F}(\mathbf{D})$, phononic part of the trace will be omitted since it does not depend on the variational coefficients. The expression for polaronic part is:

$$\begin{aligned} \mathcal{F}^{pl}(\mathbf{D}) &= -\frac{1}{\beta} \ln \sum_{\mathbf{k}} e^{-\beta E_{\mathbf{k}}}, \\ E_{\mathbf{k}} &= -\sum_{\mathbf{R}^+} J_{\mathbf{R}}(\mathbf{D}) \cos \mathbf{kR} + \sum_{\mathbf{q}} \hbar \omega_{\mathbf{q}} (D_{\mathbf{q}}^2 - 2f_{\mathbf{q}} D_{\mathbf{q}}), \\ J_{\mathbf{R}}(\mathbf{D}) &= 2t_{\mathbf{R}} e^{-\sum_{\mathbf{q}} D_{\mathbf{q}}^2 (1 - \cos \mathbf{qR}) (2n_{\mathbf{q}} + 1)}. \end{aligned} \quad (2.14)$$

$E_{\mathbf{k}}$ is the polaron band dispersion or renormalized electron band dispersion. From the last equation it can be deduced that the electron-phonon interaction, besides binding the electron (overall energy shift)⁴, also narrows the band.

Transforming the \mathbf{k} -sum into an integral over the first Brillouine zone gives:

$$\mathcal{F}^{pl}(\mathbf{D}) = \sum_{\mathbf{q}} \hbar \omega_{\mathbf{q}} (D_{\mathbf{q}}^2 - 2f_{\mathbf{q}} D_{\mathbf{q}}) - \frac{1}{\beta} \ln \left[\frac{V}{(2\pi)^3} \int_{FBZ} d^3 \mathbf{k} e^{\beta \sum_{\mathbf{R}^+} J_{\mathbf{R}}(\mathbf{D}) \cos \mathbf{kR}} \right]. \quad (2.15)$$

For convenience, further calculations will be done for cubic lattice with nearest neighbour hopping only. The integral is in this case expressible through modified Bessel functions:

$$\mathcal{F}^{pl}(\mathbf{D}) = \sum_{\mathbf{q}} \hbar \omega_{\mathbf{q}} (D_{\mathbf{q}}^2 - 2f_{\mathbf{q}} D_{\mathbf{q}}) - \frac{1}{\beta} \ln (I_0(\beta J_{\mathbf{C}_x}) I_0(\beta J_{\mathbf{C}_y}) I_0(\beta J_{\mathbf{C}_z})), \quad (2.16)$$

where \mathbf{C}_x , \mathbf{C}_y and \mathbf{C}_z are lattice vectors of tree nearest neighbors in positive directions of x , y and z axes, respectively. Cubic symmetry is manifested as:

$$J_{\mathbf{C}_x}(\mathbf{D}) = J_{\mathbf{C}_y}(\mathbf{D}) = J_{\mathbf{C}_z}(\mathbf{D}) = J_{\mathbf{C}}(\mathbf{D}). \quad (2.17)$$

⁴Note that the binding energy in the strong-coupling limit will go to $\sum_{\mathbf{q}} f_{\mathbf{q}}^2$, which is the result used for the redefinition of coupling constants in chapter 1.2.

Optimization of the free energy functional $\frac{\delta \mathcal{F}^{pl}(\mathbf{D})}{\delta D_{\mathbf{q}}} = 0$, gives equations for variational parameters:

$$D_{\mathbf{q}} = \frac{f_{\mathbf{q}}}{1 + \frac{I_1(\beta J_{\mathbf{C}}(\mathbf{D}))}{I_0(\beta J_{\mathbf{C}}(\mathbf{D}))} \frac{J_{\mathbf{C}}(\mathbf{D})}{\omega_{\mathbf{q}}} \coth \frac{\beta \omega_{\mathbf{q}}}{2} \sum_{i=x,y,z} (1 - \cos \mathbf{q} \mathbf{C}_i)}. \quad (2.18)$$

All parameters are completely determined by renormalized bandwidth, $J_{\mathbf{C}}(\mathbf{D})$, so instead of solving the system of equations, one self-consistent equation for $J_{\mathbf{C}}(\mathbf{D})$ can be solved. The equation is found by combining (2.14) and (2.18):

$$J_{\mathbf{C}}(\mathbf{D}) = 2t_{\mathbf{C}} e^{-\sum_{\mathbf{q}} \left[\frac{f_{\mathbf{q}}}{1 + \frac{I_1(\beta J_{\mathbf{C}}(\mathbf{D}))}{I_0(\beta J_{\mathbf{C}}(\mathbf{D}))} \frac{J_{\mathbf{C}}(\mathbf{D})}{\omega_{\mathbf{q}}} \coth \frac{\beta \omega_{\mathbf{q}}}{2} \sum_{i=x,y,z} (1 - \cos \mathbf{q} \mathbf{C}_i)} \right]^2 \coth \frac{\beta \omega_{\mathbf{q}}}{2} (1 - \cos \mathbf{q} \mathbf{C}_x)}. \quad (2.19)$$

Thus, optimal variational parameters are found starting from the Gibbs-Bogolyubov inequality. It is easy to see that for the weak interaction, when $f_{\mathbf{q}} \rightarrow 0$, also $D_{\mathbf{q}} \rightarrow 0$, so that the unitary transformation is close to unity. For the strong interaction, $J_{\mathbf{C}}(\mathbf{D}) \rightarrow 0$, implying $D_{\mathbf{q}} \rightarrow f_{\mathbf{q}}$, which corresponds to the usual Lang-Firsov transformation. These results were expected when the transformation was tailored and they demonstrate the adequacy of the transformation in the weak and strong coupling limits. In the intermediate regime, it is expected that transformation, as optimized, makes the non-diagonal part of the Hamiltonian small. Thus, the case is set for the application of perturbation techniques. Before that, numerical results for the variational coefficients in 1D model will be given.

2.3 Numerical Solution for the Variational Parameters in 1D Model

All numerical calculations are done for the 1D lattice model discussed in 1.2⁵:

$$H = - \sum_{\mathbf{m}} t_{\mathbf{C}} c_{\mathbf{m}+\mathbf{C}}^{\dagger} c_{\mathbf{m}} - \sum_{\mathbf{m}} t_{\mathbf{C}} c_{\mathbf{m}-\mathbf{C}}^{\dagger} c_{\mathbf{m}} + \sum_{\mathbf{q}} \hbar \omega_{\mathbf{q}} b_{\mathbf{q}}^{\dagger} b_{\mathbf{q}} - \sum_{\mathbf{m}, \mathbf{n}} \hbar \omega_0 f_{\mathbf{m}-\mathbf{n}} c_{\mathbf{n}}^{\dagger} c_{\mathbf{n}} (b_{\mathbf{m}}^{\dagger} + b_{\mathbf{m}}),$$

$$f_{\mathbf{m}-\mathbf{n}} = \alpha \cos \psi \delta_{\mathbf{m}, \mathbf{n}} + \frac{\alpha C^2 \sin \psi}{\sqrt{\kappa} |\mathbf{m} - \mathbf{n}|^2} (1 - \delta_{\mathbf{m}, \mathbf{n}}) \quad (2.20)$$

The parameters of the model are transfer integral $t_{\mathbf{C}}$ ⁶, temperature, overall coupling strength α and constant ψ that determines the nature of Hamiltonian (electron-phonon interaction range).

⁵Nearest neighbor only TBA is used for the electronic part of the Hamiltonian.

⁶From this point on, all the energies quoted for numerical results will be given in units of $\hbar \omega_0$ and momenta in units of $\frac{1}{C}$, where C is the lattice constant.

When solving equation (2.19), two distinct cases emerge. The first case is what will be called transition case and the second is transition-less case. In the transition-less case for all values of temperature and coupling constant, a single solution exists. The values of renormalized bandwidth and free-energy functional vary smoothly in the whole parameter range. In the transition case, there are two solutions of the equation (2.19). One of the solutions exists only for relatively weak interaction strength, and the other for relatively strong. They coexist in a certain range of intermediate coupling strengths. The right solution is chosen such that it gives lower value of the free-energy functional. As a consequence, free-energy functional and renormalized bandwidth do not vary smoothly. Typical free-energy functional dependence on coupling strength in both cases is shown in figure 2.1.

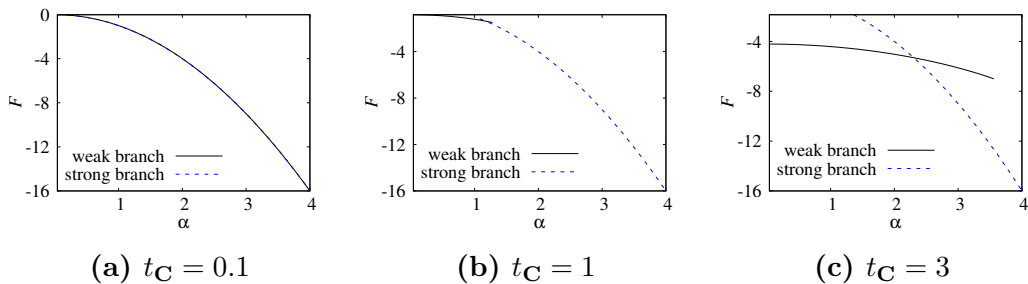


Figure 2.1: Dependence of the free-energy functional on coupling strength for different values of transfer integrals. In graphs 2.1b and 2.1c two distinct branches exist and transition can be seen. All the examples are given for the Holstein model ($\psi = 0$) and fixed temperature ($k_B T = 1$).

It must be emphasized that this apparent "transition" is the consequence of the method used. It has been rigorously proven, after some debate, that the phononic Hamiltonians of the conituum Fröhlich-like type do not undergo phase transition [16]. This group does not include lattice models studied, but it is very plausible that the phase transition is absent for them as well. However, since the free-energy functional is only the upper bound to the real free energy of the system, the results that are obtained here do not imply the existence of the phase transition.

Transition being present or not, it is desirable that the transformation makes the residual part of the electron-phonon interaction sufficiently small. This is shown to be true for the Holstein Hamiltonian [14]. The ground state energy calculated by the variational method employed here was found to be within ten percent of the value found by the exact calculations even in the intermediate regime. There are no results to be used for comparisons with Hamiltonians other than Holstein, but the success of the method in the Holstein case does provide some reassurance. Renormalized band dispersion obtained ($E_{\mathbf{k}}$), however, is the rough first approximation to the real polaronic band dispersion. It will be clear how the band structure evolves from the one regime to the other after calculating polaronic spectral properties.

In figure 2.2, temperature and coupling strength dependence of the ratio of renormalized and unrenormalized bandwidth for several characteristic values of t_C and ψ are shown. Transition is seen as a sharp jump from the light yellow region to the dark region.

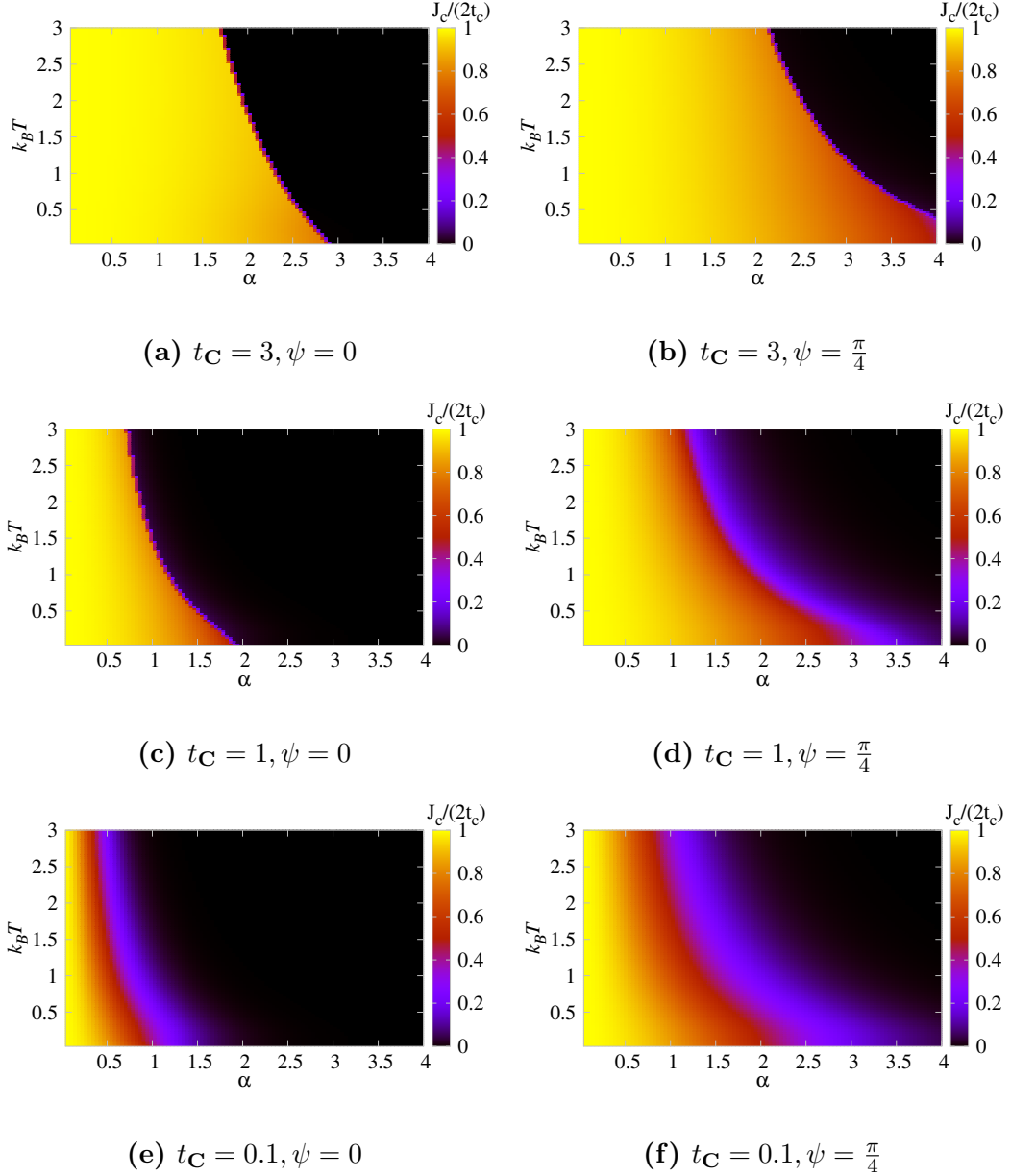


Figure 2.2: Dependence of bandwidth narrowing factor (renormalized bandwidth divided by the interaction-less bandwidth) on coupling strength and temperature. The dependence is shown for several values of transfer integral (interaction-less bandwidth) and two models - the Holstein model and the $\psi = \frac{\pi}{4}$ model.

The following can be deduced from the graphs shown and similar graphs for the unrepresented region of parameters. Transition-less case is universal for $t_{\mathbf{C}} < 1$, regardless of the nature of Hamiltonian (constant ψ) or temperature. Transition case exists for $t_{\mathbf{C}} > 1$, but the sharpness and even the existence of transition depend much on the temperature and the nature of Hamiltonian. For the Holstein model ($\psi = 0$), transition is very sharp for all temperatures. As the Hamiltonian is further from the Holstein one, transition is less and less sharp and even vanishes for lower temperatures. Coupling strengths and temperatures for which the transition occurs depend on the transfer integral ($t_{\mathbf{C}}$) as well as the nature of Hamiltonian. With increasing the transfer integral stronger coupling and higher temperatures are needed for transition. The same happens when increasing the range of interaction (increasing ψ).

Explanation for the absence of transition for $t_{\mathbf{C}} < 1$ may be implied by the free energy dependence on coupling constant in this regime (figure 2.1). The dependence resembles the strong coupling branch of the free energy in the case where the transition takes place. This suggests that the nature of the polaronic states in those two regions is similar. The similarity may be due to the both states being adiabatic in nature - when the polaron is localized (small renormalized bandwidth), phonons follow electronic motion adiabatically.

As for the dependence of the transition on the nature of the Hamiltonian, it may also be connected with the properties of strong coupling branch of polaronic state. If the electron is to be localized by the interaction with phonons, for the same overall strength of interaction, short-range interaction ($\psi \rightarrow 0$) will be more effective in the localization than the long range one. It may be expected that the long-range interaction will localized electron more gradually.

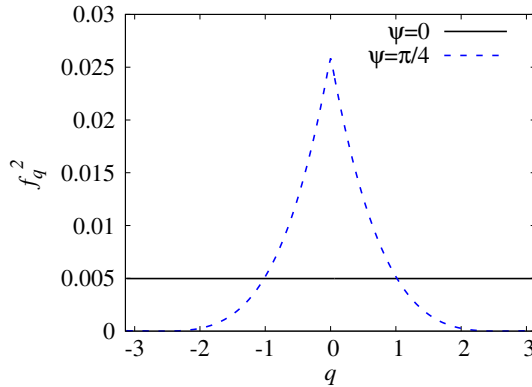


Figure 2.3: Square of interactions coefficients in the momentum space for Holstein and $\psi = \frac{\pi}{4}$ models. Coupling strength is set to $\alpha = 1$.

Temperature, transfer integral and interaction range dependence of coupling strength needed for transition to occur can also be analyzed. As for the dependence on trans-

fer integral, it is to be expected that the larger the electronic transfer between the neighboring sites, the stronger the electron-phonon interaction must be in order for localization to happen. Expression (2.14) can be used to analyse other dependencies. In the strong coupling regime $D_{\mathbf{q}} \rightarrow f_{\mathbf{q}}$, so the bandwidth decays exponentially with coupling strength. However, factor in the exponent, $\sum_{\mathbf{q}} f_{\mathbf{q}}^2 (1 - \cos \mathbf{q}\mathbf{R})(2n_{\mathbf{q}} + 1)$, is smaller for long-range interaction because of the different momentum dependence on interaction coefficients. This dependence is shown in figure 2.3 for the Holstein case and the case $\psi = \frac{\pi}{4}$. Longer range interaction is the strongest for small momenta, however, the factor $1 - \cos \mathbf{q}\mathbf{R}$ suppresses the localization by the small momentum part of the interaction. From (2.14) it can also be seen that the higher temperature (higher average number of phonons in the system) has the similar effect as the higher interaction strength.

Of particular importance is the fact that the long-range electron-phonon interaction suppresses the transition to narrow band region. Not only that, but even when the small bandwidth region is reached, exponential decrease of the bandwidth is milder than in the Holstein case. The results equivalent to these were found in Quantum Monte-Carlo calculations for a different 1D lattice polaron Hamiltonian class [17]. They are considered to open the possibility for a relatively high mobility of lattice polarons, especially in the adiabatic region and when compared to Holstein estimates. This will be explored in the chapters that follow.

Chapter 3

Approximate Solutions for Kubo Formula and Spectral Properties of Lattice Fröhlich Polaron

In this chapter, the explicit expression for the mobility of the polaron in the models investigated will be derived starting from Kubo formula. The Kubo formula will be solved approximately with the assumption that the interaction part of the Hamiltonian is small after the unitary transformation applied in chapter 2. The expression given will contain polaronic spectral functions. In order to obtain them, corresponding Matsubara Green's functions will be found via standard Dyson expansion. Analytic continuation will then give the needed retarded Green's functions and thus provide the recipe for the calculation of polaronic spectra and mobility.

3.1 Approximate Solution to Kubo Formula

The starting point of mobility calculation will be the Kubo formula variant given in equation (1.54). In order to proceed from it, the current operator for the system needs to be known. It can be shown that appropriate current operator for an electron on a lattice, under the condition that the interacting part of the Hamiltonian commutes with the local electron density operator $c_{\mathbf{m}}^\dagger c_{\mathbf{m}}$ (which is the case for Hamiltonian in consideration), takes the following form in the site representation [18]:

$$\mathbf{j} = \frac{e_0}{i\hbar} \sum_{\mathbf{m}, \mathbf{n}} (\mathbf{m} - \mathbf{n}) t_{\mathbf{m}-\mathbf{n}} c_{\mathbf{m}}^\dagger c_{\mathbf{n}}, \quad (3.1)$$

where e_0 is charge of an electron. After applying the unitary transformation given by (2.2), the current operator becomes:

$$\begin{aligned} \mathbf{j}(\mathbf{D}) &= \sum_{\mathbf{k}, \mathbf{q}, \mathbf{q}'} \mathbf{J}_{\mathbf{k}} c_{\mathbf{q}}^\dagger c_{\mathbf{q}'} \theta_{\mathbf{k}-\mathbf{q}}^\dagger \theta_{\mathbf{k}-\mathbf{q}'}, \\ \mathbf{J}_{\mathbf{k}} &= \frac{e_0}{i\hbar} \sum_{\mathbf{R}} \mathbf{R} t_{\mathbf{R}} e^{i\mathbf{k}\mathbf{R}}, \quad \theta_{\mathbf{k}} = \frac{1}{N} \sum_{\mathbf{R}} \theta_{\mathbf{R}} e^{i\mathbf{k}\mathbf{R}}. \end{aligned} \quad (3.2)$$

Using the trace invariance with regards to unitary transformations, Kubo formula can be completely rewritten in terms of transformed operators:

$$\mu_x = -\frac{\beta}{2N_c e_0} \sum_{\mathbf{k}, \mathbf{q}} \sum_{\mathbf{k}', \mathbf{q}'} \sum_{\mathbf{k}'', \mathbf{q}''} \int_{-\infty}^{\infty} dt J_{\mathbf{k}}^x J_{\mathbf{q}}^x \text{Tr} \left(\rho(\mathbf{D}) c_{\mathbf{k}'}^\dagger(t) c_{\mathbf{q}'}(t) \theta_{\mathbf{k}-\mathbf{k}'}^\dagger(t) \theta_{\mathbf{k}-\mathbf{q}'}(t) c_{\mathbf{k}''}^\dagger c_{\mathbf{q}''} \theta_{\mathbf{q}-\mathbf{k}''}^\dagger \theta_{\mathbf{q}-\mathbf{q}''} \right), \quad (3.3)$$

where $\rho(\mathbf{D})$ is statistical operator of the interacting system. Only one diagonal component of the mobility tensor will be calculated. This is sufficient to describe the whole mobility tensor for cubic lattices, since symmetry reduces it to a scalar in the principal directions basis.

Thermodynamic averages as well as time evolutions in (3.3) are to be calculated with respect to the full electron-phonon Hamiltonian. However, if the electron-phonon interaction is small, approximations that will make calculations doable are possible. The first such approximation is the separation of electronic and phononic evolutions. It is valid to expect that if the interacting part is small, electronic and phononic operators can be averaged independently:

$$\begin{aligned} &\text{Tr} \left(\rho(\mathbf{D}) c_{\mathbf{k}'}^\dagger(t) c_{\mathbf{q}'}(t) \theta_{\mathbf{k}-\mathbf{k}'}^\dagger(t) \theta_{\mathbf{k}-\mathbf{q}'}(t) c_{\mathbf{k}''}^\dagger c_{\mathbf{q}''} \theta_{\mathbf{q}-\mathbf{k}''}^\dagger \theta_{\mathbf{q}-\mathbf{q}''} \right) \\ &\approx \left\langle c_{\mathbf{k}'}^\dagger(t) c_{\mathbf{q}'}(t) c_{\mathbf{k}''}^\dagger c_{\mathbf{q}''} \right\rangle \left\langle \theta_{\mathbf{k}-\mathbf{k}'}^\dagger(t) \theta_{\mathbf{k}-\mathbf{q}'}(t) \theta_{\mathbf{q}-\mathbf{k}''}^\dagger \theta_{\mathbf{q}-\mathbf{q}''} \right\rangle \end{aligned} \quad (3.4)$$

The phononic average can further be simplified by noting that since the model in question deals with small carrier concentrations¹, the impact of interaction on phononic properties will be negligible. In fact, if this impact were to be evaluated, for example by calculating additional phononic self-energy that comes from the interaction with carriers, it would be proportional to carrier concentration. In light of this fact, all the phononic quantities can be seen as the unrenormalized ones. Applied to the average and phononic evolution in (3.4), this gives:

$$\begin{aligned} &\left\langle \theta_{\mathbf{m}}^\dagger(t) \theta_{\mathbf{n}}(t) \theta_{\mathbf{l}}^\dagger \theta_{\mathbf{j}} \right\rangle \approx \left\langle \theta_{\mathbf{m}}^\dagger(t) \theta_{\mathbf{n}}(t) \theta_{\mathbf{l}}^\dagger \theta_{\mathbf{j}} \right\rangle_0 \\ &\approx \left\langle e^{\sum_{\mathbf{q}} D_{\mathbf{q}} (b_{\mathbf{q}} e^{-i\omega_{\mathbf{q}} t} - b_{-\mathbf{q}}^\dagger e^{i\omega_{\mathbf{q}} t}) e^{-i\mathbf{q}\mathbf{m}}} e^{\sum_{\mathbf{q}'} D_{\mathbf{q}'} (b_{\mathbf{q}'}^\dagger e^{i\omega_{\mathbf{q}'} t} - b_{-\mathbf{q}'} e^{-i\omega_{\mathbf{q}'} t}) e^{i\mathbf{q}'\mathbf{n}}} \right. \\ &\quad \left. \cdot e^{\sum_{\mathbf{q}''} D_{\mathbf{q}''} (b_{\mathbf{q}''} - b_{-\mathbf{q}''}^\dagger) e^{-i\mathbf{q}''\mathbf{l}}} e^{\sum_{\mathbf{q}'''} D_{\mathbf{q}'''} (b_{\mathbf{q}'''}^\dagger - b_{-\mathbf{q}'''} e^{i\mathbf{q}'''\mathbf{j}})} \right\rangle_0 \end{aligned} \quad (3.5)$$

¹It is a single-electron model.

$$\begin{aligned}
&= \left\langle e^{\sum_{\mathbf{q}} D_{\mathbf{q}} [b_{\mathbf{q}}^{\dagger} e^{i\omega_{\mathbf{q}} t} (e^{i\mathbf{q}\mathbf{n}} - e^{i\mathbf{q}\mathbf{m}}) - b_{\mathbf{q}} e^{-i\omega_{\mathbf{q}} t} (e^{-i\mathbf{q}\mathbf{n}} - e^{-i\mathbf{q}\mathbf{m}})]} e^{\sum_{\mathbf{q}'} D_{\mathbf{q}'} [b_{\mathbf{q}'}^{\dagger} (e^{i\mathbf{q}'\mathbf{j}} - e^{i\mathbf{q}'\mathbf{l}}) - b_{\mathbf{q}'} (e^{-i\mathbf{q}'\mathbf{j}} - e^{-i\mathbf{q}'\mathbf{l}})]} \right\rangle_0 \\
&= e^{-\frac{1}{2} \sum_{\mathbf{q}} D_{\mathbf{q}}^2 |1 - e^{i\mathbf{q}(\mathbf{m}-\mathbf{n})}|^2 (2n_{\mathbf{q}}+1)} e^{-\frac{1}{2} \sum_{\mathbf{q}} D_{\mathbf{q}}^2 |1 - e^{i\mathbf{q}(\mathbf{l}-\mathbf{j})}|^2 (2n_{\mathbf{q}}+1)} \\
&\cdot e^{-\sum_{\mathbf{q}} D_{\mathbf{q}}^2 [(n_{\mathbf{q}}+1)e^{-i\omega_{\mathbf{q}} t} + n_{\mathbf{q}} e^{i\omega_{\mathbf{q}} t}] (1 - e^{i\mathbf{q}(\mathbf{n}-\mathbf{m})}) (1 - e^{-i\mathbf{q}(\mathbf{j}-\mathbf{l})}) e^{i\mathbf{q}(\mathbf{m}-\mathbf{l})}}
\end{aligned}$$

The average is calculated similarly to the average in (2.8). Additionally, the last step stems from the well known identity $e^A e^B = e^{\frac{1}{2}[A,B] + A+B}$, valid for $[A, [A, B]] = [B, [A, B]] = 0$.

Fermionic average in (3.4) will be expanded by the Wick's theorem as if it were the average over the free Hamiltonian, but the single-electron correlations that are obtained that way will be calculated by using the full interacting Green's functions. This corresponds to the non-vertex approximation for mobility. The full calculation that would include vertex corrections would be a task of significant complexity. However, vertex correction for electron-phonon interaction are thought to be proportional to the interaction strength and temperature² [6]. This can provide a basis for disregarding them, since the variational method employed is optimized for various temperatures and coupling strength so that it leaves the small interacting part. Thus, by exploiting the non-vertex approximation, the electronic average reads:

$$\left\langle c_{\mathbf{k}'}(t)^{\dagger} c_{\mathbf{q}'}(t) c_{\mathbf{k}''}^{\dagger} c_{\mathbf{q}''} \right\rangle \approx \delta_{\mathbf{k}', \mathbf{q}''} \delta_{\mathbf{q}', \mathbf{k}''} \left\langle c_{\mathbf{k}'}^{\dagger}(t) c_{\mathbf{k}''} \right\rangle \left\langle c_{\mathbf{q}'}(t) c_{\mathbf{q}''}^{\dagger} \right\rangle. \quad (3.6)$$

The additional terms that come from the Wick's theorem are disregarded, since they are proportional to the square of electron concentration.

After some straightforward Fourier transforms in momentum space, the following expression for mobility is obtained:

$$\mu_x = \frac{e_0 \beta}{2N N_c \hbar^2} \sum_{\mathbf{k}, \mathbf{q}} \int_{-\infty}^{\infty} dt \Gamma_{\mathbf{k}, \mathbf{q}}^x(t) \left\langle c_{\mathbf{k}}^{\dagger}(t) c_{\mathbf{k}} \right\rangle \left\langle c_{\mathbf{q}}(t) c_{\mathbf{q}}^{\dagger} \right\rangle, \quad (3.7)$$

where:

$$\begin{aligned}
\Gamma_{\mathbf{k}, \mathbf{q}}^x(t) &= \sum_{\mathbf{X}, \mathbf{Y}, \mathbf{Z}} t_{\mathbf{X}} t_{\mathbf{Y}} X^x Y^x e^{i(\mathbf{q}\mathbf{X} + \mathbf{k}\mathbf{Y} + \mathbf{k}\mathbf{Z} - \mathbf{q}\mathbf{Z})} \theta_{\mathbf{X}}^0 \theta_{\mathbf{Y}}^0 \theta_{\mathbf{X}, \mathbf{Y}, \mathbf{Z}}(t), \\
\theta_{\mathbf{X}}^0 &= e^{-\frac{1}{2} \sum_{\mathbf{q}} D_{\mathbf{q}}^2 |1 - e^{i\mathbf{q}\mathbf{X}}|^2 (2n_{\mathbf{q}}+1)} = \frac{J_{\mathbf{X}}(\mathbf{D})}{2t_{\mathbf{X}}} \\
\theta_{\mathbf{X}, \mathbf{Y}, \mathbf{Z}}(t) &= e^{-\sum_{\mathbf{q}} D_{\mathbf{q}}^2 [(n_{\mathbf{q}}+1)e^{-i\omega_{\mathbf{q}} t} + n_{\mathbf{q}} e^{i\omega_{\mathbf{q}} t}] (1 - e^{-i\mathbf{q}\mathbf{X}}) (1 - e^{i\mathbf{q}\mathbf{Y}}) e^{i\mathbf{q}\mathbf{Z}}}.
\end{aligned} \quad (3.8)$$

As a result of applied approximations, Kubo formula is rewritten in the terms of single electron correlators. However, since the transformation is previously applied, the electrons are already dressed by phonons, their properties thus renormalized. The scattering mechanism that limits the carrier mobility is the residual electron-phonon

²This is certainly not always the case, impurity scattering being the example where vertex corrections are as important as the non-vertex term.

interaction. It will come into play when calculating polaronic spectral functions. According to (1.28) spectral functions can be used to find the needed single electron correlators.

3.2 Matsubara Functions via Dyson Expansion

Matsubara formalism described in 1.3 will be used for perturbative calculations of polaronic spectral properties. Dyson expansion (1.23) up to the second order gives:

$$G_{\mathbf{k}}(\tau) = -\langle T_{\tau} c_{\mathbf{k}}^I(\tau) c_{\mathbf{k}}^{I\dagger} \rangle_0 + \frac{1}{\hbar} \int_0^{\hbar\beta} d\tau_1 \langle T_{\tau} c_{\mathbf{k}}^I(\tau) V^I(\tau_1) c_{\mathbf{k}}^{I\dagger} \rangle_{0,conn} \\ - \frac{1}{2\hbar^2} \int_0^{\hbar\beta} d\tau_1 \int_0^{\hbar\beta} d\tau_2 \langle T_{\tau} c_{\mathbf{k}}^I(\tau) V^I(\tau_1) V^I(\tau_2) c_{\mathbf{k}}^{I\dagger} \rangle_{0,conn}. \quad (3.9)$$

For convenience, the interaction part of the Hamiltonian is rewritten as:

$$V = V_1 + V_2 = -\frac{1}{N} \sum_{\mathbf{k}, \mathbf{q}} c_{\mathbf{k}-\mathbf{q}}^{\dagger} c_{\mathbf{k}} \mathcal{B}_{\mathbf{k}, \mathbf{q}}, \quad (3.10) \\ \mathcal{B}_{\mathbf{k}, \mathbf{q}} = N\hbar\omega_{\mathbf{q}}(f_{\mathbf{q}} - D_{\mathbf{q}})(b_{\mathbf{q}}^{\dagger} + b_{-\mathbf{q}}) + \sum_{\mathbf{m}, \mathbf{n}} t_{\mathbf{m}-\mathbf{n}}(\theta_{\mathbf{m}}^{\dagger} \theta_{\mathbf{n}} - \langle \theta_{\mathbf{m}}^{\dagger} \theta_{\mathbf{n}} \rangle_0) e^{i((\mathbf{k}-\mathbf{q})\mathbf{m}-\mathbf{k}\mathbf{n})}.$$

It is easy to see by considering phononic part of the interaction Hamiltonian that the first order contribution vanishes:

$$G_{\mathbf{k}}(\tau) = G_{\mathbf{k}}^0(\tau) - \frac{1}{2N^2\hbar^2} \sum_{\mathbf{k}', \mathbf{q}'} \sum_{\mathbf{k}'', \mathbf{q}''} \int_0^{\hbar\beta} d\tau_1 \int_0^{\hbar\beta} d\tau_2 \langle T_{\tau} \mathcal{B}_{\mathbf{k}', \mathbf{q}'}(\tau_1) \mathcal{B}_{\mathbf{k}'', \mathbf{q}''}(\tau_2) \rangle_0 \\ \langle T_{\tau} c_{\mathbf{k}}(\tau) c_{\mathbf{k}'-\mathbf{q}'}^{\dagger}(\tau_1) c_{\mathbf{k}'}(\tau_1) c_{\mathbf{k}''-\mathbf{q}''}^{\dagger}(\tau_2) c_{\mathbf{k}''}(\tau_2) c_{\mathbf{k}}^{\dagger} \rangle_{0,conn}. \quad (3.11)$$

Wick's theorem is employed for the electronic average³:

$$\langle T_{\tau} c_{\mathbf{k}}(\tau) c_{\mathbf{k}'-\mathbf{q}'}^{\dagger}(\tau_1) c_{\mathbf{k}'}(\tau_1) c_{\mathbf{k}''-\mathbf{q}''}^{\dagger}(\tau_2) c_{\mathbf{k}''}(\tau_2) c_{\mathbf{k}}^{\dagger} \rangle_{0,conn} = \\ -\delta_{\mathbf{k}, \mathbf{k}'-\mathbf{q}'} \delta_{\mathbf{k}', \mathbf{k}''-\mathbf{q}''} \delta_{\mathbf{k}'', \mathbf{k}} G_{\mathbf{k}}^0(\tau - \tau_1) G_{\mathbf{k}'}^0(\tau_1 - \tau_2) G_{\mathbf{k}}^0(\tau_2) \\ -\delta_{\mathbf{k}, \mathbf{k}''-\mathbf{q}''} \delta_{\mathbf{k}'', \mathbf{k}'-\mathbf{q}'} \delta_{\mathbf{k}', \mathbf{k}} G_{\mathbf{k}}^0(\tau - \tau_2) G_{\mathbf{k}''}^0(\tau_2 - \tau_1) G_{\mathbf{k}}^0(\tau_1) \\ +\delta_{\mathbf{k}, \mathbf{k}'-\mathbf{q}'} \delta_{\mathbf{k}', \mathbf{k}} \delta_{\mathbf{q}'', 0} G_{\mathbf{k}}^0(\tau - \tau_1) G_{\mathbf{k}}^0(\tau_1) n_F(\mathbf{k}'') \\ +\delta_{\mathbf{k}, \mathbf{k}''-\mathbf{q}''} \delta_{\mathbf{k}'', \mathbf{k}} \delta_{\mathbf{q}', 0} G_{\mathbf{k}}^0(\tau - \tau_2) G_{\mathbf{k}}^0(\tau_2) n_F(\mathbf{k}'). \quad (3.12)$$

³Terms proportional to the electronic concentration are kept because they will later disappear exactly. However, they could have been disregarded at this point without changes to the final result.

Phononic average calculated for $\tau_1 > \tau_2$ is expanded into four terms:

$$\begin{aligned}
& \langle T_\tau \mathcal{B}_{\mathbf{k}', \mathbf{q}'}(\tau_1) \mathcal{B}_{\mathbf{k}'', \mathbf{q}''}(\tau_2) \rangle_0 \\
&= N^2 \hbar^2 \omega_{\mathbf{q}'} \omega_{\mathbf{q}''} (f_{\mathbf{q}'} - D_{\mathbf{q}'})(f_{\mathbf{q}''} - D_{\mathbf{q}''}) \langle (b_{\mathbf{q}'}^\dagger(\tau_1) + b_{-\mathbf{q}'}(\tau_1))(b_{\mathbf{q}''}^\dagger(\tau_2) + b_{-\mathbf{q}''}(\tau_2)) \rangle_0 \\
&+ \sum_{\mathbf{m}, \mathbf{n}, \mathbf{l}, \mathbf{j}} t_{\mathbf{m}-\mathbf{n}} t_{\mathbf{l}-\mathbf{j}} e^{i((\mathbf{k}'-\mathbf{q}')\mathbf{m}-\mathbf{k}'\mathbf{n})} e^{i((\mathbf{k}''-\mathbf{q}'')\mathbf{l}-\mathbf{k}''\mathbf{j})} \left[\langle \theta_{\mathbf{m}}^\dagger(\tau_1) \theta_{\mathbf{n}}(\tau_1) \theta_{\mathbf{l}}^\dagger(\tau_2) \theta_{\mathbf{j}}(\tau_2) \rangle_0 \right. \\
&\quad \left. - \langle \theta_{\mathbf{m}}^\dagger(\tau_1) \theta_{\mathbf{n}}(\tau_1) \rangle_0 \langle \theta_{\mathbf{l}}^\dagger(\tau_2) \theta_{\mathbf{j}}(\tau_2) \rangle_0 \right] \\
&+ N \hbar \omega_{\mathbf{q}'} (f_{\mathbf{q}'} - D_{\mathbf{q}'}) \sum_{\mathbf{l}, \mathbf{j}} t_{\mathbf{l}-\mathbf{j}} e^{i((\mathbf{k}''-\mathbf{q}'')\mathbf{l}-\mathbf{k}''\mathbf{j})} \langle (b_{\mathbf{q}'}^\dagger(\tau_1) + b_{-\mathbf{q}'}(\tau_1)) \theta_{\mathbf{l}}^\dagger(\tau_2) \theta_{\mathbf{j}}(\tau_2) \rangle_0 \\
&+ N \hbar \omega_{\mathbf{q}''} (f_{\mathbf{q}''} - D_{\mathbf{q}''}) \sum_{\mathbf{m}, \mathbf{n}} t_{\mathbf{m}-\mathbf{n}} e^{i((\mathbf{k}'-\mathbf{q}')\mathbf{m}-\mathbf{k}'\mathbf{n})} \langle \theta_{\mathbf{m}}^\dagger(\tau_1) \theta_{\mathbf{n}}(\tau_1) (b_{\mathbf{q}''}^\dagger(\tau_2) + b_{-\mathbf{q}''}(\tau_2)) \rangle_0.
\end{aligned} \tag{3.13}$$

Averaging of the first term is straightforward. Averaging in the second term was already done in (3.5) and (2.8). The result of (2.8) can also be used to deal with the last two terms. More specifically, the expression:

$$\langle \theta_{\mathbf{m}}^\dagger \theta_{\mathbf{n}} \rangle_0 = e^{-\frac{1}{2} \sum_{\mathbf{q}} D_{\mathbf{q}}^2 |e^{i\mathbf{q}\mathbf{n}} - e^{i\mathbf{q}\mathbf{m}}|^2 (2n_{\mathbf{q}}+1)}, \tag{3.14}$$

can be differentiated with respect to the suitable parameters ($D_{\mathbf{q}}(e^{i\mathbf{q}\mathbf{n}} - e^{i\mathbf{q}\mathbf{m}})$ and its conjugate are one possible choice). Combining the expressions derived by differentiation, the averages needed for the last two terms can be obtained. However, differentiating the operator side is not trivial and the following identity, valid for $[[A, \frac{\partial A(\alpha)}{\partial \alpha}], A] = 0$, must be employed:

$$\frac{\partial e^{A(\alpha)}}{\partial \alpha} = e^{A(\alpha)} \left(\frac{\partial A(\alpha)}{\partial \alpha} - \frac{1}{2} [A, \frac{\partial A(\alpha)}{\partial \alpha}] \right) = \left(\frac{\partial A(\alpha)}{\partial \alpha} + \frac{1}{2} [A, \frac{\partial A(\alpha)}{\partial \alpha}] \right) e^{A(\alpha)} \tag{3.15}$$

The identity is proven by series expansion in appendix A. Finally, the averages in the last two terms of (3.13) are found:

$$\begin{aligned}
& \langle (b_{\mathbf{q}'}^\dagger(\tau_1) + b_{-\mathbf{q}'}(\tau_1)) \theta_{\mathbf{l}}^\dagger(\tau_2) \theta_{\mathbf{j}}(\tau_2) \rangle_0 \\
&= D_{\mathbf{q}'} [(n_{\mathbf{q}'} + 1) e^{-\omega_{\mathbf{q}'}(\tau_1-\tau_2)} - n_{\mathbf{q}'} e^{\omega_{\mathbf{q}'}(\tau_1-\tau_2)}] (e^{-i\mathbf{q}'\mathbf{j}} - e^{-i\mathbf{q}'\mathbf{l}}) \langle \theta_{\mathbf{l}}^\dagger \theta_{\mathbf{j}} \rangle_0, \\
& \langle \theta_{\mathbf{m}}^\dagger(\tau_1) \theta_{\mathbf{n}}(\tau_1) (b_{\mathbf{q}''}^\dagger(\tau_2) + b_{-\mathbf{q}''}(\tau_2)) \rangle_0 \\
&= -D_{\mathbf{q}''} [(n_{\mathbf{q}''} + 1) e^{-\omega_{\mathbf{q}''}(\tau_1-\tau_2)} - n_{\mathbf{q}''} e^{\omega_{\mathbf{q}''}(\tau_1-\tau_2)}] (e^{-i\mathbf{q}''\mathbf{n}} - e^{-i\mathbf{q}''\mathbf{m}}) \langle \theta_{\mathbf{m}}^\dagger \theta_{\mathbf{n}} \rangle_0.
\end{aligned} \tag{3.16}$$

After analogous calculation for $\tau_2 > \tau_1$ phononic part gives:

$$- \langle T_\tau \mathcal{B}_{\mathbf{k}', \mathbf{q}'}(\tau_1) \mathcal{B}_{\mathbf{k}'', \mathbf{q}''}(\tau_2) \rangle_0 = N \delta_{\mathbf{q}', -\mathbf{q}''} D_{\mathbf{k}', \mathbf{k}'', \mathbf{q}'}(\tau_1 - \tau_2), \tag{3.17}$$

where:

$$\begin{aligned}
D_{\mathbf{k}',\mathbf{k}'',\mathbf{q}'}(\tau) = & - \left[N\hbar^2\omega_{\mathbf{q}'}^2(f_{\mathbf{q}'} - D_{\mathbf{q}'})^2 [(n_{\mathbf{q}'} + 1)e^{-\omega_{\mathbf{q}'|\tau|} + n_{\mathbf{q}'}e^{\omega_{\mathbf{q}'|\tau|}}] \right. \\
& + \sum_{\mathbf{X},\mathbf{Y},\mathbf{Z}} t_{\mathbf{X}}t_{\mathbf{Y}}\theta_{\mathbf{X}}^0\theta_{\mathbf{Y}}^0 e^{i(\mathbf{k}'\mathbf{X}+\mathbf{k}''\mathbf{Y}-\mathbf{q}'\mathbf{Z})} (\theta_{\mathbf{X},\mathbf{Y},\mathbf{Z}}(|\tau|) - 1) \\
& - N\hbar\omega_{\mathbf{q}'}(f_{\mathbf{q}'} - D_{\mathbf{q}'})D_{\mathbf{q}'} [(n_{\mathbf{q}'} + 1)e^{-\omega_{\mathbf{q}'|\tau|} - n_{\mathbf{q}'}e^{\omega_{\mathbf{q}'|\tau|}}] \text{sgn}\tau \\
& \left. \cdot \sum_{\mathbf{X}} t_{\mathbf{X}}\theta_{\mathbf{X}}^0 (e^{i\mathbf{k}''\mathbf{X}} - e^{-i\mathbf{k}'\mathbf{X}})(1 - e^{i\mathbf{q}'\mathbf{X}}) \right] \\
\theta_{\mathbf{X},\mathbf{Y},\mathbf{Z}}(\tau) = & e^{-\sum_{\mathbf{q}} D_{\mathbf{q}}^2 [(n_{\mathbf{q}}+1)e^{-\omega_{\mathbf{q}\tau} + n_{\mathbf{q}}e^{\omega_{\mathbf{q}\tau}}] (1 - e^{-i\mathbf{q}\mathbf{X}})(1 - e^{i\mathbf{q}\mathbf{Y}}) e^{i\mathbf{q}\mathbf{Z}}
\end{aligned} \tag{3.18}$$

From the definition of bosonic time ordering one obtains:

$$\langle T_{\tau} \mathcal{B}_{\mathbf{k}',\mathbf{q}'}(\tau_1) \mathcal{B}_{\mathbf{k}'',\mathbf{q}''}(\tau_2) \rangle_0 = \langle T_{\tau} \mathcal{B}_{\mathbf{k}'',\mathbf{q}''}(\tau_2) \mathcal{B}_{\mathbf{k}',\mathbf{q}'}(\tau_1) \rangle_0. \tag{3.19}$$

This enables summation of the factors in the expansion of (3.11), that differ only up to the exchange of dummy variables τ_1 and τ_2 . The imaginary frequency polaronic Matsubara function is:

$$\begin{aligned}
G_{\mathbf{k}}(ip_n) = & G_{\mathbf{k}}^0(ip_n) - \frac{1}{N\hbar^2} \sum_{\mathbf{k}',\mathbf{q}'} \sum_{\mathbf{k}'',\mathbf{q}''} \int_0^{\hbar\beta} d\tau e^{ip_n\tau} \int_0^{\hbar\beta} d\tau_1 \int_0^{\hbar\beta} d\tau_2 \delta_{\mathbf{q}',-\mathbf{q}''} D_{\mathbf{k}',\mathbf{k}'',\mathbf{q}'}(\tau_1 - \tau_2) \\
& \left[\delta_{\mathbf{k},\mathbf{k}'-\mathbf{q}'} \delta_{\mathbf{k}',\mathbf{k}''-\mathbf{q}''} \delta_{\mathbf{k}'',\mathbf{k}} G_{\mathbf{k}}^0(\tau - \tau_1) G_{\mathbf{k}'}^0(\tau_1 - \tau_2) G_{\mathbf{k}}^0(\tau_2) - \delta_{\mathbf{k},\mathbf{k}'-\mathbf{q}'} \delta_{\mathbf{k}',\mathbf{k}} \delta_{\mathbf{q}'',0} G_{\mathbf{k}}^0(\tau - \tau_1) G_{\mathbf{k}}^0(\tau_1) n_F(\mathbf{k}'') \right] \\
= & G_{\mathbf{k}}^0(ip_n) - \frac{1}{N\hbar^2} \int_0^{\hbar\beta} d\tau e^{ip_n\tau} \int_0^{\hbar\beta} d\tau_1 \int_0^{\hbar\beta} d\tau_2 \\
& \left[\sum_{\mathbf{q}} D_{\mathbf{k}-\mathbf{q},\mathbf{k},-\mathbf{q}}(\tau_1 - \tau_2) G_{\mathbf{k}}^0(\tau - \tau_1) G_{\mathbf{k}-\mathbf{q}}^0(\tau_1 - \tau_2) G_{\mathbf{k}}^0(\tau_2) \right. \\
& \left. - \sum_{\mathbf{k}''} D_{\mathbf{k},\mathbf{k}'',0}(\tau_1 - \tau_2) G_{\mathbf{k}}^0(\tau - \tau_1) G_{\mathbf{k}}^0(\tau_1) n_F(\mathbf{k}'') \right].
\end{aligned} \tag{3.20}$$

With the usual definition of frequency transform for bosonic Matsubara function:

$$D_{\mathbf{k}',\mathbf{k}'',\mathbf{q}'}(\tau) = \frac{1}{\hbar\beta} \sum_n e^{-i\omega_n\tau} D_{\mathbf{k}',\mathbf{k}'',\mathbf{q}'}(i\omega_n) \quad \omega_n = \frac{2n\pi}{\hbar\beta}, \tag{3.21}$$

the polaronic Matsubara function becomes:

$$G_{\mathbf{k}}(ip_n) = G_{\mathbf{k}}^0(ip_n) - \frac{(G_{\mathbf{k}}^0(ip_n))^2}{N\hbar^2} \sum_{\mathbf{q}} \left[\frac{1}{\hbar\beta} \sum_m D_{\mathbf{k}-\mathbf{q},\mathbf{k},-\mathbf{q}}(i\omega_n - i\omega_m) G_{\mathbf{k}-\mathbf{q}}^0(ip_m) - D_{\mathbf{k},\mathbf{q},0}(0) n_F(\mathbf{q}) \right]. \tag{3.22}$$

Matsubara self-energy can be read from the last expression:

$$\Sigma_{\mathbf{k}}(ip_n) = -\frac{1}{N\hbar^2} \sum_{\mathbf{q}} \left[\frac{1}{\hbar\beta} \sum_m D_{\mathbf{k}-\mathbf{q},\mathbf{k},-\mathbf{q}}(i\omega_n - i\omega_m) G_{\mathbf{k}-\mathbf{q}}^0(ip_m) - D_{\mathbf{k},\mathbf{q},\mathbf{0}}(0) n_F(\mathbf{q}) \right]. \quad (3.23)$$

3.3 Analytic Continuation and Retarded Green's Functions

Analytic continuation is a necessary step that will provide retarded Green's functions needed from known expressions for Matsubara functions. In order to keep expressions compact, it is useful to define the following retarded and advanced phonon functions:

$$\begin{aligned} -ih(t) \langle \mathcal{B}_{\mathbf{k}',\mathbf{q}'}(t) \mathcal{B}_{\mathbf{k}'',\mathbf{q}''} - \mathcal{B}_{\mathbf{k}'',\mathbf{q}''} \mathcal{B}_{\mathbf{k}',\mathbf{q}'}(t) \rangle_0 &= N \delta_{\mathbf{q}',-\mathbf{q}''} D_{\mathbf{k}',\mathbf{k}'',\mathbf{q}'}^{ret}(t), \\ ih(-t) \langle \mathcal{B}_{\mathbf{k}',\mathbf{q}'}(t) \mathcal{B}_{\mathbf{k}'',\mathbf{q}''} - \mathcal{B}_{\mathbf{k}'',\mathbf{q}''} \mathcal{B}_{\mathbf{k}',\mathbf{q}'}(t) \rangle_0 &= N \delta_{\mathbf{q}',-\mathbf{q}''} D_{\mathbf{k}',\mathbf{k}'',\mathbf{q}'}^{adv}(t). \end{aligned} \quad (3.24)$$

These functions are calculated in the same manner as the corresponding Matsubara function $D_{\mathbf{k}',\mathbf{k}'',\mathbf{q}'}(\tau)$. In fact, the whole calculation is analogous with τ exchanged with it , the results being:

$$\begin{aligned} D_{\mathbf{k}',\mathbf{k}'',\mathbf{q}'}^{ret}(t) &= -ih(t) \left[N\hbar^2 \omega_{\mathbf{q}'}^2 (f_{\mathbf{q}'} - D_{\mathbf{q}'})^2 (-2i \sin \omega_{\mathbf{q}'} t) \right. \\ &\quad + \sum_{\mathbf{X},\mathbf{Y},\mathbf{Z}} t_{\mathbf{X}} t_{\mathbf{Y}} \theta_{\mathbf{X}}^0 \theta_{\mathbf{Y}}^0 e^{i(\mathbf{k}'\mathbf{X} + \mathbf{k}''\mathbf{Y} - \mathbf{q}'\mathbf{Z})} (\theta_{\mathbf{X},\mathbf{Y},\mathbf{Z}}(t) - \theta_{\mathbf{X},\mathbf{Y},\mathbf{Z}}(-t)) \\ &\quad \left. - N\hbar \omega_{\mathbf{q}'} (f_{\mathbf{q}'} - D_{\mathbf{q}'}) D_{\mathbf{q}'} 2 \cos \omega_{\mathbf{q}'} t \sum_{\mathbf{X}} t_{\mathbf{X}} \theta_{\mathbf{X}}^0 (e^{i\mathbf{k}''\mathbf{X}} - e^{-i\mathbf{k}'\mathbf{X}}) (1 - e^{i\mathbf{q}'\mathbf{X}}) \right] \end{aligned} \quad (3.25)$$

$$\begin{aligned} D_{\mathbf{k}',\mathbf{k}'',\mathbf{q}'}^{adv}(t) &= ih(-t) \left[N\hbar^2 \omega_{\mathbf{q}'}^2 (f_{\mathbf{q}'} - D_{\mathbf{q}'})^2 (-2i \sin \omega_{\mathbf{q}'} t) \right. \\ &\quad + \sum_{\mathbf{X},\mathbf{Y},\mathbf{Z}} t_{\mathbf{X}} t_{\mathbf{Y}} \theta_{\mathbf{X}}^0 \theta_{\mathbf{Y}}^0 e^{i(\mathbf{k}'\mathbf{X} + \mathbf{k}''\mathbf{Y} - \mathbf{q}'\mathbf{Z})} (\theta_{\mathbf{X},\mathbf{Y},\mathbf{Z}}(t) - \theta_{\mathbf{X},\mathbf{Y},\mathbf{Z}}(-t)) \\ &\quad \left. - N\hbar \omega_{\mathbf{q}'} (f_{\mathbf{q}'} - D_{\mathbf{q}'}) D_{\mathbf{q}'} 2 \cos \omega_{\mathbf{q}'} t \sum_{\mathbf{X}} t_{\mathbf{X}} \theta_{\mathbf{X}}^0 (e^{i\mathbf{k}''\mathbf{X}} - e^{-i\mathbf{k}'\mathbf{X}}) (1 - e^{i\mathbf{q}'\mathbf{X}}) \right] \end{aligned} \quad (3.26)$$

Definitions allow for the application of the analytic continuation theorem on the phononic functions:

$$\begin{aligned} D_{\mathbf{k}',\mathbf{k}'',\mathbf{q}'}(\omega + i\delta) &= D_{\mathbf{k}',\mathbf{k}'',\mathbf{q}'}^{ret}(\omega) \\ D_{\mathbf{k}',\mathbf{k}'',\mathbf{q}'}(\omega - i\delta) &= D_{\mathbf{k}',\mathbf{k}'',\mathbf{q}'}^{adv}(\omega) \end{aligned} \quad (3.27)$$

The conditions are set for summing $-\sum_m D_{\mathbf{k}-\mathbf{q},\mathbf{k},-\mathbf{q}}(i\omega_n - i\omega_m)G_{\mathbf{k}-\mathbf{q}}^0(ip_m) = -\sum_m D_{\mathbf{k}-\mathbf{q},\mathbf{k},-\mathbf{q}}(ip_n - ip_m)G_{\mathbf{k}-\mathbf{q}}^0(ip_m)$ over Matsubara frequencies. Since the sum is over fermionic thermal poles, the following function will be of help:

$$g_{\mathbf{k},\mathbf{q}}^{ip_n}(z) = \frac{1}{e^{\hbar\beta z} + 1} D_{\mathbf{k}-\mathbf{q},\mathbf{k},-\mathbf{q}}(ip_n - z)G_{\mathbf{k}-\mathbf{q}}^0(z). \quad (3.28)$$

As defined, residua around the fermionic thermal poles of $g_{\mathbf{k},\mathbf{q}}^{ip_n}$ are equal to the terms of the sum needed:

$$\text{Res}(g_{\mathbf{k},\mathbf{q}}^{ip_n}(z), z = ip_m) = -\frac{1}{\hbar\beta} D_{\mathbf{k}-\mathbf{q},\mathbf{k},-\mathbf{q}}(ip_n - ip_m)G_{\mathbf{k}-\mathbf{q}}^0(ip_m) \quad (3.29)$$

All the other poles of the function $g_{\mathbf{k},\mathbf{q}}^{ip_n}(z)$ are on the real axis, since they stem from

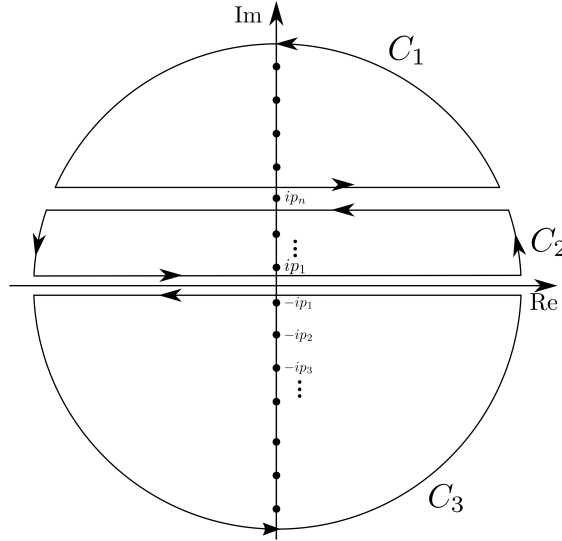


Figure 3.1: Contour used for Matsubara summation.

the D and G . For these reasons, integration of g over the contour shown in the figure 3.1 will be used to perform the summation. The complex integral being calculated is:

$$I_{\mathbf{k},\mathbf{q}}^{ip_n} = \oint_{C_1} \frac{dz}{2\pi i} g_{\mathbf{k},\mathbf{q}}^{ip_n}(z) + \oint_{C_2} \frac{dz}{2\pi i} g_{\mathbf{k},\mathbf{q}}^{ip_n}(z) + \oint_{C_3} \frac{dz}{2\pi i} g_{\mathbf{k},\mathbf{q}}^{ip_n}(z). \quad (3.30)$$

Cauchy residuum theorem gives:

$$I_{\mathbf{k},\mathbf{q}}^{ip_n} = \sum_m \text{Res}(g_{\mathbf{k},\mathbf{q}}^{ip_n}(z), z = ip_m) - \text{Res}(g_{\mathbf{k},\mathbf{q}}^{ip_n}(z), z = ip_n). \quad (3.31)$$

Using (3.29), the Matsubara summation in expression for the self-energy is done:

$$\Sigma_{\mathbf{k}}(ip_n) = \frac{1}{N\hbar^2} \sum_{\mathbf{q}} \left[I_{\mathbf{k},\mathbf{q}}^{ip_n} - \frac{1}{\hbar\beta} D_{\mathbf{k}-\mathbf{q},\mathbf{k},-\mathbf{q}}(0)G_{\mathbf{k}-\mathbf{q}}^0(ip_n) + D_{\mathbf{k},\mathbf{q},0}(0)n_F(\mathbf{q}) \right]. \quad (3.32)$$

The complex integral vanishes on the infinite circular boundary, and can thus be expressed as the sum of regular integrals over the straight contour parts:

$$\begin{aligned}
I_{\mathbf{k},\mathbf{q}}^{ip_n} &= \int_{-\infty}^{\infty} \frac{d\omega'}{2\pi i} n_F(\omega' + ip_n + i\delta) D_{\mathbf{k}-\mathbf{q},\mathbf{k},-\mathbf{q}}(-\omega' - i\delta) G_{\mathbf{k}-\mathbf{q}}^0(\omega' + ip_n + i\delta) \\
&+ \int_{\infty}^{-\infty} \frac{d\omega'}{2\pi i} n_F(\omega' + ip_n - i\delta) D_{\mathbf{k}-\mathbf{q},\mathbf{k},-\mathbf{q}}(-\omega' + i\delta) G_{\mathbf{k}-\mathbf{q}}^0(\omega' + ip_n - i\delta) \\
&+ \int_{-\infty}^{\infty} \frac{d\omega'}{2\pi i} n_F(\omega' + i\delta) D_{\mathbf{k}-\mathbf{q},\mathbf{k},-\mathbf{q}}(ip_n - \omega' - i\delta) G_{\mathbf{k}-\mathbf{q}}^0(\omega' + i\delta) \\
&+ \int_{\infty}^{-\infty} \frac{d\omega'}{2\pi i} n_F(\omega' - i\delta) D_{\mathbf{k}-\mathbf{q},\mathbf{k},-\mathbf{q}}(ip_n - \omega' + i\delta) G_{\mathbf{k}-\mathbf{q}}^0(\omega' - i\delta)
\end{aligned} \tag{3.33}$$

Additional expressions needed for the analytic continuation are:

$$\begin{aligned}
n_F(\omega' + ip_n \pm i\delta) &= -\frac{1}{e^{\hbar\beta\omega'} - 1 \pm i\hbar\beta\delta e^{\hbar\beta\omega'}} = -\text{p.v.}[n(\omega')] \pm i\pi\delta(e^{\hbar\beta\omega'} - 1) \\
&= -\text{p.v.}[n(\omega')] \pm i\frac{\pi}{\hbar\beta}\delta(\omega'), \quad n_F(\omega' \pm i\delta) = n_F(\omega).
\end{aligned} \tag{3.34}$$

Taking the limit $\delta \rightarrow 0$ in (3.33) first, and then using the analytic continuation theorem for various Matsubara functions, the following expression is obtained:

$$\begin{aligned}
I_{\mathbf{k},\mathbf{q}}(\omega) &= -\int_{-\infty}^{\infty} \frac{d\omega'}{2\pi i} n(\omega') D_{\mathbf{k}-\mathbf{q},\mathbf{k},-\mathbf{q}}^{adv}(-\omega') G_{\mathbf{k}-\mathbf{q}}^{0ret}(\omega' + \omega) \\
&+ \int_{-\infty}^{+\infty} \frac{d\omega'}{2\pi i} n(\omega') D_{\mathbf{k}-\mathbf{q},\mathbf{k},-\mathbf{q}}^{ret}(-\omega') G_{\mathbf{k}-\mathbf{q}}^{0ret}(\omega' + \omega) \\
&+ \int_{-\infty}^{\infty} \frac{d\omega'}{2\pi i} n_F(\omega') D_{\mathbf{k}-\mathbf{q},\mathbf{k},-\mathbf{q}}^{ret}(\omega - \omega') G_{\mathbf{k}-\mathbf{q}}^{0ret}(\omega') \\
&- \int_{-\infty}^{+\infty} \frac{d\omega'}{2\pi i} n_F(\omega') D_{\mathbf{k}-\mathbf{q},\mathbf{k},-\mathbf{q}}^{ret}(\omega - \omega' + i\delta) G_{\mathbf{k}-\mathbf{q}}^{0adv}(\omega') \\
&+ \frac{1}{\hbar\beta} D_{\mathbf{k}-\mathbf{q},\mathbf{k},-\mathbf{q}}(0) G_{\mathbf{k}-\mathbf{q}}^{0ret}(\omega)
\end{aligned} \tag{3.35}$$

Once again, it is useful to exploit the low carrier density approximation. In this approximation, Fermi level is far below the band minimum so that its position becomes irrelevant (Fermi distribution coincides with the Boltzmann distribution). From now on, energies are measured from the middle of the band⁴ instead from the Fermi level. In addition to terms proportional to carrier concentration in (3.35) vanishing, ap-

⁴Any other point could have been chosen, but this choice makes the form of the band dispersion simple for 1D case, $-J_C \cos \mathbf{kC}$.

proximations for the expressions appearing in the formula for mobility can be made:

$$\begin{aligned}
n_F(\omega - \frac{E_f}{\hbar})\Lambda_{\mathbf{k}}(\omega - \frac{E_f}{\hbar}) &\approx e^{-\beta\hbar(\omega - \frac{E_f}{\hbar})}\Lambda_{\mathbf{k}}(\omega - \frac{E_f}{\hbar}), \\
(1 - n_F(\omega - \frac{E_f}{\hbar}))\Lambda_{\mathbf{k}}(\omega - \frac{E_f}{\hbar}) &\approx \Lambda_{\mathbf{k}}(\omega - \frac{E_f}{\hbar}), \\
N_c &\approx \sum_{\mathbf{k}} \int_{-\infty}^{\infty} \frac{d\omega}{2\pi} e^{-\beta\hbar(\omega - \frac{E_f}{\hbar})}\Lambda_{\mathbf{k}}(\omega - \frac{E_f}{\hbar}).
\end{aligned} \tag{3.36}$$

Finally, expression for the retarded self-energy is:

$$\Sigma_{\mathbf{k}}^{ret}(\omega - \frac{E_f}{\hbar}) = \frac{1}{N\hbar^2} \sum_{\mathbf{q}} \int_{-\infty}^{\infty} \frac{d\omega'}{2\pi i} n(\omega') [D_{\mathbf{k}-\mathbf{q},\mathbf{k},-\mathbf{q}}^{ret}(-\omega') - D_{\mathbf{k}-\mathbf{q},\mathbf{k},-\mathbf{q}}^{adv}(-\omega')] G_{\mathbf{k}-\mathbf{q}}^{0ret}(\omega' + \omega - \frac{E_f}{\hbar}), \tag{3.37}$$

while the expression for mobility becomes:

$$\begin{aligned}
\mu_x &= \frac{e_0\beta}{2N(\sum_{\mathbf{k}} \int_{-\infty}^{\infty} \frac{d\omega}{2\pi} e^{-\beta\hbar\omega}\Lambda_{\mathbf{k}}(\omega - \frac{E_f}{\hbar}))} \\
&\sum_{\mathbf{k},\mathbf{q}} \int_{-\infty}^{\infty} dt \int_{-\infty}^{\infty} \frac{d\omega_1}{2\pi} \int_{-\infty}^{\infty} \frac{d\omega_2}{2\pi} e^{it(\omega_1 - \omega_2)} \Gamma_{\mathbf{k},\mathbf{q}}^x(t) e^{-\beta\hbar\omega_1} \Lambda_{\mathbf{k}}(\omega_1 - \frac{E_f}{\hbar}) \Lambda_{\mathbf{q}}(\omega_2 - \frac{E_f}{\hbar}).
\end{aligned} \tag{3.38}$$

Equations (3.37) and (3.38) can be used as given for calculations of spectra and mobilities. However, the expression for self-energy can be significantly simplified by the introduction of greater and lesser phonon Green functions, defined as:

$$\begin{aligned}
-i\langle \mathcal{B}_{\mathbf{k}',\mathbf{q}'}(t)\mathcal{B}_{\mathbf{k}'',\mathbf{q}''} \rangle_0 &= N\delta_{\mathbf{q}',-\mathbf{q}''} D_{\mathbf{k}',\mathbf{k}'',\mathbf{q}'}^{\gt}(t) \\
-i\langle \mathcal{B}_{\mathbf{k}'',\mathbf{q}''}\mathcal{B}_{\mathbf{k}',\mathbf{q}'}(t) \rangle_0 &= N\delta_{\mathbf{q}',-\mathbf{q}''} D_{\mathbf{k}',\mathbf{k}'',\mathbf{q}'}^{\lt}(t)
\end{aligned} \tag{3.39}$$

Similarly to the retarded and advanced phononic functions, explicit expressions for greater and lesser Green's functions can be found. The greater function, as will be seen, is of particular importance. It is useful to split the greater function in two parts:

$$D_{\mathbf{k}',\mathbf{k}'',\mathbf{q}'}^{\gt}(t) = D_{\mathbf{k}',\mathbf{k}'',\mathbf{q}'}^{\gt 1}(t) + D_{\mathbf{k}',\mathbf{k}'',\mathbf{q}'}^{\gt 2}(t), \tag{3.40}$$

each being:

$$\begin{aligned}
D_{\mathbf{k}',\mathbf{k}'',\mathbf{q}'}^{\gt 1}(t) &= -i \left[N\hbar^2\omega_{\mathbf{q}'}^2(f_{\mathbf{q}'} - D_{\mathbf{q}'})^2 [(n_{\mathbf{q}'} + 1)e^{-i\omega_{\mathbf{q}'}t} + n_{\mathbf{q}'}e^{i\omega_{\mathbf{q}'}t}] \right. \\
&\quad - N\hbar\omega_{\mathbf{q}'}(f_{\mathbf{q}'} - D_{\mathbf{q}'})D_{\mathbf{q}'} [(n_{\mathbf{q}'} + 1)e^{-i\omega_{\mathbf{q}'}t} - n_{\mathbf{q}'}e^{i\omega_{\mathbf{q}'}t}] \\
&\quad \left. \cdot \sum_{\mathbf{X}} t_{\mathbf{X}}\theta_{\mathbf{X}}^0(e^{i\mathbf{k}''\mathbf{X}} - e^{-i\mathbf{k}'\mathbf{X}})(1 - e^{i\mathbf{q}'\mathbf{X}}) \right], \\
D_{\mathbf{k}',\mathbf{k}'',\mathbf{q}'}^{\gt 1}(\omega) &= -2i\pi \left[N\hbar^2\omega_{\mathbf{q}'}^2(f_{\mathbf{q}'} - D_{\mathbf{q}'})^2 [(n_{\mathbf{q}'} + 1)\delta(\omega - \omega_{\mathbf{q}'}) + n_{\mathbf{q}'}\delta(\omega + \omega_{\mathbf{q}'})] \right. \\
&\quad - N\hbar\omega_{\mathbf{q}'}(f_{\mathbf{q}'} - D_{\mathbf{q}'})D_{\mathbf{q}'} [(n_{\mathbf{q}'} + 1)\delta(\omega - \omega_{\mathbf{q}'}) - n_{\mathbf{q}'}\delta(\omega + \omega_{\mathbf{q}'})] \\
&\quad \left. \cdot \sum_{\mathbf{X}} t_{\mathbf{X}}\theta_{\mathbf{X}}^0(e^{i\mathbf{k}''\mathbf{X}} - e^{-i\mathbf{k}'\mathbf{X}})(1 - e^{i\mathbf{q}'\mathbf{X}}) \right], \\
D_{\mathbf{k}',\mathbf{k}'',\mathbf{q}'}^{\gt 2}(t) &= -i \sum_{\mathbf{X},\mathbf{Y},\mathbf{Z}} t_{\mathbf{X}}t_{\mathbf{Y}}\theta_{\mathbf{X}}^0\theta_{\mathbf{Y}}^0 e^{i(\mathbf{k}'\mathbf{X} + \mathbf{k}''\mathbf{Y} - \mathbf{q}'\mathbf{Z})} (\theta_{\mathbf{X},\mathbf{Y},\mathbf{Z}}(t) - 1), \\
D_{\mathbf{k}',\mathbf{k}'',\mathbf{q}'}^{\gt}(\omega) &= \int_{-\infty}^{\infty} dt e^{i\omega t} D_{\mathbf{k}',\mathbf{k}'',\mathbf{q}'}^{\gt}(t).
\end{aligned} \tag{3.41}$$

Expanding (3.39) in the free phonon basis, the connection between greater and lesser functions is found:

$$\begin{aligned}
D_{\mathbf{k}',\mathbf{k}'',\mathbf{q}'}^{\gt}(t) &= -ie^{\beta\Omega} \sum_{i,j} e^{-\frac{(E_i - E_j)t}{\hbar}} e^{-\beta E_i} \langle i | \mathcal{B}_{\mathbf{k}',\mathbf{q}'} | j \rangle \langle j | \mathcal{B}_{\mathbf{k}'',\mathbf{q}''} | i \rangle, \\
D_{\mathbf{k}',\mathbf{k}'',\mathbf{q}'}^{\lt}(t) &= -ie^{\beta\Omega} \sum_{i,j} e^{-\frac{(E_i - E_j)t}{\hbar}} e^{-\beta E_j} \langle i | \mathcal{B}_{\mathbf{k}',\mathbf{q}'} | j \rangle \langle j | \mathcal{B}_{\mathbf{k}'',\mathbf{q}''} | i \rangle.
\end{aligned} \tag{3.42}$$

From these expressions, it is found that:

$$D_{\mathbf{k}',\mathbf{k}'',\mathbf{q}'}^{\gt}(\omega) = e^{\beta\omega} D_{\mathbf{k}',\mathbf{k}'',\mathbf{q}'}^{\lt}(\omega). \tag{3.43}$$

On the other side, definitions imply:

$$D_{\mathbf{k}',\mathbf{k}'',\mathbf{q}'}^{\gt}(t) - D_{\mathbf{k}',\mathbf{k}'',\mathbf{q}'}^{\lt}(t) = D_{\mathbf{k}',\mathbf{k}'',\mathbf{q}'}^{ret}(t) - D_{\mathbf{k}',\mathbf{k}'',\mathbf{q}'}^{adv}(t). \tag{3.44}$$

Combining the last two expressions yields:

$$n(\omega') [D_{\mathbf{k}-\mathbf{q},\mathbf{k},-\mathbf{q}}^{ret}(-\omega') - D_{\mathbf{k}-\mathbf{q},\mathbf{k},-\mathbf{q}}^{adv}(-\omega')] = -D_{\mathbf{k}-\mathbf{q},\mathbf{k},-\mathbf{q}}^{\gt}(-\omega'). \tag{3.45}$$

Self-energy can now be rewritten as:

$$\begin{aligned}\Sigma_{\mathbf{k}}^{ret}(\omega - \frac{E_f}{\hbar}) &= \frac{i}{2\pi N\hbar^2} \sum_{\mathbf{q}} \int_{-\infty}^{\infty} d\omega' D_{\mathbf{k}-\mathbf{q},\mathbf{k},-\mathbf{q}}^>(-\omega') G_{\mathbf{k}-\mathbf{q}}^{0ret}(\omega' + \omega - \frac{E_f}{\hbar}) \\ &= \frac{i}{N\hbar^2} \sum_{\mathbf{q}} \int_{-\infty}^{\infty} dt e^{i(\omega - \frac{E_f}{\hbar})t} D_{\mathbf{k}-\mathbf{q},\mathbf{k},-\mathbf{q}}^>(t) G_{\mathbf{k}-\mathbf{q}}^{0ret}(t).\end{aligned}\quad (3.46)$$

It is convenient to divide the self-energy in the same way as the greater phonon function:

$$\Sigma_{\mathbf{k}}^{ret}(\omega - \frac{E_f}{\hbar}) = \Sigma_{\mathbf{k}}^1(\omega - \frac{E_f}{\hbar}) + \Sigma_{\mathbf{k}}^2(\omega - \frac{E_f}{\hbar}), \quad (3.47)$$

with corresponding parts being:

$$\begin{aligned}\Sigma_{\mathbf{k}}^1(\omega - \frac{E_f}{\hbar}) &= \frac{1}{N\hbar^2} \sum_{\mathbf{q}} \left[N\hbar^2 \omega_{\mathbf{q}}^2 (f_{\mathbf{q}} - D_{\mathbf{q}})^2 [(n_{\mathbf{q}} + 1) G_{\mathbf{k}-\mathbf{q}}^{ret}(\omega - \omega_{\mathbf{q}} - \frac{E_f}{\hbar}) \right. \\ &\quad \left. + n_{\mathbf{q}} G_{\mathbf{k}-\mathbf{q}}^{ret}(\omega + \omega_{\mathbf{q}} - \frac{E_f}{\hbar})] \right. \\ &\quad \left. - N\hbar \omega_{\mathbf{q}} (f_{\mathbf{q}} - D_{\mathbf{q}}) D_{\mathbf{q}} [(n_{\mathbf{q}} + 1) G_{\mathbf{k}-\mathbf{q}}^{ret}(\omega - \omega_{\mathbf{q}} - \frac{E_f}{\hbar}) - n_{\mathbf{q}} G_{\mathbf{k}-\mathbf{q}}^{ret}(\omega + \omega_{\mathbf{q}} - \frac{E_f}{\hbar})] \right. \\ &\quad \left. \cdot \sum_{\mathbf{X}} t_{\mathbf{X}} \theta_{\mathbf{X}}^0 (e^{i\mathbf{k}\mathbf{X}} - e^{-i(\mathbf{k}-\mathbf{q})\mathbf{X}}) (1 - e^{-i\mathbf{q}\mathbf{X}}) \right],\end{aligned}\quad (3.48)$$

$$\Sigma_{\mathbf{k}}^2(\omega - \frac{E_f}{\hbar}) = \frac{i}{N\hbar^2} \sum_{\mathbf{q}} \int_{-\infty}^{\infty} dt e^{i(\omega - \frac{E_f}{\hbar})t} D_{\mathbf{k}-\mathbf{q},\mathbf{k},-\mathbf{q}}^{>2}(t) G_{\mathbf{k}-\mathbf{q}}^{ret}(t). \quad (3.49)$$

In the last expressions, free fermionic Green's functions on the right are replaced by the full ones. This is equivalent to the summation of an infinite series of diagrams that stem from the basic diagram calculated here from the first nontrivial order in Dyson series. Summing this series of diagrams for the self energy is known as the self-consistent Born approximation [19]. Equations (3.47), (3.48) and (3.49), together with Dyson equation (1.26), form a self-consistent system. It is the system that will be solved numerically in order to obtain the polaronic spectral properties.

Chapter 4

Polaron Mobility Estimates in Extreme Parameter Regions

The results of the previous chapter are lengthy expressions for polaron mobility and self-energy. Any numerical calculation based on them can carry errors, some of which, like errors made during discretization, can be hard to estimate. For this reason, a simple analytical or semi-analytic benchmark result is needed. One such result is the low temperature weak coupling nonadiabatic limit for mobility. It is a well established result for various electron-phonon Hamiltonians [6]. Additionally, a low temperature weak coupling adiabatic estimate as well as a high temperature strong coupling estimate for mobility will be derived in this chapter. Together, all the limits not only provide benchmarks for evaluating the success of numerical calculations¹, but they also shed light on the nature of processes that influence polaronic mobility and spectra. For compactness and because they are only needed for comparison with numerical results, all the results in this chapter will be presented for the 1D model. Extensions to the more general case are straightforward.

4.1 Low Temperature and Weak Coupling Limit for Polaron Mobility

In the weak coupling limit, mobility can be expressed as a power series over inverse coupling constant [6]. The results for the first nontrivial terms in the series will be found. The starting point for approximations is equation (3.38).

¹There are cases where the later two estimates will not be accurate, as will be seen. The first limit mentioned, should, in the region of parameters it applies to, always be close to the numerical results.

The first approximation to be made is for the phononic factor $\Gamma_{\mathbf{k},\mathbf{q}}^x(t)$. Since for $\alpha \ll 1^2$ and $\beta \gg 1$ (which implies $n \ll 1$)³ the leading term in the expansion of Γ is α^0 and the next are proportional to positive powers of α , only the leading term will be retained. Using the equation (3.8), the approximation proceeds as follows:

$$\begin{aligned}\theta_{\mathbf{X},\mathbf{Y},\mathbf{Z}}(t) &\approx 1 \\ \Gamma_{\mathbf{k},\mathbf{q}}^x(t) &= \sum_{\mathbf{X},\mathbf{Y},\mathbf{Z}} t_{\mathbf{X}} t_{\mathbf{Y}} X^x Y^x e^{i(\mathbf{q}\mathbf{X}+\mathbf{k}\mathbf{Y}+\mathbf{k}\mathbf{Z}-\mathbf{q}\mathbf{Z})} \theta_{\mathbf{X}}^0 \theta_{\mathbf{Y}}^0 \theta_{\mathbf{X},\mathbf{Y},\mathbf{Z}}(t), \\ &\approx \frac{J_{\mathbf{C}}^2}{4t_{\mathbf{C}}^2} \sum_{\mathbf{X},\mathbf{Y},\mathbf{Z}} t_{\mathbf{X}} t_{\mathbf{Y}} X^x Y^x e^{i(\mathbf{q}\mathbf{X}+\mathbf{k}\mathbf{Y}+\mathbf{k}\mathbf{Z}-\mathbf{q}\mathbf{Z})} = -\frac{J_{\mathbf{C}}^2 N}{2} (1 - \cos 2\mathbf{q}\mathbf{C}) \delta_{\mathbf{k},\mathbf{q}}\end{aligned}\quad (4.1)$$

When coupling strength and the average number of phonons are small, it is to be expected that the electron-phonon interaction will give only small corrections to the self-energy. If this is the case, spectral function and its square, given by (1.27), have the following limits⁴:

$$\begin{aligned}\Lambda_{\mathbf{k}}(\omega - \frac{E_f}{\hbar}) &= \frac{-2\text{Im}[\Sigma_{\mathbf{k}}^{\text{ret}}(\omega - \frac{E_f}{\hbar})]}{\left(\omega - \frac{E_{\mathbf{k}}}{\hbar} + \text{Re}[\Sigma_{\mathbf{k}}^{\text{ret}}(\omega - \frac{E_f}{\hbar})]\right)^2 + \left(\text{Im}[\Sigma_{\mathbf{k}}^{\text{ret}}(\omega - \frac{E_f}{\hbar})]\right)^2} \\ &\xrightarrow[\text{Re}\Sigma \rightarrow 0]{\text{Im}\Sigma \rightarrow 0} 2\pi \delta\left(\omega + \frac{J_{\mathbf{C}} \cos \mathbf{k}\mathbf{C}}{\hbar}\right) \\ \left[\Lambda_{\mathbf{k}}(\omega - \frac{E_f}{\hbar})\right]^2 &\xrightarrow[\text{Re}\Sigma \rightarrow 0]{\text{Im}\Sigma \rightarrow 0} -\frac{2\pi}{\text{Im}[\Sigma_{\mathbf{k}}^{\text{ret}}(-\frac{J_{\mathbf{C}} \cos \mathbf{k}\mathbf{C} + E_f}{\hbar})]} \delta\left(\omega + \frac{J_{\mathbf{C}} \cos \mathbf{k}\mathbf{C}}{\hbar}\right)\end{aligned}\quad (4.2)$$

After inserting results (4.1) and (4.2) into (3.38) and performing the integrations, the Kubo formula for mobility in the low temperature and weak coupling limit becomes:

$$\mu_x = \frac{e_0 C^2 \beta J_{\mathbf{C}}^2}{4 \sum_{\mathbf{k}} e^{\beta J_{\mathbf{C}} \cos \mathbf{k}\mathbf{C}}} \sum_{\mathbf{k}} (1 - \cos 2\mathbf{k}\mathbf{C}) e^{\beta J_{\mathbf{C}} \cos \mathbf{k}\mathbf{C}} \frac{1}{\text{Im}[\Sigma_{\mathbf{k}}^{\text{ret}}(-\frac{J_{\mathbf{C}} \cos \mathbf{k}\mathbf{C} + E_f}{\hbar})]} \quad (4.3)$$

To obtain the mobility the imaginary part of the self-energy has to be obtained in this limit. From (3.48), (3.49) and (2.19) it can be shown that the self-energy can be expanded into series over positive powers of α^2 . The consequence is the expected expansion of mobility into the power series over $\frac{1}{\alpha^2}$. Depending on the nature of

²Weak coupling region for polaron lattice Hamiltonian is actually determined by $\frac{\alpha^2}{t_{\mathbf{C}}} \ll 1$, but approximations made in this chapter are valid for $\alpha \ll 1$. Weak coupling denomination is used in broader sense than defined in 1.2.

³For the weak coupling low temperature approximations, both $\alpha \ll 1$ and $\beta \gg 1$ conditions are necessary. However, since α and n are always found in a product of form $\alpha^2 n$, only $\alpha \ll 1$ will be invoked, but it will also imply the application of $\beta \gg 1$.

⁴Limits are valid under integral.

scattering processes accessible to the polaron in specific parameter regions, the leading term in this expansion will be either $\frac{1}{\alpha^2}$ or $\frac{1}{\alpha^4}$.

4.1.1 Non-Adiabatic Regime ($J_C > \hbar\omega_0$)

When the renormalized bandwidth is such that $J_C > \hbar\omega_0$, band is wide enough that all the states can take part in single-phonon scatterings, either absorptions, emissions, or both. The scatterings broaden polaronic spectral lines, thus giving rise to the finite mobility. Imaginary part of the self-energy needed for the evaluation of (4.3) will be found using (3.48) and (3.49) expanded up to the α^2 order. This means that the full fermionic Green's functions on the right-hand side are replaced by the corresponding free propagators (the first order approximation when solving the self-consistent system for self-energy). Additionally, for Σ^2 part of the self-energy, exponent in the greater phonon function is expanded to the first order:

$$\begin{aligned}
D_{\mathbf{k}',\mathbf{k}'',\mathbf{q}'}^{>2}(t) &= -i \sum_{\mathbf{X},\mathbf{Y},\mathbf{Z}} t_{\mathbf{X}} t_{\mathbf{Y}} \theta_{\mathbf{X}}^0 \theta_{\mathbf{Y}}^0 e^{i(\mathbf{k}'\mathbf{X} + \mathbf{k}''\mathbf{Y} - \mathbf{q}'\mathbf{Z})} (\theta_{\mathbf{X},\mathbf{Y},\mathbf{Z}}(t) - 1), \\
D_{\mathbf{k}-\mathbf{q},\mathbf{k},-\mathbf{q}}^{>2}(t) &\approx i \frac{J_C^2 N}{4t_C^2} D_{\mathbf{q}}^2 \sum_{\mathbf{X},\mathbf{Y}} t_{\mathbf{X}} t_{\mathbf{Y}} e^{i\mathbf{k}(\mathbf{X}+\mathbf{Y})} e^{-i\mathbf{q}\mathbf{X}} (1 - e^{i\mathbf{q}\mathbf{X}}) (1 - e^{-i\mathbf{q}\mathbf{Y}}) [(n+1)e^{-i\omega t} + ne^{i\omega t}].
\end{aligned} \tag{4.4}$$

Using this expansion and summing over the nearest neighbours, self-energy up to the first order in α^2 becomes:

$$\begin{aligned}
\Sigma_{\mathbf{k}}^{ret}(\omega - \frac{E_f}{\hbar}) &\approx \sum_{\mathbf{q}} \left[\omega_0^2 (f_{\mathbf{q}} - D_{\mathbf{q}})^2 [(n+1)G_{\mathbf{k}-\mathbf{q}}^{0ret}(\omega - \omega_0 - \frac{E_f}{\hbar}) \right. \\
&\quad + nG_{\mathbf{k}-\mathbf{q}}^{0ret}(\omega + \omega_0 - \frac{E_f}{\hbar})] - 2J_C [\cos \mathbf{k}\mathbf{C} - \cos(\mathbf{k} - \mathbf{q})\mathbf{C}] \omega_0 (f_{\mathbf{q}} - D_{\mathbf{q}}) D_{\mathbf{q}} \\
&\quad \cdot [(n+1)G_{\mathbf{k}-\mathbf{q}}^{0ret}(\omega - \omega_0 - \frac{E_f}{\hbar}) - nG_{\mathbf{k}-\mathbf{q}}^{0ret}(\omega + \omega_0 - \frac{E_f}{\hbar})] \\
&\quad + J_C^2 D_{\mathbf{q}}^2 [(n+1)G_{\mathbf{k}-\mathbf{q}}^{0ret}(\omega - \omega_0 - \frac{E_f}{\hbar}) + nG_{\mathbf{k}-\mathbf{q}}^{0ret}(\omega + \omega_0 - \frac{E_f}{\hbar})] \\
&\quad \left. \cdot [\cos \mathbf{k}\mathbf{C} - \cos(\mathbf{k} - \mathbf{q})\mathbf{C}]^2 \right].
\end{aligned} \tag{4.5}$$

From the expression above, the required imaginary part is:

$$\begin{aligned}
\text{Im}[\Sigma_{\mathbf{k}}^{ret}(-\frac{J_C \cos \mathbf{k}\mathbf{C} + E_f}{\hbar})] &= -\pi \sum_{\mathbf{q}} \hbar \omega_0^2 f_{\mathbf{q}}^2 \left[(n+1)\delta(-J_C \cos \mathbf{k}\mathbf{C} + J_C \cos(\mathbf{k} - \mathbf{q})\mathbf{C} - \hbar\omega_0) \right. \\
&\quad \left. + n\delta(-J_C \cos \mathbf{k}\mathbf{C} + J_C \cos(\mathbf{k} - \mathbf{q})\mathbf{C} + \hbar\omega_0) \right].
\end{aligned} \tag{4.6}$$

The first term in (4.6) corresponds to phonon emission - polaron in the state \mathbf{k} with corresponding energy $-J_{\mathbf{C}} \cos \mathbf{k} \cdot \mathbf{C}$ scatters to the state with energy $-J_{\mathbf{C}} \cos \mathbf{k} \cdot \mathbf{C} - \hbar\omega_0 = -J_{\mathbf{C}} \cos (\mathbf{k} - \mathbf{q}) \cdot \mathbf{C}$ and momentum corresponding to it, while emitting the phonon of energy $\hbar\omega_0$ and appropriate momentum. Analogously, the second term in (4.6) corresponds to phonon absorption. After transformation of sums in (4.6) into integrals and evaluation of these integrals, one obtains:

$$\begin{aligned} \text{Im}[\Sigma_{\mathbf{k}}^{ret}(-\frac{J_{\mathbf{C}} \cos \mathbf{k} \cdot \mathbf{C} + E_f}{\hbar})] = & -\frac{N}{2} \sum_{+,-} \hbar\omega_0^2 \left[f_{\mathbf{q}_1^\pm}^2 \frac{n+1}{\sqrt{J_{\mathbf{C}}^2 - (J_{\mathbf{C}} \cos \mathbf{k} \cdot \mathbf{C} + \hbar\omega_0)^2}} \right. \\ & \left. + f_{\mathbf{q}_2^\pm}^2 \frac{n}{\sqrt{J_{\mathbf{C}}^2 - (J_{\mathbf{C}} \cos \mathbf{k} \cdot \mathbf{C} - \hbar\omega_0)^2}} \right], \end{aligned} \quad (4.7)$$

where:

$$\mathbf{q}_1^\pm = \mathbf{k} \mp \arccos \frac{\hbar\omega_0 + J_{\mathbf{C}} \cos \mathbf{k} \cdot \mathbf{C}}{J_{\mathbf{C}}}, \quad \mathbf{q}_2^\pm = \mathbf{k} \mp \arccos \frac{-\hbar\omega_0 - J_{\mathbf{C}} \cos \mathbf{k} \cdot \mathbf{C}}{J_{\mathbf{C}}}. \quad (4.8)$$

The first term in (4.7) is defined and should be included only when $-J_{\mathbf{C}} \cos \mathbf{k} > -J_{\mathbf{C}} + \omega_0$, which corresponds to the range of initial states \mathbf{k} for which the single-phonon intraband emission is allowed. Similar is valid for the second term and absorption. In order for mobility to be finite in this approximation all the states in the band must be able to participate in at least one of the processes. It is not hard to see that this is possible for $J_{\mathbf{C}} > \hbar\omega_0$, as already implied. With (4.7), the self-energy, and thus mobility, are found in the low temperature weak coupling non-adiabatic regime. It should be noted that expressions for mobility in this regime derived after the unitary transformation are identical (up to the change of renormalized bandwidth with unrenormalized) to the ones that could have been derived starting from the untransformed Hamiltonian.

From the expressions (4.3) and (4.7) several features can be deduced. Mobility dependence on coupling constant is $\frac{1}{\alpha^2}$. The temperature dependence is roughly $\frac{1}{n}$, since the absorption term dominates for small temperatures for which only the bottom of the band is populated. This is in agreement with the polaron mobility features in weak coupling regime described in 1.1. Because the approximations used for the derivation of the result all naturally follow for weak couplings and low temperatures, the results for the mobility in this parameter region are expected to be a good benchmark for the validity of full numerical calculations.

4.1.2 Adiabatic Regime ($J_{\mathbf{C}} < \frac{\hbar\omega_0}{2}$)

When $J_{\mathbf{C}} < \frac{\hbar\omega_0}{2}$, no state in the polaron band can participate in the single-phonon processes. First contributions to the scattering come from the two-phonon processes,

more specifically from the processes that include simultaneous absorption and emission of phonons.

When calculating the imaginary self-energy contribution from two-phonon processes, both terms Σ^1 and Σ^2 contain two-phonon contributions. Contributions from Σ^1 come from the second order of self-consistent Born approximations. However, the spectral line is infinitely narrow in the first order, since single-phonon processes are forbidden, so calculating the second order simply by inserting the first order correction in (4.5) to calculate second terms would give no contribution. This suggests that the majority of two-phonon contributions stem from Σ^2 part, specifically from the higher terms in the expansion of the exponent in the greater phonon function.

With this in mind, the greater phonon function from (3.49) is expanded to the second order in α^2 and terms corresponding to simultaneous absorption and emission are kept (double absorptions and emissions which also appear in the second order expansion are forbidden processes). Self-energy is given by:

$$\begin{aligned} \Sigma_{\mathbf{k}}^{ret}(\omega - \frac{E_f}{\hbar}) &\approx \frac{1}{4N} \sum_{\mathbf{q}} G_{\mathbf{k}-\mathbf{q}}^{0ret}(\omega - \frac{E_f}{\hbar}) \sum_{\mathbf{X}, \mathbf{Y}, \mathbf{Z}} J_{\mathbf{X}} J_{\mathbf{Y}} e^{i\mathbf{k}(\mathbf{X}+\mathbf{Y})} e^{i\mathbf{q}(\mathbf{Z}-\mathbf{X})} \\ &\cdot \sum_{\mathbf{q}', \mathbf{q}''} D_{\mathbf{q}'}^2 D_{\mathbf{q}''}^2 n(n+1) (1 - e^{-i\mathbf{q}'\mathbf{X}}) (1 - e^{i\mathbf{q}'\mathbf{Y}}) e^{i\mathbf{q}'\mathbf{Z}} (1 - e^{-i\mathbf{q}''\mathbf{X}}) (1 - e^{i\mathbf{q}''\mathbf{Y}}) e^{i\mathbf{q}''\mathbf{Z}} \end{aligned} \quad (4.9)$$

Taking the imaginary part and performing the integrals involving the emerging delta function gives:

$$\text{Im}[\Sigma_{\mathbf{k}}^{ret}(-\frac{J_{\mathbf{C}} \cos \mathbf{kC} + E_f}{\hbar})] \approx -\frac{J_{\mathbf{C}} N}{8\hbar |\sin \mathbf{kC}|} n(n+1) \sum_{\mathbf{q}} [D_{\mathbf{q}}^4 F_{\mathbf{k}, \mathbf{q}, 0}^1 + D_{\mathbf{q}}^2 D_{\mathbf{q}+2\mathbf{k}}^2 F_{\mathbf{k}, \mathbf{q}, 2\mathbf{k}}^1], \quad (4.10)$$

where:

$$F_{\mathbf{k}, \mathbf{q}, \mathbf{q}'}^1 = \sum_{\mathbf{X}, \mathbf{Y}}^{n.n.} e^{i(\mathbf{k}-\mathbf{q}')\mathbf{X}} e^{i\mathbf{k}\mathbf{Y}} (1 - e^{i(\mathbf{q}+\mathbf{q}')\mathbf{X}}) (1 - e^{-i(\mathbf{q}+\mathbf{q}')\mathbf{Y}}) (1 - e^{-i\mathbf{q}\mathbf{X}}) (1 - e^{i\mathbf{q}\mathbf{Y}}). \quad (4.11)$$

The first term in (4.10) corresponds to the two-phonon process in which polaron is scattered via phonon absorption and emission from the state \mathbf{k} to the same state. The second term corresponds to the process in which final state is $-\mathbf{k}$, with the same energy as state \mathbf{k} . One sum over momenta remains because momenta of the two phonons that participate in the process can be distributed arbitrarily subject to the constraint that total phonon momentum must be either 0 (for the first term) or $2\mathbf{k}$ (for the second term).

Nearest neighbour sums are easily calculated:

$$\begin{aligned} F_{\mathbf{k}, \mathbf{q}, 0}^1 &= 8(1 + \cos 2\mathbf{kC})(1 - \cos \mathbf{qC})^2 \\ F_{\mathbf{k}, \mathbf{q}, 2\mathbf{k}}^1 &= 16(1 - \cos(2\mathbf{k} + \mathbf{q})\mathbf{C})(1 - \cos \mathbf{qC}) + 4 \cos(2\mathbf{k} + \mathbf{q})\mathbf{C} \end{aligned} \quad (4.12)$$

Equation (4.10) together with (4.12) determines the imaginary part of self-energy needed for mobility calculations in (4.3). From its form it can be deduced that the mobility in the adiabatic regime will depend on the coupling constant as $\frac{1}{\alpha^4}$, as expected for the two-phonon scattering governed mobility. Temperature dependence in the low temperature limit is still $\frac{1}{n(n+1)} \approx \frac{1}{n}$. The results for the mobility in the adiabatic regime, however, are not an ideal benchmark for the comparison with full numerical calculation to the extent that non-adiabatic regime results are. They should be used more as an order of magnitude calculation. The reason is that the approximations used cannot capture the contribution from Σ^1 self-energy term.

4.1.3 Mixed Regime ($\frac{\hbar\omega_0}{2} < J_C < \hbar\omega_0$)

In the region of bandwidths for which $\frac{\hbar\omega_0}{2} < J_C < \hbar\omega_0$ is valid, single-phonon processes are allowed for some states in the band. More precisely, absorption is allowed for the states with energies between $-J_C$ and $J_C - \omega_0$ while emission is allowed between $-J_C + \omega_0$ and J_C . However, since the states in the middle of the band cannot participate in one phonon processes, the mobility calculated with single-phonon approximation only would be infinite.

Simple solution to this problem is possible because mobility contributions from various states in the band are independent in the weak coupling approximation, as implied by (4.3). Self-energy estimates for the states for which single-phonon processes are forbidden can be obtained in the two-phonon approximation given by (4.10). Self-energy for the states that can scatter via single-phonon processes is obtained by (4.7). Consequently, the mobility is finite. It is expected that the final result will be closer to the adiabatic case, since the main contribution to mobility comes from the populated bottom of the band.

4.2 High Temperature and Strong Coupling Limit for Polaron Mobility

The basic approximation made in the strong coupling and high temperature limit is the form of the Green's function:

$$G^{ret}(\omega - \frac{E_f}{\hbar}) = \frac{1}{\omega - \frac{E}{\hbar} - i\text{Im}\Sigma^{ret}(\frac{E}{\hbar})} \implies G^{ret}(t) = -ih(t)e^{\text{Im}\Sigma^{ret}(\frac{E}{\hbar})t}e^{-i\frac{E}{\hbar}t} \quad (4.13)$$

Several assumptions are contained in this expression. Firstly, flat-band dispersion is assumed. This is approximate, since the band exponentially narrows in the strong coupling limit as seen in 2.3. Real part of the self-energy can be combined with the band energy in one quantity, E , which itself is arbitrary because of the low carrier

density approximation. However, in the regime of interest, polaronic spectrum can be complicated, as will be seen from numerical results. In addition to the main band, additional bands do appear at energies $\hbar\omega_0$ separated from the initial one, although weaker by spectral weight. This fact is not included in the approximation and will effect the validity of the strong coupling limit. Furthermore, the spectral line profile is assumed to be Lorentzian. Also, the imaginary part of the self-energy does not depend on the polaron momentum. Both of the last two assumptions will be justified in the following calculations.

Imaginary part of self-energy is to be calculated from self-consistent system given by (3.48) and (3.49). The great simplification comes from the fact that Σ^1 part of the self energy is negligible in the strong coupling limit. This is easily seen by noting that $J_{\mathbf{C}} \ll 1$ implies $f_{\mathbf{q}} - D_{\mathbf{q}} \propto J_{\mathbf{C}}$, so that both terms in Σ^1 fall off exponentially with coupling strength and temperature, as does the renormalized bandwidth. Exponentially small bandwidth in Σ^2 is compensated by the exponential factor $\theta_{\mathbf{X},\mathbf{Y},\mathbf{Z}}(t)$. Equations (3.14), (3.18) and (3.48) combined with (4.13) give:

$$\begin{aligned} \Sigma^{ret}(\omega - \frac{E_f}{\hbar}) &= \frac{1}{N\hbar^2} \int_{-\infty}^{\infty} dt e^{i(\omega - \frac{E_f}{\hbar})t} G^{ret}(t) \sum_{\mathbf{q}} \sum_{\mathbf{X},\mathbf{Y},\mathbf{Z}} t_{\mathbf{X}} t_{\mathbf{Y}} \theta_{\mathbf{X}}^0 \theta_{\mathbf{Y}}^0 e^{i((\mathbf{k}-\mathbf{q})\mathbf{X} + \mathbf{k}\mathbf{Y} + \mathbf{q}\mathbf{Z})} (\theta_{\mathbf{X},\mathbf{Y},\mathbf{Z}}(t) - 1) \\ &= \frac{1}{\hbar^2} \int_{-\infty}^{\infty} dt e^{i(\omega - \frac{E_f}{\hbar})t} G^{ret}(t) \sum_{\mathbf{X},\mathbf{Y}} t_{\mathbf{X}} t_{\mathbf{Y}} e^{i\mathbf{k}(\mathbf{X} + \mathbf{Y})} e^{-2\sum_{\mathbf{q}} D_{\mathbf{q}}^2 (1 - \cos \mathbf{q}\mathbf{X})(2n+1)} \\ &\quad \cdot \left(e^{\sum_{\mathbf{q}} D_{\mathbf{q}}^2 [(n+1)e^{-i\omega_0 t} + ne^{i\omega_0 t}]} \left(1 - e^{i\mathbf{q}\mathbf{X}} - e^{i\mathbf{q}\mathbf{Y}} + e^{i\mathbf{q}(\mathbf{X} + \mathbf{Y})} \right) - 1 \right). \end{aligned} \tag{4.14}$$

Two types of terms arise in the nearest neighbor sum, the ones with $\mathbf{X} = -\mathbf{Y}$ and the ones with $\mathbf{X} = \mathbf{Y}$. Only the terms of the first type will be kept because in that case second exponential factor can compensate band narrowing exponent for $t = mT$, where $m \in \mathcal{Z}$ and $T = \frac{2\pi}{\omega_0}$. For the terms of the second type, band narrowing exponent cannot be compensated regardless of time, so the contribution from this term is always exponentially small. As an additional consequence, self-energy becomes momentum independent, which is consistent with the approximation already used in (4.13):

$$\begin{aligned} \Sigma^{ret}(\omega - \frac{E_f}{\hbar}) &= \frac{2t_{\mathbf{C}}^2}{\hbar^2} \int_{-\infty}^{\infty} dt e^{i(\omega - \frac{E_f}{\hbar})t} G^{ret}(t) g(t), \\ g(t) &= e^{-4E_a} \left[2n+1 - (n+1)e^{-i\omega_0 t} - ne^{i\omega_0 t} \right], \\ E_a &= \frac{1}{2} \sum_{\mathbf{q}} D_{\mathbf{q}}^2 (1 - \cos \mathbf{q}\mathbf{C}). \end{aligned} \tag{4.15}$$

Further simplification comes from the fact that for strong coupling and high temperatures, the function $g(t)$ peaks prominently for $t = mT$, reaching its maximum value of 1. Away from the points $t = mT$, g decays as $e^{-E_a(2n+1)\omega_0 t}$. In comparison to this, retarded Green's function decays as $e^{\text{Im}\Sigma^{ret}t}$. It is to be expected that for strong limit

$E_a(2n+1) \gg \text{Im}\Sigma^{ret}$, since $E_a \propto \alpha^2$ and self-energy should not be large because the unitary transformation nearly diagonalizes the Hamiltonian. Consequently, Green's function varies slowly on the timescales on which g varies, so it can be approximated by its value in points $t = mT$ for the application of the mean value theorem. By exploiting this fact, as well as periodicity of the function g , one obtains:

$$\begin{aligned} \Sigma^{ret}(\omega - \frac{E_f}{\hbar}) &= \frac{2t_{\text{C}}^2}{\hbar^2} \left[\gamma_1 G^{ret}(0) + \gamma_2 \sum_{m=1}^{\infty} e^{i(\omega - \frac{E_f}{\hbar})mT} G^{ret}(mT) \right], \\ \gamma_1 &= \int_0^{\frac{T}{2}} dt g(t), \quad \gamma_2 = \int_{-\frac{T}{2}}^{\frac{T}{2}} dt g(t). \end{aligned} \quad (4.16)$$

It follows from (4.15) that $\Sigma^{ret}(\omega - \frac{E_f}{\hbar})$ is the most significant for $\omega - \frac{E_f}{\hbar} = \frac{E}{\hbar}$, since the sum over m vanishes for oscillating summands. After inserting the form of G^{ret} and taking imaginary parts, a self-consistent equation for $\text{Im}\Sigma^{ret}(\frac{E}{\hbar})$ is obtained:

$$\text{Im}\Sigma^{ret}(\frac{E}{\hbar}) = -\frac{2t_{\text{C}}^2}{\hbar^2} \left[\text{Re}(\gamma_1) + \text{Re}(\gamma_2) \frac{e^{\text{Im}\Sigma^{ret}(\frac{E}{\hbar})T}}{1 - e^{\text{Im}\Sigma^{ret}(\frac{E}{\hbar})T}} \right]. \quad (4.17)$$

Although (4.17) must be solved numerically, it is a single equation and can be solved very reliably.

With the self-energy calculated, the spectral function needed for the evaluation of mobility via (3.38) is straightforward:

$$\Lambda(\omega - \frac{E_f}{\hbar}) = \frac{-2\text{Im}\Sigma^{ret}(\frac{E}{\hbar})}{(\omega - \frac{E}{\hbar})^2 + (\text{Im}\Sigma^{ret}(\frac{E}{\hbar}))^2} \implies \Lambda(t) = e^{\text{Im}\Sigma^{ret}(\frac{E}{\hbar})|t|} e^{-i\frac{E}{\hbar}t} \quad (4.18)$$

In (3.38), a spectral function is convolved with thermal factor $e^{-\beta\omega}$. However, for high temperatures for which $\text{Im}\Sigma^{ret}(\frac{E}{\hbar}) \ll \frac{1}{\beta}$ is satisfied, thermal factor varies much slower than spectral function. Thus, its value can be approximated with the value for $\omega = \frac{E}{\hbar}$, for which the spectral function reaches its maximum. With this accounted for, mobility in the strong coupling approximation becomes:

$$\mu_x = \frac{e_0\beta}{2N^2} \int_{-\infty}^{\infty} dt e^{2\text{Im}\Sigma^{ret}(\frac{E}{\hbar})|t|} \sum_{\mathbf{k}, \mathbf{q}} \Gamma_{\mathbf{k}, \mathbf{q}}^x(t) \quad (4.19)$$

The momentum sums are exactly evaluated to give:

$$\frac{1}{N^2} \sum_{\mathbf{k}, \mathbf{q}} \Gamma_{\mathbf{k}, \mathbf{q}}^x(t) = -2t_{\text{C}}^2 C^2 g(t). \quad (4.20)$$

Using the same mean value approximation as for the self-energy in (4.15), mobility is found to be⁵:

$$\mu_x = -e_0 \beta t_{\mathbf{C}}^2 C^2 \gamma_2 \left[1 + 2 \frac{e^{2\text{Im}\Sigma^{ret}(\frac{E}{\hbar})T}}{1 - e^{2\text{Im}\Sigma^{ret}(\frac{E}{\hbar})T}} \right]. \quad (4.21)$$

Expressions (4.17) and (4.21) completely determine the mobility in the strong coupling approximation. One specific feature of mobility in the strong coupling region is the fact that it scales as the square of the transfer integral, while the mobility in the weak coupling region scales almost linearly with transfer integral.

Because of the assumptions made while deriving it, the strong coupling approximation is not an ideal benchmark to which numerical results can be compared. However, it is expected that it will be in agreement in at least some region of parameters in which all assumptions are satisfied. It is not simple to determine this region beforehand because the validity of approximation depends on the details of the polaronic spectrum which will be found numerically. Furthermore, it is expected that the approximation will provide at least an order of magnitude estimate in the whole strong-coupling region. Lastly, the importance of the strong coupling approximation also lies in the fact that it represents a generalization of the strong coupling estimate discussed in section 1.1 [9]. As such, by comparing the results of the approximation with the ones obtained by the full numerical approach, the range of applicability of the estimate from chapter 1.1 and the underlying theory of small polaron transport will be investigated.

⁵At first glance, mobility may not seem to be real, but it is not hard to see γ_2 is a real quantity, although γ_1 is not.

Chapter 5

Numerical Results

In this chapter numerical results for the polaron mobility will be presented. In addition, mobility calculated by the weak and strong coupling approximations of chapter 4 will be provided for comparison. Before the mobility results are presented, the intermediate results, more specifically the polaronic spectra and the current-current correlations, will be discussed. These will provide an insight into the nature of polaronic states.

5.1 Parameters of Numerical Calculation

Full numerical calculations are based on the approximate solution of the Kubo formula given by equation (3.38). The self-energy function needed is calculated self-consistently from the system given by (3.47), (3.48) (3.49), and (1.26). Calculations for the mobility in the weak and the strong coupling limits are done according to expressions (4.3) and (4.21), respectively.

All the calculations are done for $N = 100$ lattice sites. It has been found that increasing the number of sites changes the mobility negligibly. Discretization in time, or equivalently, frequency domain with variable frequency range and density of points adjusted such that the total number of points is $2^{13} = 8192$. The range of frequencies is tuned such that all the relevant energies are included in calculation. The range is determined by the phononic factor $D^{>2}$ which is needed for self-energy and thus Green's function calculation. Factor $D^{>2}$ have Fourier components in multiples of $\hbar\omega_0$. The strongest Fourier component of $D^{>2}$ scales as $\alpha^2 n$ with interaction strength and temperature. The frequencies four times higher than that of the main Fourier component of phononic factor are included. The consequence is that density of frequency points decreases with increasing temperature and coupling strength. In order for calculation to be considered valid, spectral lines must be several frequency points

wide. In some cases, this cannot be achieved with 2^{12} total points, and thus no result for the mobility is given. This usually happens in the low temperature region where spectral lines are narrow. In cases where spectral lines are too narrow, the self-consistent system for the self-energy also has difficulties converging or does not converge. As an additional check of the consistency of numerical calculations, the function $C(t) \propto \langle j^x(t)j^x(0) \rangle$ is examined and if the correlations do not fall off in the time range of calculation or the peaks contain too few points, the calculation is discarded. This happens when spectral lines are too narrow or the self-consistency calculation does not converge.

Parameter ranges investigated with full numeric calculations include transfer integrals $t_{\mathbf{C}}$ in the range of 0.1 – 3, temperatures $k_B T$ in the range 0.2 – 3, coupling constants α in the range 0.7 – 4.0, and the ψ parameter in the range of $0 - \frac{\pi}{3}$. In all the results presented, energies are measured in units of $\hbar\omega_0$, while momenta are measured in units of $\frac{1}{C}$. The difficulties with extending the range of calculations are mainly in direction of smaller temperatures and coupling strengths. However, in the majority of cases, the ranges investigated are sufficient to show the behavior in the regimes of interest and to allow comparison with appropriate limits¹.

5.2 Polaronic Spectra

In this chapter, calculated polaronic spectra for several representative cases are presented. In figures 5.1 and 5.2, the dependence of polaronic spectra on coupling strength is shown for two distinct transfer integrals. The spectra are shown for relatively low temperature, $k_B T = 0.4$.

The features seen in spectra for narrow unrenormalized bandwidth case, $t_{\mathbf{C}} = 0.2$, are as follows. Firstly, the band narrowing is gradual, as already implied in section 2.3 for the case where the transition in bandwidth does not occur. However, additional feature seen is the appearance of the second band at ω_0 distance from the original. In fact, it can be seen with more careful analyses that the sequence of increasingly darker bands at distances of ω_0 do form. The bands are consequences of single-phonon and multi-phonon scatterings and as such their spectral weight and number increases with coupling strength. They are equivalent to vibrational energy levels of independent molecules, as expected for low transfer integrals.

The spectra for a wide band, $t_{\mathbf{C}} = 3$, shows somewhat more complicated behaviour. The first feature that arises is the band splitting at ω_0 above the band minimum. With increasing the coupling strength, the additional splittings arise and thus a sequence of bands each at the distance ω_0 forms, with the lowest one being more and more

¹Particularly, the lower boundary of coupling constant range of 0.7 seems high, but the relevant interaction strength is α^2 , so that it correspond to interaction strength of 0.5, the strength at which first-order weak coupling approximations in phononic systems still perform well [5].

prominent. This is in contrast with the picture acquired in section 2.3, in which a single band of almost unrenormalized bandwidth exists until the sharp transition from which one very narrow band arises. The rough picture is only a first approximation and spectra here show that the apparent transition arises in a much smoother way - by splitting the initial band into a number of narrower ones which are at the end each narrowed strongly according to the results from section 2.3. This picture corresponds well to previous calculations of spectra for the Holstein model [20].

In figure 5.2 one additional, interesting feature may be seen. At coupling strengths close to the strength at which transition occurs (according to 2.3), the ground state band is inverted - its minimum being at the momentum different from zero. This feature may seem very implausible for the electronic system, however, it is not that uncommon for polaronic systems. It has been shown that even in the SCBA approximation, as well as in more exact treatments, although for the somewhat different Hamiltonian of Peierls, a similar band inversion occurs in some parameter ranges. According to [19], the inversion is likely to happen when the electron-phonon interaction range increases. Similar effect can be seen for the cases investigated here - while the inversion is either very slight or absent in the Holstein case, as the interaction range increases, it becomes more prominent. However, it cannot be considered with any certainty that the band inversion indeed happens in the system investigated, since it may be a feature specific to SCBA approximation used or it may stem from the fact that the unitary transformation used is the least reliable in parameter ranges near the transition.

The influence of temperature on polaronic spectra is shown in figure 5.3 in comparison with corresponding spectra in figures 5.1 and 5.2. Firstly, as expected from the results of section 2.3, the increase of temperature acts to some extent in the same way as the increase of coupling strength, causing the transition to occur at lower couplings, as can be inferred from figures 5.2e, 5.3e and 5.3f. Furthermore, the temperature strongly widens the spectral lines. In the low transfer integral case, the additional bands that form become more prominent. One important consequence of spectral broadening for further analyses is the fact that with high enough temperatures, a series of narrow bands formed at high interaction strengths may merge to form a single band as seen in 5.3e and 5.3f.

Finally, in figure 5.4, the influence of electron-phonon interaction range on polaronic spectra is presented. It can be inferred that for qualitatively similar spectra, interaction strengths are different. More specifically, the higher interaction strength is needed for longer-range interaction models in order to have the same effect as for the Holstein model. It must be emphasized that the band minimum shift (binding energy) is roughly the same for the same value of α in both models. However, the effects on the band structure are much stronger in the Holstein case. This is in agreement with the results for the effect of interaction range on transition point presented in section 2.3. It can be deduced that when the effects on band structure are considered, longer interaction range effectively lowers the electron-phonon interaction influences

such as band splitting and narrowing. This gives another indication that long-range interaction will yield a more mobile polaron for the same binding energy.

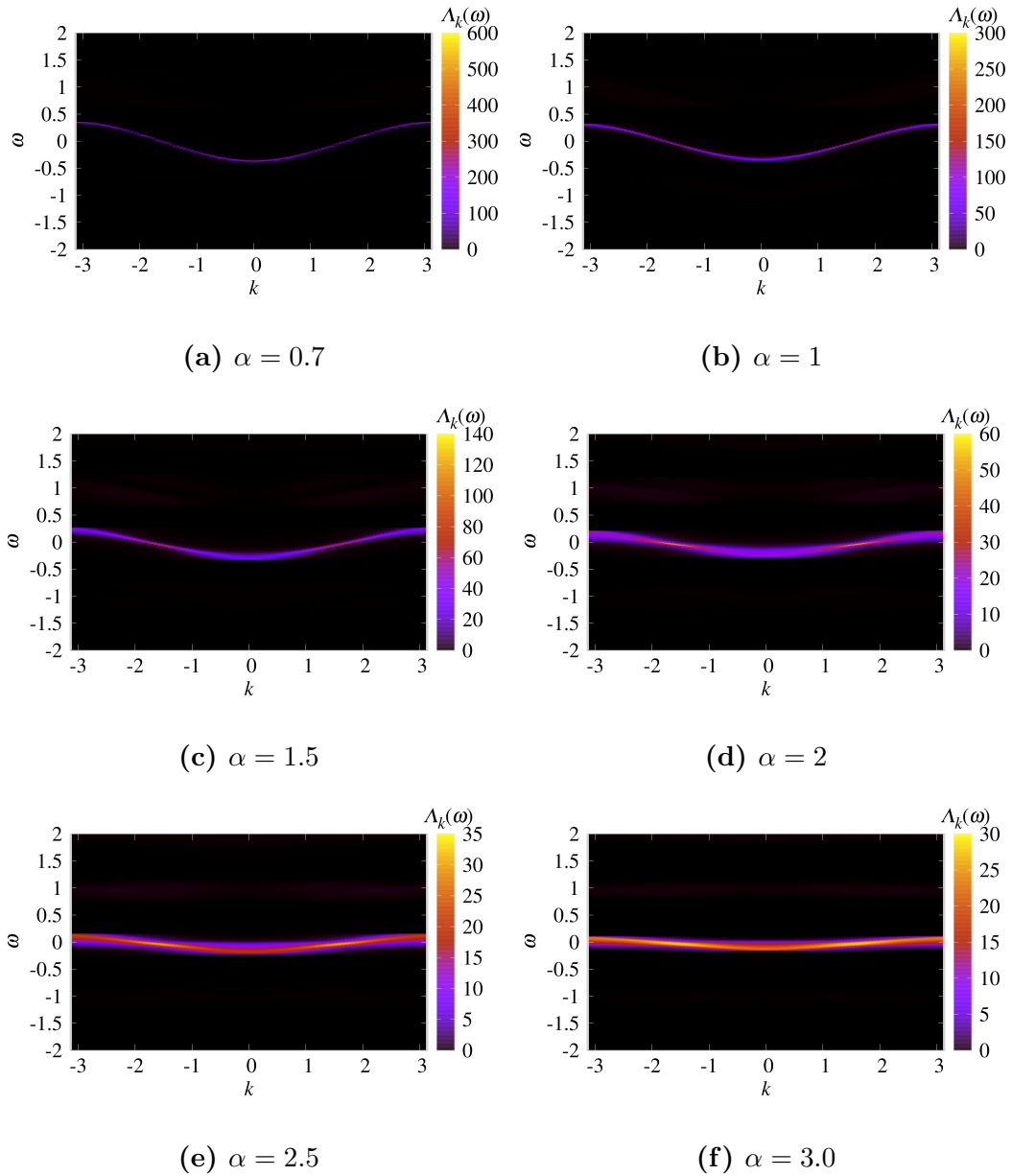


Figure 5.1: Polaron band spectra for different coupling strengths and fixed $t_C = 0.2$, $\psi = \frac{\pi}{4}$, and $k_B T = 0.4$.

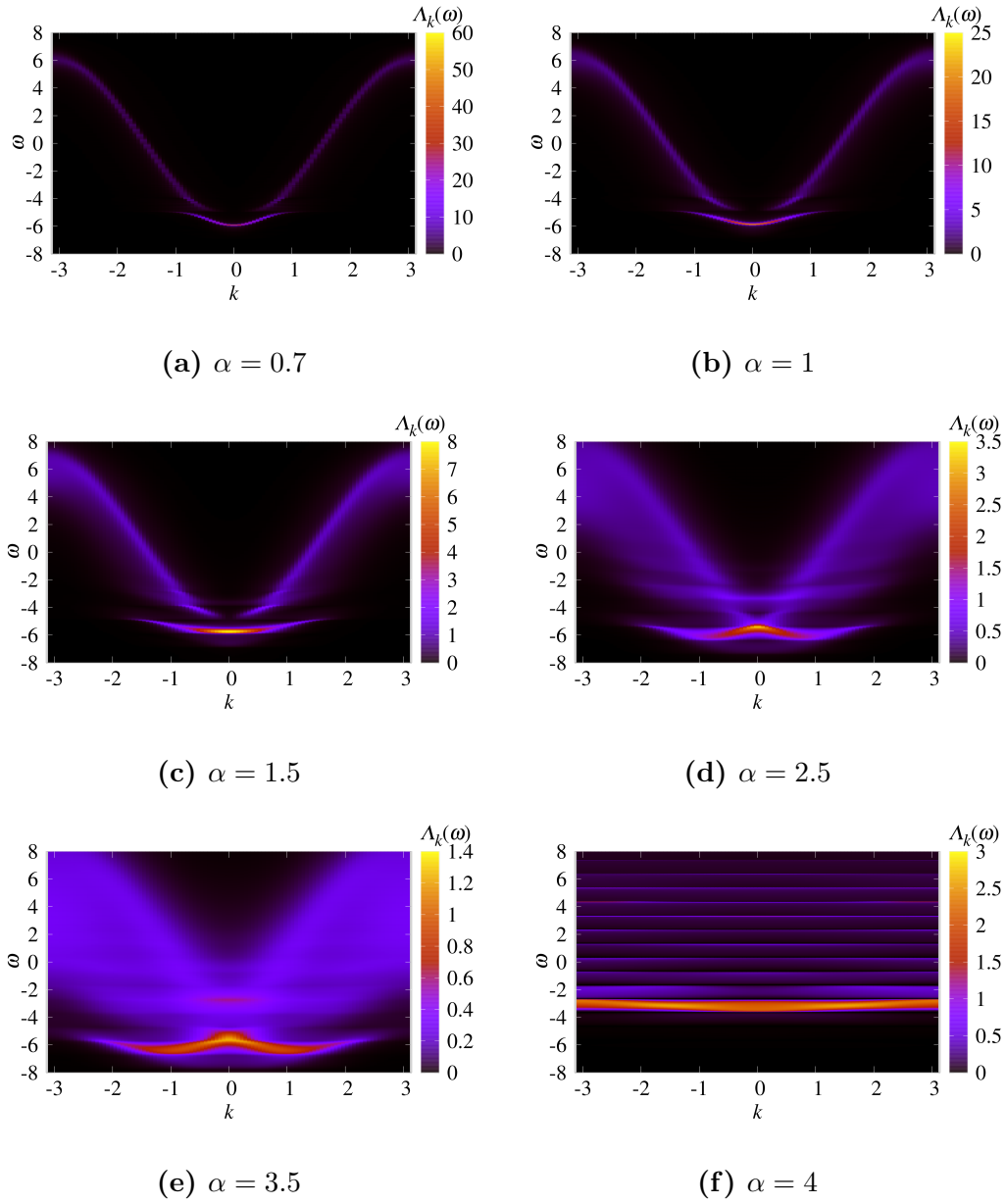


Figure 5.2: Polaron band spectra for different coupling strengths and fixed $t_C = 3.0$, $\psi = \frac{\pi}{4}$, and $k_B T = 0.4$.

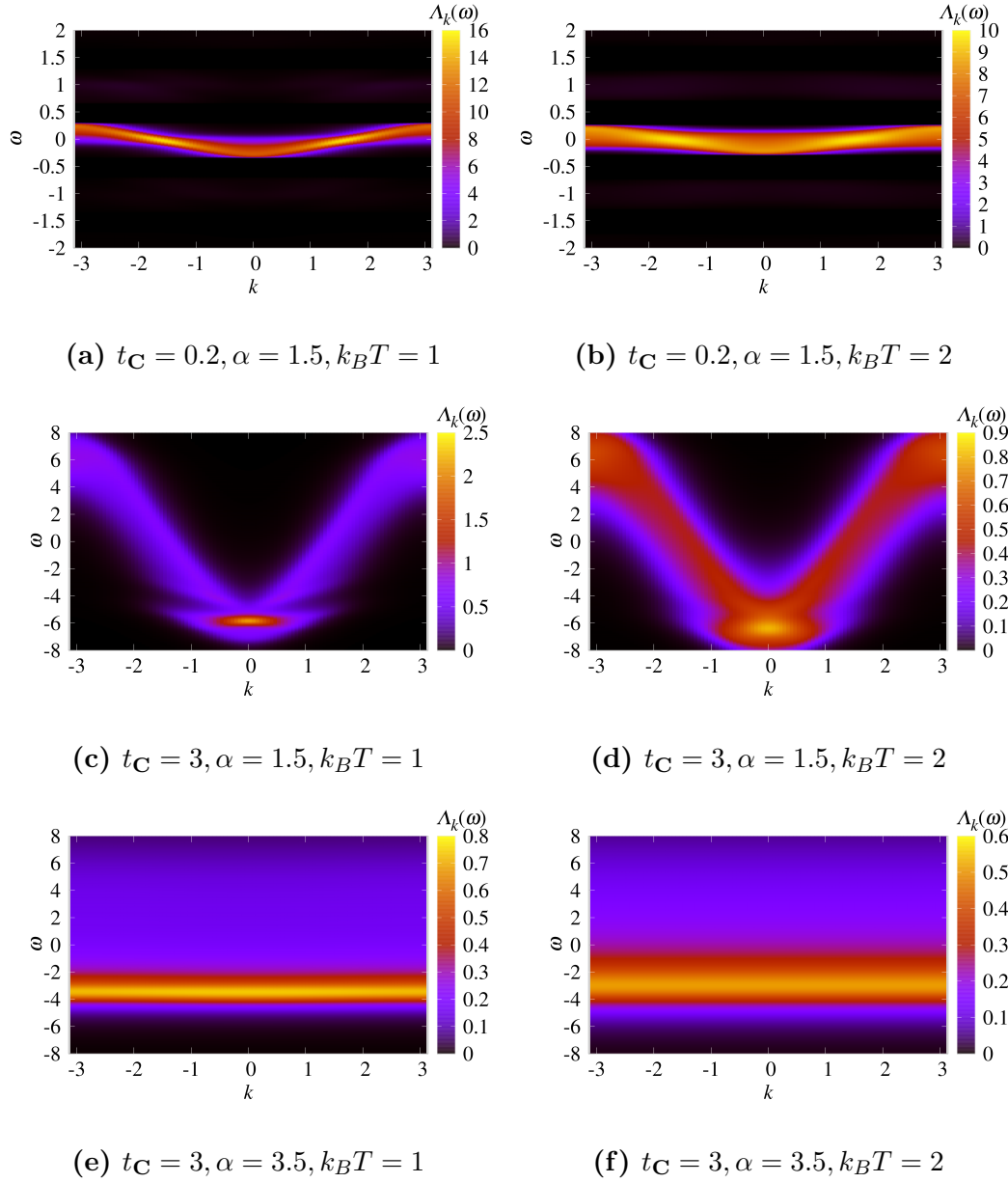


Figure 5.3: The effect of temperature on polaron band spectra. The spectra are given for higher temperatures than the respective ones in figures 5.1 and 5.2. In all the cases shown, $\psi = \frac{\pi}{4}$

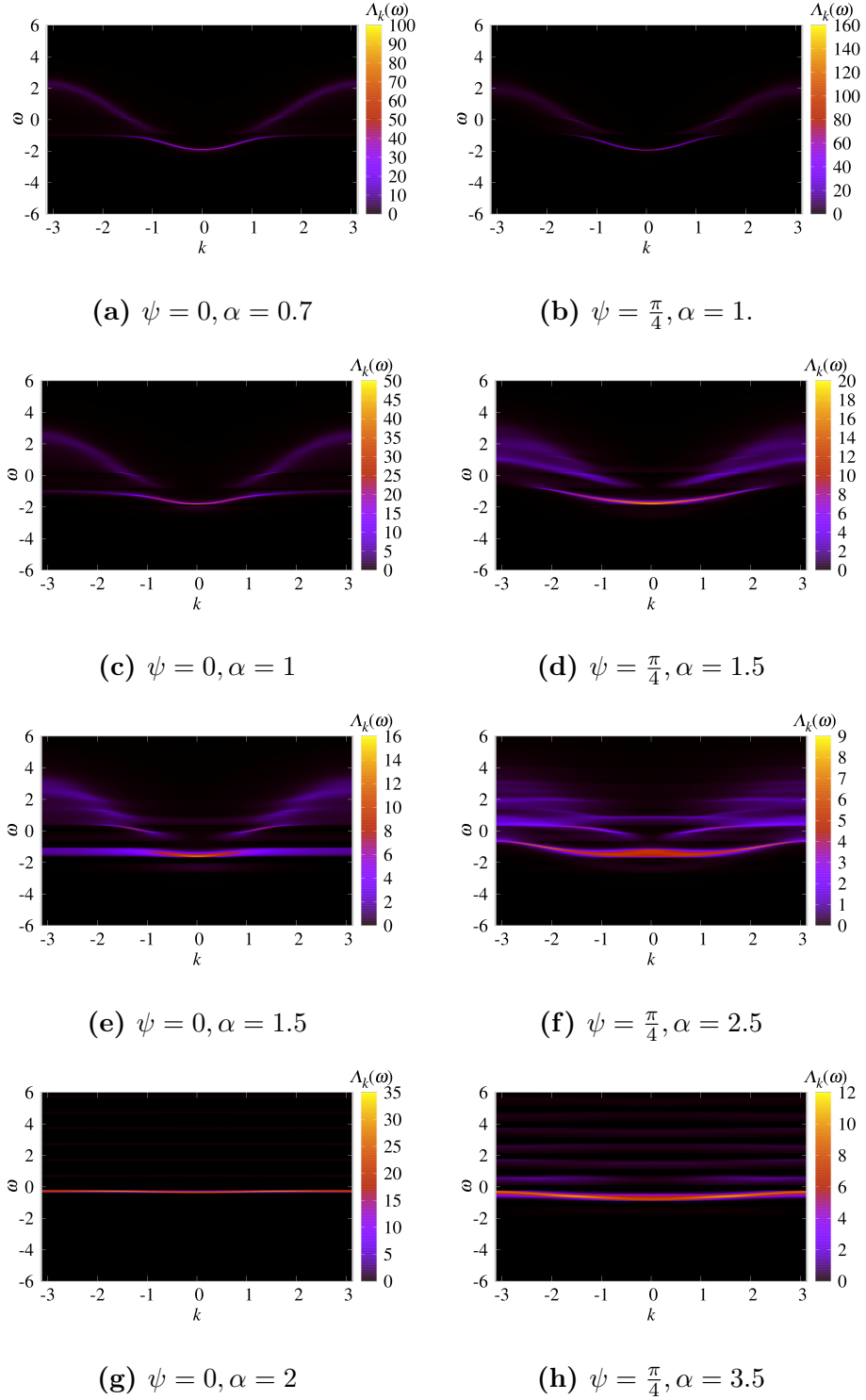


Figure 5.4: Comparison of polaron spectra for different electron-phonon interaction ranges. The spectra on the left correspond to the Holstein case with $\psi = 0$, while the spectra on the right correspond to $\psi = \frac{\pi}{4}$. In the figures shown $t_C = 1$ and $k_B T = 0.3$ is fixed.

5.3 Current-Current Correlations

Quantity proportional to current-current correlations is shown in figure 5.5. Its dependence on coupling strength and temperature is presented. From these and similar plots, it can be deduced that there are two distinct regimes for low temperatures.

The first regime is the weak coupling regime ($\frac{\alpha^2}{2t_C} < 1$). The main feature of correlation function is that it is wide, with phononic ringing, recognized by peaks located at integer multiples of $\frac{2\pi}{\omega_0}$, being only a secondary effect. This suggests that the polaron is in the regime of band-like transport, where the width of the correlation function is limited by scattering. With increasing the temperature, correlations do become narrow, ultimately ending as a delta-like peak.

On the other hand, figures 5.5b, 5.5d, and 5.5f show the features of distinctively different strong-coupling regime ($\frac{\alpha^2}{2t_C} > 1$). The narrow phononic peaks are the main feature of the correlations. The effects of scattering and temperature determine their envelope. As the temperature increases, temperature envelopeme becomes more and more narrow and at high enough temperatures all phononic peaks except the central one vanish. Thus, in the extreme limit of high temperatures, phononic correlations show the same behaviour independent of the electron-phonon coupling strength. It is worth noting that the regime of delta-like correlations is reached for different temperatures at different coupling strength. For very strong and very weak coupling, it takes higher temperature to narrow the central peak or eliminate the neighbouring peaks. Subsequently, delta-like limit is most easily reached at intermediate coupling strengths.

The delta-like limit in correlations can be related to the hopping-like transfer, as described in section 1.1. The narrow correlations enable the carrier hopping to be modeled by a Markovian process, thus entering the regime of the validity of the expression (1.9).

Lastly, it should be noted that the current-current correlations show a clear interdependence with polaronic spectra shown in previous chapter, as expected. The wide band regime corresponds to wide correlations with phonon ringing as a secondary effect. The narrow band regime corresponds to correlations that are dominated by numerous phononic peaks. With the temperature increased to the point for which narrow polaronic bands merge into a single, spectraly wide band, correlations reach the delta-like limit. Thus, when analyzing the mobility results, the analyses based on spectra and correlations are essentially equivalent.

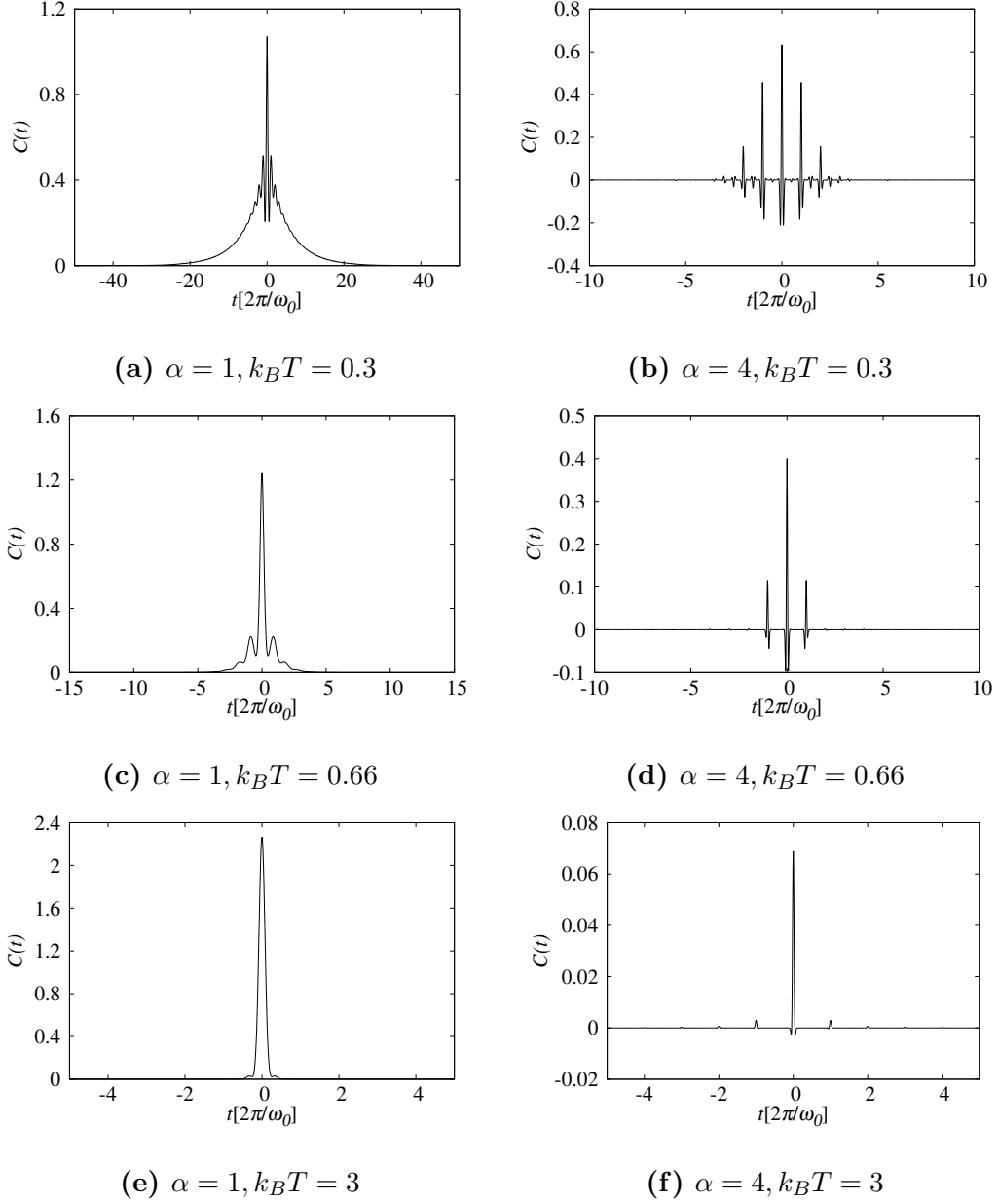


Figure 5.5: Current-current correlations for different coupling strength and temperatures. The plotted quantity $C(t)$ is directly proportional to $\langle j^x(t)j^x(0) \rangle$. In the figures shown $t_C = 1$ and $\psi = \frac{\pi}{4}$ is fixed.

5.4 Mobility

Results of the mobility calculations are presented in figure 5.6. Along with the data obtained by full numerical calculations, weak and strong coupling limits are shown. The data points missing for the full numerical calculation are the ones that did not properly converge, as noted in 5.1. The data points missing for the strong coupling limit are the ones for which the condition $\text{Im}\Sigma < k_B T$ is not satisfied, thus making one of the approximations in the derivation completely unjustified. The mobility in the figures (μ) is shown in units such that the following is valid for mobility in real units (μ_r):

$$\mu = \frac{\mu_r}{\frac{e_0 C^2}{\hbar}}, \quad \mu_r \approx 0.152 \frac{\text{cm}^2}{\text{Vs}} \left(\frac{C}{1\text{\AA}}\right)^2 \mu. \quad (5.1)$$

General features of the mobility obtained are as follows:

- For the realistic lattice constants mobility ranges from $10^{-3} \frac{\text{cm}^2}{\text{Vs}}$ to $10^3 \frac{\text{cm}^2}{\text{Vs}}$. This is in agreement with the orders of magnitude for mobility measured in materials for which the polaronic effects are assumed to be dominant [11]. However, more detailed comparisons are not viable, at least because the model explored is one-dimensional.
- Mobility shows monotonous decrease with temperature. However, while the low temperature decrease is nearly exponential, as can be seen by comparing the result with the weak limit, the high temperature decrease corresponds to a power law with exponent between 1 and 2².
- Transition between the two regions of temperature dependence is smooth. Some non-smoothness, however, can be seen for large transfer integrals. This corresponds to the region in parameter space where the transition described in 2.3 occurs. It can be assumed that the non-smoothness seen is the consequence of the unitary transformation being the least successful in this region.
- Mobility decreases with increasing the coupling strength. The decrease is stronger in adiabatic region with $t_C < 0.5$. In a rough approximation for the low temperature regime, the decrease in the adiabatic region is $\propto \frac{1}{\alpha^4}$, while in the non-adiabatic region, the $\frac{1}{\alpha^2}$ decrease can be observed. This is to be expected from the discussion done in chapter 4.1, regarding the nature of allowed scattering processes (single-phonon and two-phonon ones being dominant in the weak limit).
- Mobility increases with increasing the transfer integral. In high temperature region, the increase is roughly $\propto t_C^2$, while in the low temperature region, mobility scales as $\propto t_C$. This is to be expected from limiting results (4.21), (4.3) and (4.7).

²Power law exponent is close to 1.5 when taking into account the points for the highest temperatures.

- Mobility for the long-range electron-phonon interaction is significantly higher than for a short range one, especially in the high-temperature region and non-adiabatic region. This result was expected from the analyses of renormalized bandwidths and polaronic spectra, but it is now ultimately confirmed. Apart from the weak coupling, low temperature and high transfer integral region where it is small or nonexistent, the difference between the Holstein case and here presented $\psi = \frac{\pi}{4}$ case is significant and reaches a decade for high temperature region.

Comparison with the limiting cases derived in chapter 4 does not only confirm the numerics but also sheds light on the properties of mobility described. The best benchmark for the results is the comparison with very reliable low temperature and weak coupling limit in non-adiabatic regime from chapter 4.1.1. As can be seen from the corresponding regions in figures 5.6e, 5.6f, 5.6g, and 5.6h, the agreement for $\alpha = 0.7$ and even $\alpha = 1$ is very good³. Comparison with this limit, and more specifically expressions (4.3) and (4.7), also leads to the conclusions about temperature ($\mu \propto \frac{1}{n}$), coupling strength ($\mu \propto \frac{1}{\alpha^2}$), and transfer integral ($\mu \propto t_{\mathbf{C}}$) dependence of mobility for the region in question. Thus the mobility features correspond to the band-like transport with dominant scattering mechanisms being the single-phonon processes.

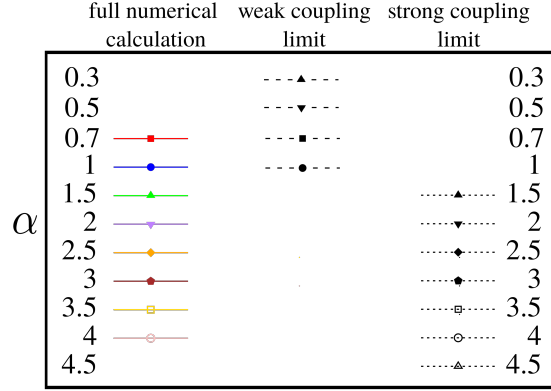
The weak adiabatic limit is not a good benchmark for the results, but it nevertheless shows to be at least a valid estimate. For the very low transfer integrals (real adiabatic behaviour), it becomes more exact as seen in figure 5.6b. The reason is that the terms it omits are proportional to either $(f_{\mathbf{q}} - D_{\mathbf{q}})^2 \propto J_{\mathbf{C}}^2$ ($J_{\mathbf{C}} \rightarrow 0$) or $J_{\mathbf{C}}^2$ directly. The comparison, however, explains the temperature, coupling strength ($\frac{1}{\alpha^4}$) and transfer integral dependence of mobility in the region, in the similar way the non-adiabatic limit does. Mobility in the weak coupling, low temperature adiabatic limit is thus band-like with two-phonon processes dominating the scattering.

The comparison with the high temperature, strong coupling limit is particularly revealing. The derivation of the formula in that limit includes assumptions, the result being that it is not always in agreement with the results. However, in all the cases, for sufficiently high temperatures, strong-coupling limit and full numerical results are seen to either be in good agreement or difference between them becoming gradually smaller. If the full numerical results had been available for arbitrarily high temperatures, it can be expected that the full agreement would be reached in all the cases.

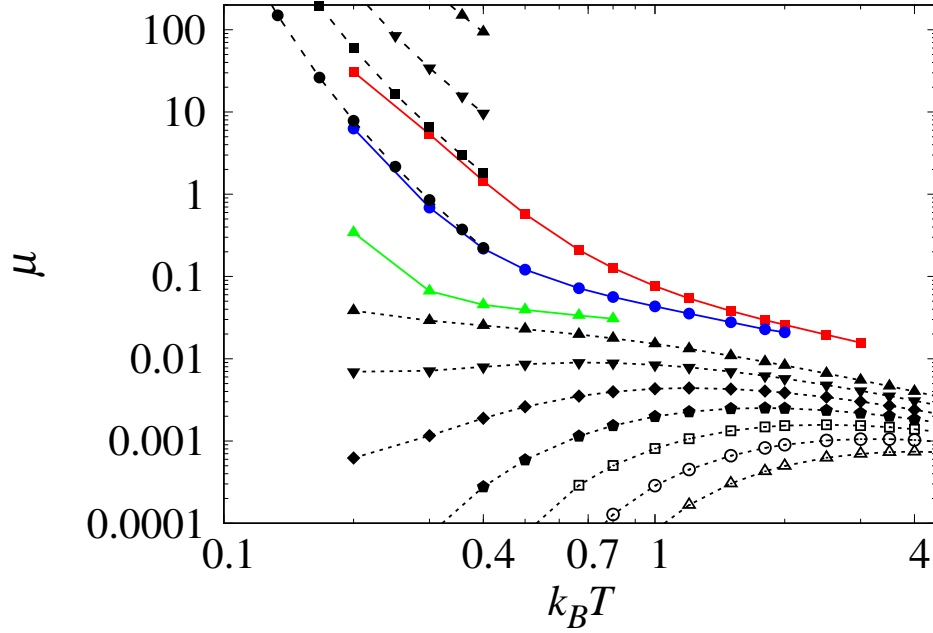
The strong coupling limit itself shows an activating behaviour for lower temperatures, followed by transition to power law decay at high temperatures. The limit itself is a generalization of the formula (1.9) [9]. Activation energy in (1.9) can be shown to

³Slight discrepancies can be attributed to the interaction strength α^2 not being extremely low. The numerical calculations become more and more resource demanding for lower temperatures and coupling strength, but the agreement for the cases shown makes the demanding full calculations unnecessary in the extreme limit.

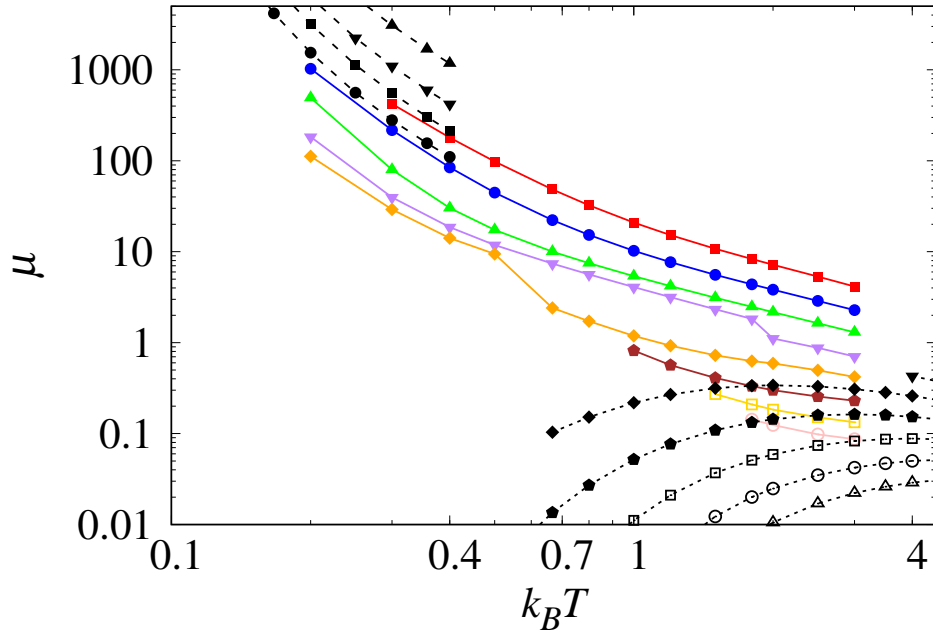
correspond exactly to E_a from (4.15). Formula (1.9) suggests activation behaviour at lower temperatures, dominated by $e^{-\beta E_a}$ factor, while the mobility maximum is reached for $k_B T = \frac{2}{3} E_a \propto \alpha^2$. Its position thus moves to the right with increasing the coupling strength, which is readily seen in figure 5.6. The high temperature dependence is dominated by power law from (1.9), $\mu \propto T^{-\frac{3}{2}}$.



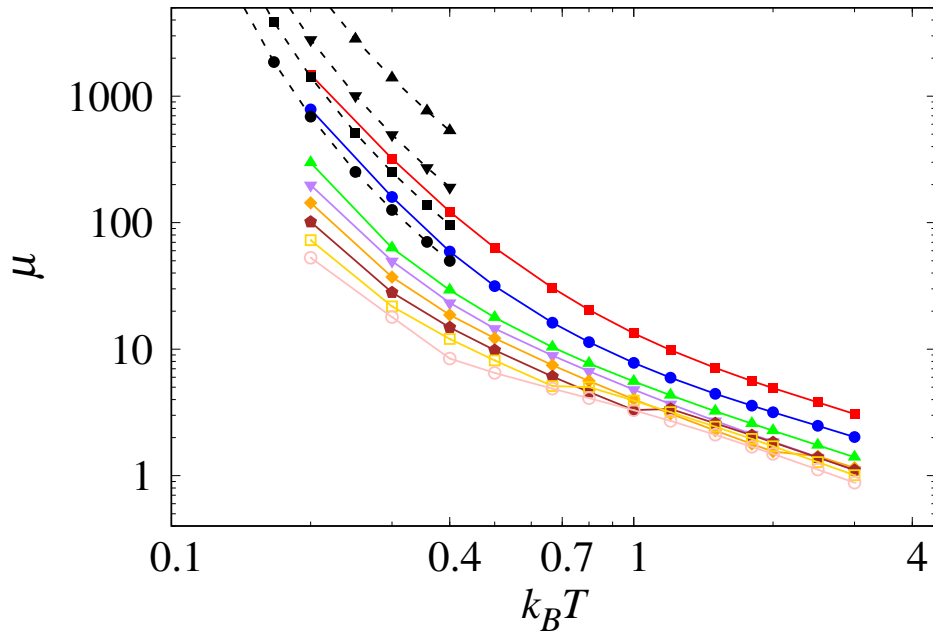
(a) Key for reading the coupling strength from the mobility plots shown below. The data connected with solid colored lines stem from full numerical calculations, while the data connected with dashed black lines are obtained by weak and strong coupling limits described in chapter 4. In cases where the results exist for full numerical calculation as well as the calculations done by strong and weak coupling approximations, data points are labeled by symbol of the same shape and filling.



(b) $t_C = 0.1, \psi = 0$



(g) $t_C = 3, \psi = 0$



(h) $t_C = 3, \psi = \frac{\pi}{4}$

Figure 5.6: Polaron mobility as a function of temperature and coupling strength for several different transfer integrals and interaction ranges. In each figure shown, transfer integral and interaction range are fixed.

When compared to full numerical results, the strong coupling limit deviates significantly in the activation region. No activation is observed for the parameters explored. It is not until the power law decay region is reached that the results start to coincide. However, the discrepancy can be explained by considering current-current correlations or spectra, equivalently. When current-current correlations are delta-like, the two results are in good agreement. Since the high temperatures lead eventually to delta-like correlations, it is expected that for all cases, agreement should be reached at sufficiently high temperature. As already noted when analyzing the correlations, the random-walk approximation is justified for such short-time correlations. Alternatively, in the way the limit was derived in chapter 4.2, the spectra can show to what extent the initial approximation of single flat band is justified. It is not a surprise that the regions where the polaronic spectra does consist of single flat band (chapter 5.2) correspond to the delta-like correlation region. In addition, as already noted, higher temperature makes spectral lines widen, ultimately merging the bands in a single one.

It turns out that the region of delta-like correlation coincides with the power law decay region for the strong limit and thus in actual results no activation is observed. There is no principle that would exclude the activation region to be present in real systems, it is only a question if the temperature is high enough for the strong coupling approximation to be valid. The results of the Monte-Carlo mobility calculations for Holstein model with $t_C = 1$ [21] show that the activation region exists for low temperatures and high coupling strengths, the region where the full numerical calculation presented here did not converge. The numerical results show satisfactory agreement with Monte-Carlo results from [21] in other parameter regions. Thus, it may be that the region of parameters accessible to full numerical calculation in the Holstein case did not include activation regions.

It is often taken that the activation is a signature of hopping-like mobility, while decay is specific to band-like mobility [10]. However, power law decay is perfectly consistent with hopping-like approximation. While the activation predicted by hopping like-approximation may or may not be present, depending on the applicability of the limit for intermediate temperatures, its absence is not a definite sign of the band-like transport.

With the above presented analyses done, mobility features in the strong coupling high temperature region, such as power law decay with respect to temperature and scaling with transfer integral as t_C^2 are explained by the strong coupling limit picture of hoping-like transfer in a flat band.

One additional point is of importance - the dependence of strong-coupling limit result on the range of electron-phonon interaction. The expression for activation energy, $E_a = \frac{1}{2} \sum_{\mathbf{q}} D_{\mathbf{q}}^2 (1 - \cos \mathbf{q} \cdot \mathbf{C})$ implies that the low momentum electron-phonon coupling contribution is suppressed. However, the long-range models have the highest interaction contribution from the low momenta, in sharp contrast with the Holstein model

which shows no momentum dependence of the coupling coefficients (figure 2.3). The lower activation energy has as a consequence the less prominent activation behavior, since the exponential factor $e^{-\beta E_a}$ is not as sharp. This can readily be seen from mobility results in strong coupling limit and for two different models presented ($\psi = 0$ and $\psi = \frac{\pi}{4}$), the best example being figures 5.6e and 5.6f. Thus, longer-range electron-phonon interaction not only suggests a significantly higher mobility in the strong coupling limit, but it also suppresses the activation region and makes it less prominent. Therefore it can be expected that in the experiments in which activation region is measured and is prominent, the electron-phonon interaction is probably of a shorter range type. Of course, mobility measurements alone cannot provide the information about the interaction range.

In conclusion, the mobility results obtained by the full numerical calculation from the approximate solution of the Kubo formula used show a reasonable agreement with both weak and strong regime limits. The general features of mobility are possible to understand in the scopes of these limits, and transition between the distinct regions is smooth overall. The discrepancies of the results and strong limit for insufficiently high temperatures are as expected from the analyses of current-current correlations and spectra. The longer range electron-phonon interaction significantly increases polaron mobility in the strong coupling region. This is as expected from the hopping activation energy being lower for a more non-locally bound polaron. The longer range lattice polaron models provide a possibility of higher mobility than the Holstein model allows together with a less prominent or absent activation region.

Chapter 6

Conclusion

The main theme of the thesis has been mobility for a family of lattice polaron models in a wide range of coupling strengths and temperatures. Electron-phonon interaction range differs between the models in the family. In order for the calculations based on perturbative techniques to be made possible, a variant of Lang-Firsov unitary transformation was applied. The transformation diagonalizes the Hamiltonian exactly in the limit of infinite coupling strength and its applicability for small and intermediate couplings is made possible by inserting the variational parameters in the transformation. The equations for variational parameters as well as the polaron properties were found by minimizing the free energy functional obtained from the Gibbs-Bogolyubov bound. Numerical results were presented for variational parameters and polaron properties were found for the 1D variant of the model. Mobility calculations are based on an approximate solution of the Kubo formula. Expressions for the spectral properties needed are found with standard Matsubara formalism. The resulting self-consistent equations for the self-energy were solved numerically for the 1D model and the mobility was calculated. For comparison, semi-analytic expressions for mobility are derived in the strong and weak coupling regime. Polaronic spectra and current-current correlations were analyzed in order to gain insight into the nature of polaron transport and relation of full numerical results with corresponding limits. Mobility results show a satisfactory agreement with the weak and strong coupling cases in the extreme parameter regimes, as well as mostly smooth transition between these regimes. Band-like exponential decrease of mobility for low temperatures crosses into hopping-like power law decay at high temperatures. No activation region is found, but its existence in the real systems cannot be excluded. When comparing the models with different electron-phonon interaction range, longer interaction range results in a significantly more mobile polarons. Further work with regards to the extension of numerical calculations to the 3D model is desirable, as well as first principle calculations that would extract the parameters of the model and thus enable quantitative comparisons with experimental results.

Appendix A

The Proof of Expressions Used for the Calculations of Phonon Thermal Averages

In this appendix, proof of the following identities will be presented:

$$\langle e^{\mu b^\dagger + \nu b} \rangle_0 = e^{\frac{1}{2}(2n+1)\mu\nu}, \quad (\text{A.1})$$

$$\frac{\partial e^{A(\alpha)}}{\partial \alpha} = e^{A(\alpha)} \left(\frac{\partial A(\alpha)}{\partial \alpha} - \frac{1}{2}[A, \frac{\partial A(\alpha)}{\partial \alpha}] \right) = \left(\frac{\partial A(\alpha)}{\partial \alpha} + \frac{1}{2}[A, \frac{\partial A(\alpha)}{\partial \alpha}] \right) e^{A(\alpha)}, \quad (\text{A.2})$$

the second one being valid under condition $[[A, \frac{\partial A(\alpha)}{\partial \alpha}], A] = 0$.

In order to prove the first result, the operator exponential on the right hand side will be transformed with the help of the well known identity $e^A e^B = e^{\frac{1}{2}[A, B] + A + B}$, applicable for $[A, [A, B]] = [B, [A, B]] = 0$. Since the phonon creation and annihilation operators give a scalar commutator, the identity can be applied to give:

$$\langle e^{\mu b^\dagger + \nu b} \rangle_0 = \langle e^{\mu b^\dagger} e^{\nu b} e^{-\frac{1}{2}\mu\nu[b^\dagger, b]} \rangle_0 = e^{\frac{1}{2}\mu\nu} \sum_{m, n} \frac{\mu^m \nu^n}{m!n!} \langle (b^\dagger)^m b^n \rangle_0. \quad (\text{A.3})$$

Only averages of expressions that conserve number of phonons are non-zero, thus only the terms with $m = n$ contribute to the sum in (A.3). Using the Wick's theorem gives:

$$\begin{aligned} e^{\frac{1}{2}\mu\nu} \sum_{m, n} \mu^m \nu^n \langle (b^\dagger)^m b^n \rangle_0 &= e^{\frac{1}{2}\mu\nu} \sum_m \frac{\mu^m \nu^m}{(m!)^2} \langle (b^\dagger)^m b^m \rangle_0 = e^{\frac{1}{2}\mu\nu} \sum_m \frac{\mu^m \nu^m}{(m!)^2} \langle b^\dagger b \rangle_0^m m! \\ &= e^{\frac{1}{2}\mu\nu} \sum_m \frac{\mu^m \nu^m}{m!} n^m = e^{\mu\nu(n+\frac{1}{2})}, \end{aligned} \quad (\text{A.4})$$

which completes the first proof.

For the second result, only one of the identities will be proven, the other one being obtainable in an analogous way or by applying the BCH formula on the already proven one. When taking the derivative of the exponential term by term, the non-commutativity must be taken into account:

$$\frac{\partial e^{A(\alpha)}}{\partial \alpha} = \frac{\partial}{\partial \alpha} \left(\sum_{n=0}^{\infty} \frac{A^n}{n!} \right) = \sum_{n=0}^{\infty} \frac{1}{n!} \sum_{m=0}^{n-1} A^{n-m-1} \frac{\partial A(\alpha)}{\partial \alpha} A^m. \quad (\text{A.5})$$

Operator $\frac{\partial A(\alpha)}{\partial \alpha}$ must now be commuted to the right of all A operators in each individual term. Every commutation leaves the term $-A^{n-2}[A, \frac{\partial A(\alpha)}{\partial \alpha}]$ and moves $\frac{\partial A(\alpha)}{\partial \alpha}$ operator one place to the right. In a term where $\frac{\partial A(\alpha)}{\partial \alpha}$ is m places from the right end, m transpositions need to be done:

$$\begin{aligned} \sum_{n=0}^{\infty} \frac{1}{n!} \sum_{m=0}^{n-1} A^{n-m-1} \frac{\partial A(\alpha)}{\partial \alpha} A^m &= \sum_{n=0}^{\infty} \frac{1}{n!} \sum_{m=0}^{n-1} \left(A^{n-1} \frac{\partial A(\alpha)}{\partial \alpha} - m A^{n-2} [A, \frac{\partial A(\alpha)}{\partial \alpha}] \right) \\ &= \sum_{n=0}^{\infty} \frac{1}{n!} \left(n A^{n-1} \frac{\partial A(\alpha)}{\partial \alpha} - \frac{(n-1)n}{2} A^{n-2} [A, \frac{\partial A(\alpha)}{\partial \alpha}] \right) = e^{A(\alpha)} \left(\frac{\partial A(\alpha)}{\partial \alpha} - \frac{1}{2} [A, \frac{\partial A(\alpha)}{\partial \alpha}] \right), \end{aligned} \quad (\text{A.6})$$

thus completing the proof of the first identity in (A.2).

Bibliography

- [1] L. D. Landau. *Phys. Z. Sowjetunion*, 3:664, 1933.
- [2] H. Fröhlich. *Adv. Phys.*, 3(11):325, 1954.
- [3] N. Prodanović, N. Vukmirović, Z. Ikonić, P. Harrison, and D. Indjin. *J. Phys. Chem. Lett*, 5(8):1335, 2014.
- [4] Y. E. Shchadilova, F. Grusdt, A. N. Rubtsov, and E. Demler. *Phys. Rev. A*, 93(4):043606, 2016.
- [5] A. S. Alexandrov and J. T. Devreese. *Advances in Polaron Physics (Springer Series in Solid-State Sciences)*. Springer, 2009.
- [6] G. D. Mahan. *Many-Particle Physics (Physics of Solids and Liquids)*. Springer, 2000.
- [7] J. T. Devreese. *Fröhlich Polarons (Lecture course including detailed theoretical derivations)*. arXiv:1012.4576.
- [8] T. Holstein. *Ann. Phys. (N.Y.)*, 8(3):343, 1959.
- [9] N. Prodanović. *Semiconductor Quantum Dots: Intraband Electronic, Optical and Carrier Dynamical Properties*. PhD thesis, University of Leeds, 2014.
- [10] J. Choi, A. T. Fafarman, S. J. Oh, D. Ko, D. K. Kim, B. T. Diroll, S. Muramoto, J. G. Gillen, C. B. Murray, and C. R. Kagan. *Nano Lett.*, 12(5):2631, 2012.
- [11] D. Keroack, Y. Lepine, and J. L. Brebner. *J. Phys. C*, 17(5):833, 1984.
- [12] A. S. Alexandrov and P. E. Kornilovitch. *Phys. Rev. B*, 82(4):807, 1999.
- [13] V. Janković. *Non-Equilibrium Optical Conductivity in a System with Localized Electronic States*. Master thesis, University of Belgrade, 2014.
- [14] Y. Cheng and R. J. Silbey. *J. Chem. Phys.*, 128(11):114713, 2008.
- [15] R. W. Munn and R. J. Silbey. *J. Chem. Phys.*, 83(4):1854, 1985.
- [16] B. Gerlach and H. Löwen. *Phys. Rev. B*, 35(9):4281, 1987.

- [17] P. E. Spencer, J. H. Samson, P. E. Kornilovitch, and A. S. Alexandrov. *Phys. Rev. B*, 71(18):184310, 2005.
- [18] A. L. Kuzemsky. *Electronic Transport in Metallic Systems and Generalized Kinetic Equations*. arXiv:1109.5532.
- [19] Q. Liu. *Phys. Lett. A*, 376(14):1219, 2012.
- [20] M. Berciu and G. A. Sawatzky. *EPL*, 81(5):57008, 2008.
- [21] A. S. Mishchenko, N. Nagaosa, G. De Filippis, A. de Candia, and V. Cataudella. *Phys. Rev. Lett.*, 114(14):146401, 2015.